FABRICATION OF INTEGRATED FLUIDIC SYSTEMS AND METHODS TO PERFORM SINGLE-MOLECULE DNA ANALYSIS

by

Venkat Ram Dukkipati

A dissertation submitted in partial fulfillment
of the requirements for the degree of
Doctor of Philosophy
(Electrical Engineering)
in The University of Michigan
2008

Doctoral Committee:

Professor Stella W. Pang, Chair
Professor David T. Burke
Professor Ronald G. Larson
Assistant Professor Wei Lu

To my parents Arun Kumar Dukkipati and Nirmala Dukkipati, my sister Nandita Dukkipati, my aunt Devi Tummala, my uncle Ram Mohan Lal Tummala

ACKNOWLEDGMENTS

I am deeply grateful to my advisor, Professor Stella W. Pang for her supervision, inspiration, and encouragement throughout the course of this study. Her continuous support was essential in progress and success of this work. I wish also to express my sincere gratitude to the members of my dissertation and prelim committee, Professor Ronald G. Larson, Professor David T. Burke, and Professor Wei Lu for their time and effort in reviewing this work.

TABLE OF CONTENTS

LIST OF FIGURES

LIST OF TABLES

LIST OF APPENDICES

LIST OF SYMBOLS

ac	Alternating Current
Al	Aluminum
APTES	Aminopropyltriethoxy Silane
Au	Gold
BSA	Bovine Serum Albumin
bp	Base Pair
Cl_2	Chlorine
cm	Centimeter
CNT	Carbon Nanotube
Cr	Chromium
C_4F_8	Perfluroisobutene
CM	Clausius-Mossoti
d	Channel Depth
d_m	Molecular Diameter
d_s	Stokes Diameter
D	Diffusivity
D_p	Dipole
dc	Direct Current
DEP	Dielectrophoresis
DI	De-Ionized
DNA	Deoxyribose Nucleic Acid

dNTP	Di-nucleotriphosphate
DRIE	Deep Reactive Ion Etching
dsDNA	Double Strand Deoxyribose Nucleic Acid
E	Electric Field
E_{ll}	Parallel Component of Electric Field
fN	Femto Newton
F	Force Stretching DNA Molecule
F_c	Capillary Force
F_D	Dielectrophoretic Force
F_E	Electrothermal Force per Unit Volume
g	Grams
H_2SO_4	Sulfuric Acid
H_2O	Water
H_2O_2	Hydrogen Peroxide
HCl	Hydrochloric Acid
HF	Hydrofluoric Acid
h	Hour
Hz	Hertz
ICEO	Induce Charge Electro-Osmosis
I_2	Iodine
IPA	Isoproponal Alcohol
K	Thousand
kb	Kilo Base
k_B	Boltzmann Constant
kbp	Kilo Base Pairs
KHz	Kilohertz
KI	Potassium Iodide

l	Channel Length
L_c	Contour Length
m	Meter
MES	2-Morpholinoethanesulphonic Acid
MHz	Megahertz
min	Minute
ml	Milli Liter
mm	Millimeter
mM	Millimolar
MPa	Megapascal
ms	Millisecond
mTorr	Millitorr
MV	Mega volts
n	Number of DNA Molecules Immobilized
n_θ	Normal Component of Electric Field
N	Newton
N_o	Constant to Fit Equation Describing Distribution of Immobilized DNA Molecules in Microchannel
N_2	Nitrogen
ng	Nanogram
NH_2	Amine
nm	Nanometer
nM	Nanomolar
NMOS	Negative Metal Oxide Semiconductor
NTP	Neuclotriphosphate
n-type	Negative-type
O_2	Oxygen

p	Persistence Length
P	Pressure
PADI	Protein Assisted DNA Immobilization
PCB	Printed Circuit Board
PCR	Polymerase Chain Reaction
PDMS	Polydimethylsiloxane
PECVD	Plasma Enhanced Chemical Vapor Deposition
pg	Picograms
pH	Pondus Hydrogenii
pM	Picomolar
PMMA	Polymethylmethacrylate
PMOS	Positive Metal Oxide Semiconductor
pN	Piconewton
PNA	Peptide Nucleic Acid
t-type	Positive-type
Q	Charge of ions
q_f	Flow Rate
r	Radius
R_g	Radius of Gyration
Re	Real Part of a Complex Number
rf	Radio Frequency
RNA	Ribonucleic Acid
RNAP	Ribonucleic Acid Polymerase
rpm	Rotations Per Minute
s	Second
S	Siemens
sccm	Standard Cubic Centimeters per Minute

Si	Silicon
SF_6	Sulfur Hexafluoride
t	Time
T	Temperature
T_r	Torque
Ti	Titanium
TRIF	Total Internal Reflection Fluorescence
TRIS-EDTA	Tris Ethylenediamine Tetraacetic Acid
u_s	Slip Velocity
UV	Ultraviolet
UTP	Uridinetriphosphate
v	Velocity of Fluid
V	Volts
V_m	Mean Velocity of Fluid
V_1	Voltage 1
V_2	Voltage 2
V_3	Voltage 3
w	Width
W	Watt
wt	Weight
x	DNA Stretch Length Between Radius of Gyration and Contour Length
X	Distance Moved by Capillary Meniscus in Channel
X_t	Multiplication
X_{inlet}	Distance Traveled Before DNA Immobilization
y	Distance from Center of Channel
z	Electrophoretic Mobility
2-D	Two Dimensional

3-D	Three Dimensional
°C	Degrees Celsius
µ	Micro
µm	Micrometer
µM	Micromolar
µS	Micro Siemens
-OH	Hydroxyl
λ	Lambda
σ	Conductivity
µl	Microliter
~	Approximate
%	Percentage
=	Equal
>	Greater Than
<	Lesser Than
Δp	Pressure Gradient
γ	Surface Tension of Fluid in Air
γ_{sa}	Surface Tension Between Channel Surface and Air
γ_{sl}	Surface Tension Between Channel Surface and Fluid
θ	Contact Angle
ν	Viscosity
$	Dollar
I	One
II	Two
III	Three
×	Magnification
±	Variation

-	Negative
ε	Dielectric Constant
ε_f	Dielectric Constant of Fluid
ε_p^*	Complex Permittivity of Particle
ε_m^*	Complex Permittivity of Medium
ς	Zeta Potential
∇	Gradient
ω	Frequency
@	At

ABSTRACT

Stretching DNA from its coiled state into a linear form is an important requirement in DNA-protein interaction studies and DNA sequencing. Immobilization of stretched DNA molecules is required to analyze protein interactions and presence of molecules along the DNA strand. The ability to perform DNA immobilization and stretching in microfabricated fluidic systems is a step towards enhancing the applications of DNA studies. Forces derived from hydrodynamic flow and electric field in channels are used to immobilize and stretch DNA molecules.

Electrodes integrated in fluidic channels are used to stretch DNA molecules using electric field. Fabrication technology for integrating electrodes with Si micro- and nano-channels using polymethylmethacrylate bonding was developed. Bonding is performed at low temperature to form integrated channels without leakage and the channels are hydrophilic, allowing introduction of fluid and biomolecules into the channels by capillary action. A novel DNA immobilization technique called protein assisted DNA immobilization (PADI) was developed to immobilize and stretch hundreds of DNA molecules using hydrodynamic flow in a microchannel. The DNA molecules are not overstretched and the immobilization is performed at physiological pH of 8.0 while maintaining continuous hydration of DNA molecules in the channel. Optical mapping and single-molecule transcription were demonstrated in microchannels using the PADI technique. Precise DNA immobilization and stretching across electrode gaps in microchannels were demonstrated using an ac voltage. Using the ac electric field, large

numbers of DNA molecules are immobilized on the electrodes without chemical modifications to the DNA or electrode surface. A mechanism based on induced charge electro-osmosis (ICEO) has been developed to induce motion in suspended particles and move them away from the electrodes. The ICEO induces motion of particles in channels without using fluid flow, unlike dc or ac electro-osmosis, or pressure driven flow. The mechanism is applied to control the motion of DNA molecules in channels using low ac voltage, and a DNA velocity of 24 μm/s has been demonstrated at a distance of 500 μm away from the electrodes.

CHAPTER 1
INTRODUCTION

The objective of this work is to fabricate integrated micro- and nano-fluidic systems for single-molecule deoxyribose nucleic acid (DNA) analysis and to develop methods that enable single-molecule analysis to be performed in the integrated systems. Fluorescence based single-molecule DNA analysis is applied to DNA mapping [1] and DNA-protein interaction studies [2]. DNA immobilization and stretching [3], which are essential steps in single-molecule analysis, can be achieved using hydrodynamic flow [4] and electric field [5]. Current methods are limited in throughput of single-molecule analysis for DNA mapping and lack of control over location of DNA molecules in channels. In this thesis, high throughput DNA immobilization and stretching are studied using hydrodynamic flow in microfluidic systems. In addition, ac voltage is used to control the placement of stretched DNA molecules in the fluidic system with integrated electrodes. DNA molecules are immobilized and stretched at specific locations across electrode gaps in channels. Voltage induced motion of DNA molecules is used to control the location of stretched DNA molecules in channels. These methods have been developed to ultimately achieve the control over the location of protein interactions with the DNA strand.

In this chapter, the advantages of single-molecule technology over conventional methods will be discussed first. Then current techniques for single-molecule DNA analysis and their features will be discussed. Finally, our approach to performing single-

molecule DNA analysis in micro- and nano-fluidic systems for applications in DNA mapping and DNA-protein interaction studies will be presented.

1.1. Biomolecular Analysis Techniques

Analyzing biomolecules such as DNA and proteins is an important step towards understanding their functionality [6], [7]. Detection and analysis of biomolecules are an integral part of disease diagnostics and biomarker discovery [8], [9]. The most common method used for detecting biomolecules is fluorescent microscopy [10]. Detection is performed by exciting fluorescent labels attached to the biomolecules using a single wavelength light. The light emitted from the labels is detected by the microscope and either a group or individual fluorescent bio-molecules are analyzed. In this section, two classes of biomolecular analysis called bulk and single-molecule technology will be discussed and their performance compared.

1.1.1. Bulk Technology

One of the most common techniques used for analyzing fluorescent labeled DNA and protein molecules is gel electrophoresis [11]. In this method, the biomolecules are separated in a gel either by their molecular weight or charge. Separation is achieved by transporting the molecules through the gel using an electric field [12]. The gel is a solid porous matrix that allows molecules of different sizes and charges to be transported through the pores at different speeds, resulting in the separation of biomolecules. Following separation, the biomolecules in the gel are viewed using fluorescent microscopy.

Often the concentration of the original DNA sample is insufficient for fluorescent detection [13] and polymerase chain reaction (PCR) must be used to perform amplification of the DNA molecules [14]. In both gel electrophoresis and PCR, the biomolecules are analyzed by imaging fluorescent signals emanated by hundreds of molecules; hence, these techniques are often referred to as bulk techniques.

1.1.2. Single-Molecule Technology

Over the past 20 years, several techniques to detect and analyze individual biomolecules have been developed [15]. Single-molecule technology has evolved into a new field due to its potential applications and advantages over conventional bulk techniques [16]. Detection of individual biomolecules enables more sensitive analysis compared to bulk techniques [3], which has significant implications in DNA and protein analysis. Currently no technology exists that can amplify low concentrations proteins [17]. Thus protein detection will benefit from development of single-molecule technologies. In DNA analysis, the higher sensitivity obviates the need for PCR amplification of DNA molecules. PCR is a complex procedure involving numerous steps such as heating, cooling, and enzymatic reactions between DNA and proteins. Procedures not requiring the PCR step will significantly lower the complexity and cost of performing DNA analysis [18]. These procedures can benefit molecular diagnostics and biomarker discovery, which require DNA analysis to be performed on large population [19]. This is apparent in the race for DNA sequencing technologies that are being developed to achieve the goal of $1000 human genome sequencing [20].

A second advantage of single-molecule analysis is the capability to detect and quantify the motion and interactions of enzymes with high precision. An enzymatic

action is performed in series of consecutive steps, where each step is constituted of motion and physical/chemical interactions with a different molecule [21]. In bulk techniques, only the average characteristics of protein interactions can be measured from a collection of biomolecules [22]. On the other hand, in single-molecule analysis, interactions occurring in isolated molecules can be characterized, which is more accurate than the average value [23].

1.2. Single-Molecule DNA Analysis

DNA is a semi-flexible polymer composed of di-nucleotriphosphates (dNTPs) that are joined together by phosphodiester bonds. Common examples include bacteriophage DNA molecules, such as λ and T7, which have been extensively used as templates for studying DNA-protein interactions and performing DNA mapping. The radius of gyration R_g of a self-avoiding polymer, such as a coiled DNA, quantifies its physical size in solution, and can be expressed as:

$$R_g = \left(\mathrm{pd_m}\right)^{1/5} \mathrm{L_c}^{3/5} \tag{1.1}$$

where p is the persistence length (which is proportional to the molecular stiffness), d_m is molecular diameter, and L_c is contour length of DNA [3]. For bacteriophage DNA in aqueous solution, R_g is typically on the order of a μm. These coiled DNA molecules in a solution experience Brownian motion and hence are undergoing continuous random motion at equilibrium. In order to perform single-molecule analysis, the DNA molecules need to be stabilized and is achieved by immobilizing the molecules. Single-molecule DNA analysis typically involves sequence detection and protein interaction studies along the strand, which is difficult to achieve on randomly coiled DNA strands since all sections of the strand are not accessible in the coiled state. Hence they must be stretched

from their coiled state into a linear form, which enables high resolution imaging of the DNA strand. The stretched state enables the detection of motion and interactions of proteins along the DNA strand [24]. DNA mapping is performed on stretched DNA molecules by detection of specific sequences and separation between the sequences along the strand [25].

Several methods of immobilization and stretching of DNA molecules have been developed over the last decade. The methods defer by the procedures used for immobilization and stretching of the DNA strands. Some methods manipulate one DNA molecule during an experiment, while others generate hundreds of immobilized and stretched DNA molecules [15]. In DNA-protein interaction studies, protein interactions are measured from a single DNA molecule. In DNA mapping, statistical data on location of specific sequences along the strand is gathered from hundreds of immobilized and stretched DNA molecules.

In existing methods, immobilization is carried out as the first step, followed by stretching of the DNA strand. Typically immobilization is performed by one of the following methods: chemical modification of the ends of DNA to enable attachment of the ends to a surface such as an electrode [26], attachment of the ends of DNA to a micro bead and subsequent optical or magnetic trapping of the bead [27], attachment of the DNA to a hydrophobic surface driven by hydrophobic-hydrophobic interactions [28], or attachment of the DNA to a positively charged surface driven by electro-static interactions [29]. Stretching is performed by a force exerted by either one of the sources: laser, magnet, entropy, fluid flow, and electric field. The length of the elongated strand depends on the force exerted on the DNA molecule. In this section, fluorescent and non-

fluorescent techniques of single-molecule analysis are presented and their applications to DNA mapping and protein interaction studies are discussed. Methods utilizing laser and magnetic field detect biomolecules though a force feedback mechanism and are classified as non-fluorescent techniques. DNA molecules manipulated by electric field, fluid flow and entropic force are detected using fluorescent microscopy.

1.2.1. Non-Fluorescent Based Single-Molecule DNA Analysis

In optical tweezers method, the micro-beads attached to the ends of DNA molecules by chemical modification are trapped in a laser light. A laser beam is focused through a high numerical aperture microscope objective, creating forces on the bead in all directions. Two types of force, gradient and scattering forces, are produced since the laser light can be both transmitted and reflected from the bead. The forces balance when the bead is centered at the point of maximum light intensity, and when the bead drifts from this position, the resulting unbalanced force pushes the bead back into the center of focus of the beam, trapping the bead at the focal point of the laser. One end of the DNA molecule is fixed to the substrate and the beaded end is pulled by the laser [30]. The DNA strand unravels as the bead moves away from the surface. Force exerted on the stretched DNA molecule by protein interactions causes the bead to shift from its trapped position. Protein interactions are quantified by converting the shift to an equivalent force, typically in the order of fN to pN. Optical tweezers are primarily used to quantify forces driving DNA-protein interactions [31]. The experiments are performed in flow cells and do not rely on fluorescent detection but on forces detected by the trapping laser. Only one DNA molecule can be immobilized and stretched during the experiment, as the laser is capable of trapping only one bead.

Magnetic tweezers operate similarly to optical tweezers, the difference being the trapping force is derived from magnets [32]. Typically one end of the DNA molecule is attached to substrate and the other end is attached to a magnetic bead. The bead is trapped in an electromagnetic gradient generated by the magnets. Experiments are performed on open substrates and do not rely on fluorescent detection but on forces detected by the magnetic trap. Magnetic tweezers manipulate only one DNA molecule during an experiment and are primarily used for DNA-protein interaction studies [33].

1.2.2. Fluorescent Based Single-Molecule DNA Analysis

In fluorescent based single-molecule analysis, imaging is performed after immobilization and stretching of DNA molecules. The immobilization and stretching is typically performed either on open substrates or in sealed channels. One of the fluorescent based techniques uses ac field applied across microfabricated electrodes to immobilize and stretch DNA molecules [34]. Spatially varying ac field lead to molecular movement induced by polarization, which is known as dielectrophoresis (DEP). In order to overcome the random thermal forces experienced by the DNA in solution, the electric field required for stretching is typically very high ~10^6 V/m. This force can be generated using microfabricated electrodes, since gaps between electrodes can be made small. Often in such experiments, one end of the DNA molecule is first immobilized on one electrode, followed by stretching the other end using an ac field [34]. The DNA molecules are attached to the electrodes either by using an electrochemical process or thiol labeling at the ends of the DNA molecules [35]. This method is capable of analyzing multiple DNA molecules in a single experiment and has been used in studies of protein motion along the DNA strands [5]. However, the number of DNA molecules immobilized

is not sufficient to perform DNA mapping. The current ac field techniques suffer from inefficient immobilization of DNA molecules to the electrodes, which results in either DNA immobilization at random locations on electrodes [34] or very few DNA immobilized on electrodes [35]. In some cases immobilization is performed after chemical modifications to DNA molecules and electrode surface [36].

DNA molecules can also be stretched using force generated from either fluid flow or air-fluid meniscus. Typically, in fluid flow based stretching techniques DNA molecules are immobilized either on a hydrophobic surface or on a positively charged surface. DNA combing method uses the hydrophobic nature of DNA to interact with a hydrophobic surface to obtain immobilization [37]. The combing method is carried out in three steps. In the first step the DNA is mixed in a buffer solution at pH of 5-7, below the physiological pH of 8.0 in order to slightly denature DNA causing the exposure of hydrophobic bases to the solvent. In the second step a hydrophobic substrate is dipped into the DNA-containing solution and as the last step the substrate is slowly pulled out of the solution, leaving highly aligned DNA molecules firmly attached to the substrate. The stretching and anchoring of the DNA is believed to come about in the following way. First, a free end of the DNA sticks to the hydrophobic substrate, presumably due to its affinity to the exposed hydrophobic bases at the end of the DNA; then the DNA molecule is stretched out by the force exerted on the rest of the DNA by the receding meniscus; and finally the other end also sticks to the substrate as it dries.

DNA combing generates hundreds of immobilized and stretched DNA molecules on an open substrate. The force exerted on the DNA by the receding water meniscus is strong enough to “overstretch” the dsDNA by as much as 60% beyond the length of its

native double helix structure. Overstretching is not desirable as it hinders the interactions of DNA strands with proteins and fluorescent labels. This method is primarily used in DNA mapping of sequences between 7 to 150 kbp using sequence specific fluorescent labels [38]. Smaller sequences cannot be detected since the force exerted on the DNA molecule is large enough to denature smaller fluorescent labels. Mapping is performed by first immobilizing the DNA molecules followed by denaturing the double strand resulting in two single strands. The single strands are hybridized with the fluorescent labels at specific sequences and their positions are scanned using a fluorescent microscope. The method requires extensive processing steps and is incapable of detecting small sequences. It nevertheless demonstrates the power of single-molecule DNA mapping as it avoides the costly and time consuming step of enzymatic synthesis of bases, which is an integral step in the PCR technique.

Positive charge surfaces have also been used to immobilize DNA molecules. An aminopropyltriethoxy silane (APTES) treated glass surface results in a monolayer of positively charged $-NH_2$ on the surface. The negatively charged DNA molecules are attached to the APTES coated surface [39] followed by stretching the DNA strand using fluid flow. Hundreds of immobilized and stretched DNA molecules are generated on the glass surface. High resolution DNA mapping of 6 bp sequences has been demonstrated using this method. DNA-protein interactions cannot be performed as the entire DNA strand is fixed to the substrate leaving little room for protein motion [24]. A second drawback is that the coating of APTES is non-uniform over a large surface area, resulting in non-uniform DNA immobilization [40]. The silane coated glass surface is sensitive to dust particles and must be preserved in an ethanol solution when not in use [40].

Entropy based force is also used to perform DNA stretching. For example, 50 kb DNA molecules unravel to over half the contour length in channels of widths <100 nm have been demonstrated. The walls of the nanochannels constrain the DNA molecules, forcing them to remain stretched [41]. This phenomenon is referred to as entropy. The length of the DNA molecules increases with decrease in cross-section of the nanochannels. DNA mapping has been demonstrated in nanochannels. DNA molecules are continuously driven into the nanochannels using electric field. Sufficient numbers of DNA molecules are analyzed to obtain a statistical distribution of sequences along the DNA strand. Nanofluidic systems have also been used to study DNA-protein interactions [42]. The locations of protein binding along the DNA strands are detected in nanochannels.

While the entropic method of stretching DNA molecules overcomes the drawbacks of surface interactions and overstretching, current nanofluidic systems have limitations when used for performing DNA mapping and DNA-protein interaction studies. The number of DNA molecules driven into the nanochannels by electric field is limited, resulting in low throughput of DNA analysis. The DNA molecules are often broken when forced into the channels. Current nanofluidic systems lack control over the placement of DNA molecules in the channels. Hence, protein interaction studies at specific sequences on the DNA strand cannot be performed.

1.3. DNA Analysis in Integrated Fluidic Systems

DNA molecules are analyzed at single-molecule level with and without fluorescence detection. In non-fluorescent based techniques, one DNA molecule is stretched during an experiment and all biomolecules are detected using a force feedback

mechanism. These techniques have provided a wealth of information on forces driving DNA-protein interactions. However, they are not applicable to DNA mapping and DNA-protein interaction studies such as protein translocation along the DNA strand, which can be detected only using fluorescence. On the other hand, fluorescent based techniques such as DNA combing suffer from over stretching. The method is incapable of high-resolution DNA mapping and DNA-protein interaction studies. While current nanofluidic systems prevent overstretching of DNA molecules, they require electric field to drive DNA molecules into the channels, which limits the throughput and causes breakage of DNA molecules. In addition, the position of DNA molecules cannot be controlled in nanochannels.

In this work, we focused on fluorescence based single-molecule DNA analysis in micro- and nano-fluidic systems. Our efforts are geared towards developing integrated fluidic systems that would allow single-molecule DNA analysis to be performed in micro- and nano-channels for DNA mapping and DNA-protein interaction studies at specific location on the DNA strands. Integrated fluidic systems are fabricated where electrodes are integrated with micro- and nano-channels. We have developed methods that allow fluid flow and electric field in the channels to control DNA immobilization and motion. These methods help overcome the limitations of existing techniques such as low throughput DNA mapping and uncontrolled positioning of DNA molecules in channels.

1.3.1. DNA Immobilization in Microchannels for High Throughput Analysis

We have developed a DNA immobilization technique in microchannels called protein assisted DNA immobilization (PADI) that allows high throughput single-

molecule analysis to be performed in microfluidic systems [43]. Applying microfluidic flow to perform DNA stretching offers several advantages. First, overstretching is avoided in microchannels by using shear flow to stretch DNA molecules. It has been shown that shear flow does not stretch DNA molecules beyond the full DNA length [44]. Second, a capillary flow is used to introduce DNA molecules in the microchannel, which results in immobilization of hundreds of stretched DNA molecules within minutes. The throughput is higher compared to nanofluidic systems where DNA molecules are driven into the channels using an electric field. The immobilization process in the PADI technique uses DNA-interacting proteins that bind to the DNA molecules and immobilize on the hydrophobic surface of the microchannels. Since no surface treatment is required, this technique produces repeatable and uniform DNA immobilization. The PADI technique can also be used to perform fluorescent-based DNA-protein interaction experiments, since the degree of immobilization of the DNA strand to the surface can be controlled by varying the concentration of DNA-interacting proteins.

1.3.2. Electric Field Controlled DNA Motion and Immobilization in Integrated Fluidic System

In all the existing single-molecule techniques, proteins randomly diffuse in solution and interact with DNA molecules. To date, control over the location of protein interactions with the DNA molecules has not been possible due to the lack of a technology capable of precise placement of stretched DNA molecules in channels. The electric field method is a promising tool to control the placement of stretched DNA molecules since the DNA molecules are negatively charged, and they can be polarized by an electric field.

Current electric field based techniques lack control over the placement of stretched DNA molecules and only a few DNA molecules are immobilized on the electrodes. On the other hand, large numbers of DNA molecules are immobilized on the electrodes present on an open substrate by extensive chemical modifications to DNA molecules and electrode surface. The chemical modifications to the electrodes require heating cycles upto 100 °C [36]. At this temperature, fluidic systems made of polymer tend to flow and possibly causing damage to the systems. Hence performing DNA immobilization by chemical modification of electrodes integrated with channels in fluidic systems made of typical polymer is not practical.

We have developed an integrated fluidic system in which electrodes are integrated with Si micro- and nano-channels [45]. The system is fabricated by bonding the electrodes on a glass substrate to channels in Si using PMMA as an adhesive layer. PMMA bonding does not clog small channels during the bonding process. The PMMA bond strength is sufficient to withstand the capillary pressure in the nanochannels. These features enabled us to integrate electrodes in nanochannels while maintaining the integrity of the channels. The fluidic system has good wetting property, enabling the pumping of fluid into the channels by the capillary action. This obviates the need for high-pressure syringe pump or electric field to force the fluid and suspended particles into micro- and nano-channels.

Using an appropriate electrode design and fluid with the desired pH, large numbers of DNA molecules are immobilized at specific location on the electrodes. The DNA molecules are immobilized without any chemical modification either to the ends of

DNA or the surface of the electrodes. This feature enabled us to immobilize DNA molecules on electrodes integrated with sealed micro- and nano-channels.

We have also developed an approach to control the motion and position of DNA molecules using an ac voltage in integrated channels [46]. The two most common forces to move particles in channels are electro-osmosis and pressure gradient. Electro-osmosis typically requires large dc voltage across a channel to generate a fluid flow that moves the particles in the channel [47]. In pressure driven flow, the pressure required to generate flow increases as channel dimensions reduce [48]. Using asymmetrical electrodes in microfluidic channels, ac electro-osmotic fluid pumping has been demonstrated where fluid flow along the channels is generated by the electric field [49]. A drawback of having fluid flow along the channels is that the resistance to flow increases in smaller channels. In this thesis, we have demonstrated ac field induced motion of DNA molecules in micro- and nano-channels. The motion is caused by the interactions of electric field with the particles and not due to field induced fluid flow along the channels. Compared to particles moved by fluid flow in the channels induced by applied pressure or voltage, moving only the particles and not the fluid makes it easier to move particles in channels with smaller dimensions and to precisely position DNA molecules in the channels. The velocity of the particles is controlled by the magnitude of the voltage. The position of the DNA molecules in nanochannels is precisely controlled by using a dual electrode pair system. The two electrode pairs enable the direction of the particles in the channels to be controlled and allow the particles to be transported to a specific location in the channels.

The content and structure of the rest of this dissertation are described as follows. In chapter 2, the fabrication of the integrated fluidic system for single-molecule DNA analysis will be described. The wetting property and sealing of the fluidic system are characterized. In chapter 3, DNA immobilization method in microchannels using DNA-interacting proteins will be presented. Results of DNA mapping and DNA-protein interactions in microchannels will also be discussed. In chapter 4, electric field is used to immobilize and stretch DNA molecules at specific location in the fluidic system. The position of DNA molecules in channels is controlled using an ac voltage. In chapter 5, the mechanisms related to ac voltage induced motion of DNA molecules and 20 nm polystyrene particles will be discussed. Through simulations and experimental results, it is shown that the motion of the particles is caused by the interactions of electric field with the particles. In chapter 6, the thesis is summarized and future plans to develop the next generation integrated fluidic system for DNA-protein interactions will be discussed.

CHAPTER 2
FABRICATION OF INTEGRATED FLUIDIC SYSTEMS FOR SINGLE MOLECULE DNA ANALYSIS

2.1. Introduction

DNA immobilization and stretching at specific locations in micro- and nano-channels will enable DNA-protein interaction studies that cannot be performed with existing methods. For example, DNA-protein interaction studies at specific sequences on a DNA strand can be performed by precise placement of stretched DNA molecules in nanochannels.

Current single-molecule techniques lack the capability of controlling the position of stretched DNA molecules in channels [50]. Electric field is a promising tool to control the spatial location of the DNA molecules. The DNA stretched length can also be controlled by varying the magnitude of voltage [45]. Due to the negative charge of DNA molecules, they are readily polarized by electric field and hence their positions and stretched lengths can be controlled using an appropriate electric field distribution in the channels.

Microfabricated electrodes integrated with micro- and nano-channels allow electric field to be applied in the channels. A number of fabrication techniques exist to integrate electrodes in microchannels, however, integrated nanochannels have not been demonstrated yet [51]. Current fabrication processes often require nanochannel sealing with a planar substrate [52], hence they cannot be applied to integrate structures such as

electrodes in the sealed nanochannels. 3-dimensional SU-8 (Microchem, MA) nanochannels have been demonstrated using reversal nanoimprint [53]. Existing integrated microfluidic systems are often fabricated from hydrophobic polymers [51]. Hydrophobic channels require cumbersome techniques such as electro-osmosis [51] and the application of pressure gradient [54] to generate fluid flow. A new fabrication technology is developed to realize integrated nanochannels with good wetting property.

We have developed a fabrication technology to integrate electrodes in sealed Si micro- and nano-channels. The Si channels are hydrophilic, enabling DNA molecules and their surrounding fluid to be introduced into the micro- and nano-channels by capillary action. Electrodes integrated with sealed micro- and nano-channels do not compromise the channel sealing. The sealed channels are capable of withstanding high capillary pressure up to ~3 MPa.

In this chapter the fabrication technology for the integrated fluidic system will be introduced in section 2.2. Fabrication of an integrated fluidic system that enables control of the motion of DNA molecules outside the electrodes is also presented in section 2.2. Characterization results of bond strength, sealing, and wetting of the fluidic system are presented in section 2.3.

2.2. Fabrication of Integrated Fluidic System

Fabrication of fluidic systems generally involves several processes such as lithography, thin film deposition, wafer bonding, and etching [55]. Lithography is performed to define micro- and nano-channels on the substrate followed by etching the channels into the substrate. Wafer bonding is performed to seal the micro- and nano-channels with a second substrate. In this section, we discuss wafer bonding applied to

sealing of the micro- and nano-channels followed by fabrication technology of our integrated fluidic system. Successful fabrication of integrated micro- and nano-fluidic systems is demonstrated.

2.2.1. Wafer Bonding

Several bonding techniques have been developed for fabrication of MEMS systems such as anodic bonding, polymer bonding, and eutectic bonding [56]. Anodic [57] and polymer bonding [58] are often used to seal fluidic channels. In anodic bonding, a pyrex glass wafer is bonded to Si channels by applying voltage and temperature. The voltage allows electrostatic attraction of Si and glass surfaces to maintain a good contact necessary for uniform bonding. Anodic bonding is very sensitive to surface non-uniformities, therefore it is not applicable to systems with structures such as electrodes deposited on either the Si or glass surface. On the other hand, polymer bonding is insensitive to surface non-uniformities, since the polymer flows during the bonding process, thereby planarizing the surface [58]. In addition, a thicker polymer layer can be spin coated on the structures present on the substrate, resulting in a planar polymer coating. This results in a homogenous contact of the polymer surface with a second substrate, enabling uniform bonding. Another advantage of polymer bonding is that it is compatible with materials having different linear expansion coefficient. However, using polymer as an intermediate layer for bonding results in a gap between the substrates and reduces the channel confinement. Moreover, sealing small channels using polymers is a challenging task since polymers tend to flow into the nanochannels, resulting in blockage during bonding.

Several polymers such as polymethylmethacrylate (PMMA) [51], polydimethylsiloxane (PDMS) [59], and SU-8 [60] are regularly used to seal microfluidic systems. However their application to seal nanochannels has to be carefully characterized to prevent blockage of the channels due to polymer flow. SU-8 sealing of nanochannels has been demonstrated using UV cross-linking to ensure the SU-8 does not block the channels [53]. Performing cross-linking and thermal bonding in the same step cannot be carried out in standard thermal bonders and requires specialized equipment such as a nanoimprinter.

PDMS is an elastomer, commonly used to duplicate channels from a mold. Following duplication, the PDMS channels are sealed with a glass substrate. Fabrication of PDMS microchannels is a simple technology that does not require clean room processing. However, PDMS cannot be used to seal channels <500 nm in width or depth since the PDMS tends to sag into small channels [59].

It has been demonstrated that PMMA is capable of sealing small channels [61]. Due to its high viscosity at low temperature, it does not clog the small channels during the bonding process [62]. We have used 950 K PMMA to seal micro- and nano-channels with integrated electrodes. These sealed channels have good wetting property with dimensions as small as 350 nm wide and 100 nm deep. Fluid filling by capillary action in the integrated channels is demonstrated and the channels have no leakage in the presence of electrodes.

2.2.2. Fabrication Technology of Integrated Fluidic System

Fig. 2.1 shows the fabrication technology of integrating electrodes with Si channels by bonding Si and glass substrates using PMMA as an adhesive layer [46]. The

100 μm thick glass is cleaned in a 1:1 H_2SO_4:H_2O_2 solution for 20 min, followed by dehydration bake at 200 °C for 1 h. 20/50 nm thick Cr/Au layer is deposited on glass and patterned using optical lithography and wet etching, as shown in Fig. 2.1(a). It is important to ensure that no photoresist residue is left on the glass since this will result in poor bonding. The glass is dehydrated again at 200 °C for 1 h. 6% 950K PMMA is spincoated on the glass with patterned electrodes to a thickness of 600 nm, as shown in Fig. 2.1(b). 10 nm thick Ti layer is evaporated on the PMMA to define areas over which the PMMA is etched, as shown in Fig. 2.1(c). The thin Ti layer prevents the solvents in the photoresist and the PMMA layers from interacting with each other. Following photoresist patterning, the Ti layer is etched in 20:1:1 H_2O:H_2O_2:HF solution. The exposed PMMA is then etched in an O_2 plasma with 100 W rf power, 250 mTorr, and 100 sccm of O_2 for 12 min as shown in Fig. 2.1(d). The photoresist and Ti layers are removed, leaving Cr/Au electrodes and patterned PMMA on glass as shown in Fig. 2.1(e).

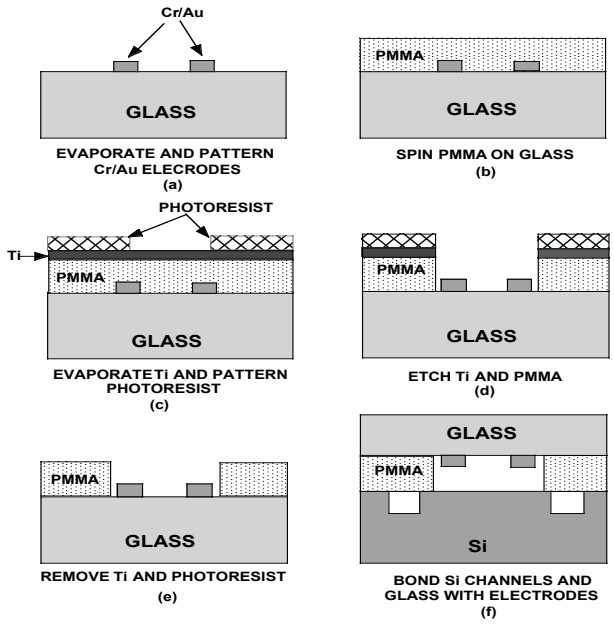

Fig. 2.1 Schematic of fabrication technology of integrated fluidic system by bonding Si and glass substrates using PMMA as adhesive layer.

The channels are etched in a Si substrate using plasma etching. Fluidic ports of 300 μm diameter to access the channels are defined by etching through the 550 μm thick Si substrate using similar etch conditions with total etch time of 3 h. The Si substrate with the etched channels and fluidic ports are cleaned in 1:1 H_2SO_4:H_2O_2 before bonding. The Si and glass substrates are first aligned and then transferred to the bonder for bonding. Bonding is carried out in vacuum at 75 Torr. This prevents the formation of air gaps and helps to improve the contact uniformity across the substrate. The bonding is performed above the glass transition temperature of PMMA (109 °C) for 15 min at a pressure of 0.4 MPa, resulting in electrodes integrated with fluidic channels as illustrated in Fig. 2.1(f).

2.2.2.1. Integrated Microfluidic System

Figure 2.2 is an optical micrograph of an integrated microfluidic system with two intersecting channels. The system consists of electrodes on a 100 μm thick glass aligned and bonded to a Si substrate containing channels perpendicular to each other. Channels are etched in Si using deep Si etching process consisting of alternate etch and passivation steps. The etch process is switched between the SF_6 etch step and the C_4F_8 passivation step to obtain fast Si etch rate and vertical etch profile. A source power of 75 W and a stage power of 12 W are used at 26 mTorr with 105 sccm SF_6 in the 14-s etch cycles. A 75 W source power is applied with no stage power at 16 mTorr and 40 sccm C_4F_8 in the 4-s passivation cycles. Conditions used for bonding the substrates are 110 °C and 0.4 MPa for 15 min at 75 Torr. The Cr/Au electrodes on the glass are 20/50 nm thick. The electrode pair consists of a sharp and a straight edge electrodes separated by 30 μm. The PMMA is patterned over the 30 μm gap to expose the electrodes to the Si microchannels.

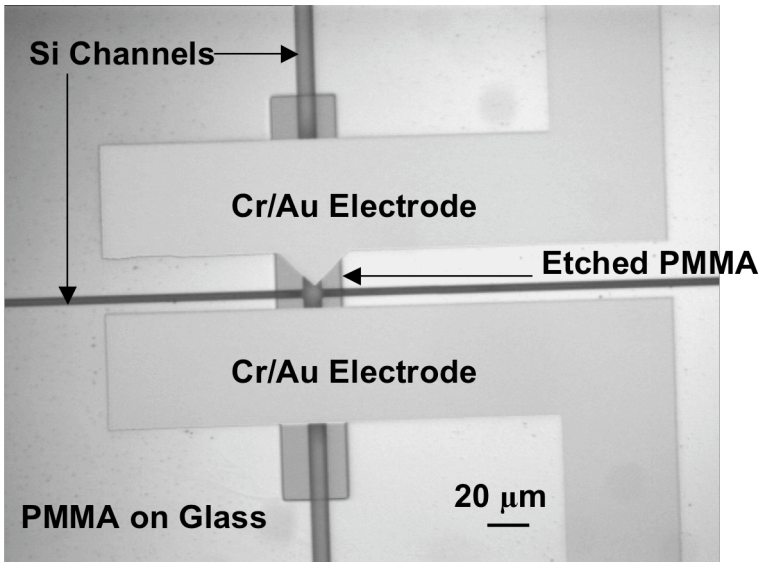

Fig. 2.2 20/50 nm thick Cr/Au electrodes on 100 μm thick glass bonded to 30 μm deep, 3 and 10 μm wide Si channels.

2.2.2.2. Integrated Nanofluidic System

PMMA bonding is used to seal nanochannels, thus giving us the capability to integrate electrodes in channels with smaller dimensions. We demonstrate fluidic systems where electrodes are integrated with 350 nm wide and 100 nm deep Si channels. 350 nm wide channels are fabricated in Si by first transferring the patterns from a Si mold to the Si substrate using nanoimprint followed by dry etching. Mold with nanochannels is imprinted on 400 nm thick PMMA spun on a Si substrate at 180 °C and 4 MPa for 15 min. The channels are transferred to the Si substrate with dry etching using Cl_2 with 600/100 W rf power and 5 mTorr for 45 s. Fluidic ports of 300 μm in diameter are etched through the entire Si substrate by dry etching in SF_6 and C_4F_8 for 3 h using alternating etch and passivation cycles. A source power of 100 W and a stage power of 40 W are used at 26 mTorr with 105 sccm SF_6 in the 14-s etch cycles. A 400 W source power is

applied with no stage power at 16 mTorr and 40 sccm C_4F_8 in the 7-s passivation cycles. The Si substrate with the etched channels and fluidic ports are cleaned in 1:1 H_2SO_4:H_2O_2 before bonding. The Si and glass substrates are aligned and bonded in vacuum at 75 Torr. Figure 2.3 shows an optical micrograph of Cr/Au electrodes integrated with 350 nm wide and 100 nm deep channels. PMMA bonding allows sealing of small channels without the polymer clogging the channels. The PMMA in the electrode gap is etched, which exposes the electrodes to the fluid and DNA molecules in the channels, thus enabling the electric field to influence and control the DNA molecules in channels.

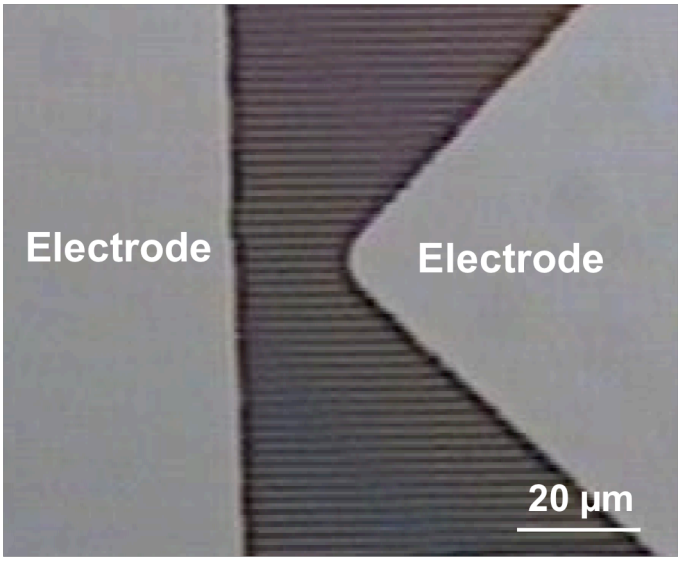

Fig. 2.3 20/50 nm thick Cr/Au electrodes on glass integrated with 350 nm wide, 100 nm deep Si nanochannels using PMMA bonding.

2.2.2.3. Wide Channel Interfaced to Narrow Channel Array

A fluidic system is fabricated to introduce DNA molecules in narrow channels and control the motion of molecules using integrated electrodes. In order to introduce DNA molecules in 1 µm wide and 400 nm deep channel array, it is interfaced to a 150 µm wide and 1 µm deep channel as shown in Fig 2.4. The DNA molecules are partially stretched by the flow in the wider channel before arriving at the interface and this allows

greater number of DNA molecules to enter the narrow channels compared to if the DNA molecules were in the coiled state. The PMMA is etched over the electrodes, allowing electric field to control the velocity of DNA molecules in the 1 μm wide channel array. However, the PMMA is not etched over the channel array to maintain confinement of the DNA molecules in the channels.

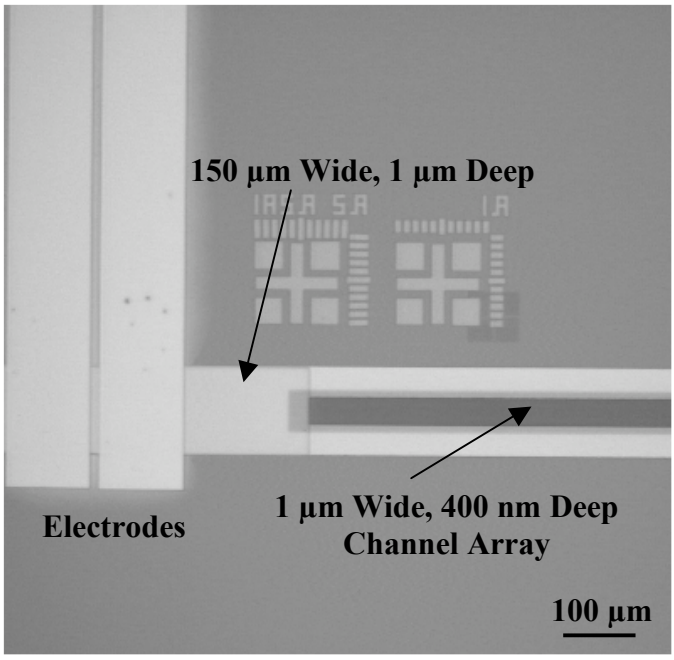

Fig. 2.4 Fluidic system with 150 μm wide channel connected to 1 μm wide channel array. Integrated electrodes in 150 μm wide channel control motion of DNA molecules in 1 μm wide channel array.

2.2.2.4. External Connections to Fluidic System

DNA and protein molecules are introduced into the channels at controlled flow rate using a syringe pump. The pump is connected to the fluidic ports in the Si substrate through a PDMS interface. The PDMS interface is prepared by mixing the PDMS silicone elastomer base with a cross-linking agent, followed by heating the mixture at 50 °C for 4 h. The heating cross-links the PDMS mixture and it is solidified. This hardened PDMS mixture is cut to a size of 2 × 2 mm^2 and 500 μm diameter holes are

punched through the PDMS. The PDMS pieces are glued to the Si substrate using an UV curable adhesive. A fluidic connector from the syringe pump is fixed to the fluidic ports in the Si substrate through the PDMS interface. The flow rate in the system is controlled by varying the values in the syringe pump.

Fluorescent labeled particles and biomolecules in the channels are imaged using a Nikon TE2000 inverted fluorescence microscope and a front-illuminated charge-coupled device camera with a minimum integration time of 100 ms for each frame. The illumination is performed through an objective piece located at the base of the microscope. The fluidic system with the glass substrate facing the microscope base is placed on the objective piece and focused manually towards the channels. The Si substrate faces upwards, thereby the fluidic ports in Si are accessible for fluid injection from the top. Following DNA/protein injection into the channels, images of the molecules in the channels are captured by the camera typically with an integration time of 100 ms. The captured image is then displayed using a software provided by the microscope supplier.

2.3. Characterization of Fluidic System

The bond strength, channel wetting and sealing of the fluidic system are characterized. The bond strength should be high enough to withstand capillary pressure during operation. A pressure gradient across the air-fluid meniscus exists during the capillary filling of the channels. The pressure increases with reducing channel dimensions. The relationship between capillary pressure Δp and the channel dimensions is given by the Young's equation [63]:

$$\Delta p = \frac{2\gamma\cos\theta}{r} \tag{2.1}$$

where γ is surface tension of fluid in air, θ is contact angle of fluid with channel surface, and r is given by:

$$r = \frac{wd}{w + d} \tag{2.2}$$

where w is channel width and d is channel depth. For example, with DI water in 100 nm deep channels, the capillary pressure can reach upto 1 MPa. The bond strength should be greater than the capillary pressure to avoid fluid leakage. When the channels are properly sealed in the fluidic system both the fluid and the suspended particles are well confined in the channels during the operation. With the developed bonding technology, we have demonstrated the sealing of nanochannels with integrated electrodes.

Another important feature of fluidic system is the wetting property of the channels. In hydrophobic fluidic systems, fluid is pumped into the channels either by pressure gradient or electro-osmosis. As the channel dimensions are reduced, higher pressure is required to pump fluid through the channels since the fluid resistance increases with decreasing channel dimensions. Electro-osmosis requires large dc voltage to generate fluid flow in channels, which often results in bubble formation. On the other hand in hydrophilic channels, capillary force can be used to fill the channels and generate continuous fluid flow. This obviates the need for high pressure gradient and large dc voltage to drive fluid in the channels. We measured the wetting property of the fluidic system by monitoring the velocity of the capillary meniscus during filling of 50 and 100 nm deep channels.

2.3.1. Bond Strength Measurements

Bond strength is measured to optimize the bonding conditions using PMMA as an adhesive layer. Figure 2.5 shows the variation of the bond strength with temperature. The Si and glass substrates are bonded with 600 nm thick PMMA at different temperatures for 15 min, applying 0.4 MPa pressure at 75 Torr vacuum. The bonded substrates are diced into 3.75 × 2.5 cm^2 chips, and are glued in between two metal fixtures. The size of the metal fixtures is slightly less than the bonded chips to ensure that the glue from the fixtures would not glue the fixtures together. By using a pull tester, the bonded chips are separated and the force required to separate them is measured. The bond strength measurements typically show an error bar within 2% due to sample and run-to-run variations.

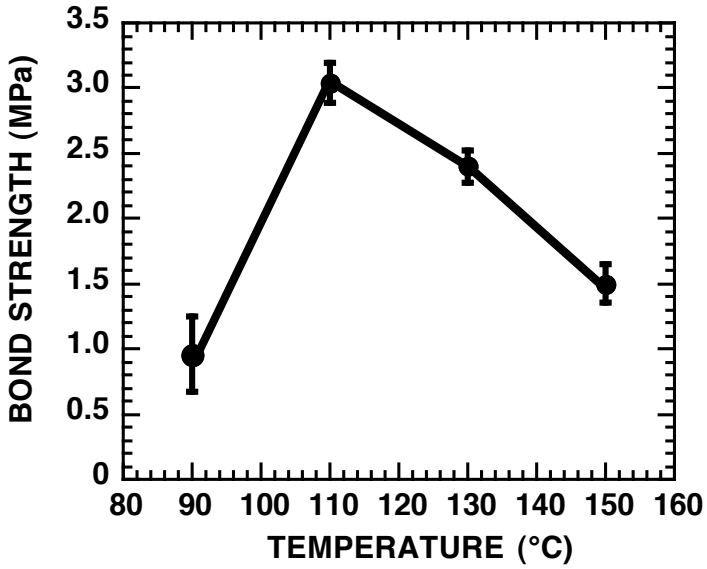

Fig. 2.5 Bond strengths at different temperatures for Si and glass substrates bonded using PMMA as adhesive layer.

The maximum bond strength of 3 MPa is obtained by bonding at 110 °C. The initial increase of bond strength with temperature is due to the added mobility of the polymer chains leading to increase in interactions between the PMMA chains and the Si surface. At higher temperature, the bond strength begins to decrease, probably due to the mismatch of the linear expansion coefficients between the glass and Si, which results in stress being produced during bonding. After the Si and glass substrates are separated by the pull test, it is observed more than 80% of the Si surface is covered with PMMA. This indicates that the PMMA-to-Si bonding is stronger than the PMMA-to-glass bonding.

The dependence of bond strength between Si and glass on PMMA thickness is also investigated. The PMMA thickness is varied from of 100 nm to 1.5 μm. The bonding is carried out at 110 °C and 0.4 MPa pressure for 15 min at 75 Torr vacuum. Figure 2.6 shows the variation of bond strength for different PMMA thicknesses. For a 100 nm thick PMMA the bond strength is lower compared to thicker layers of PMMA.

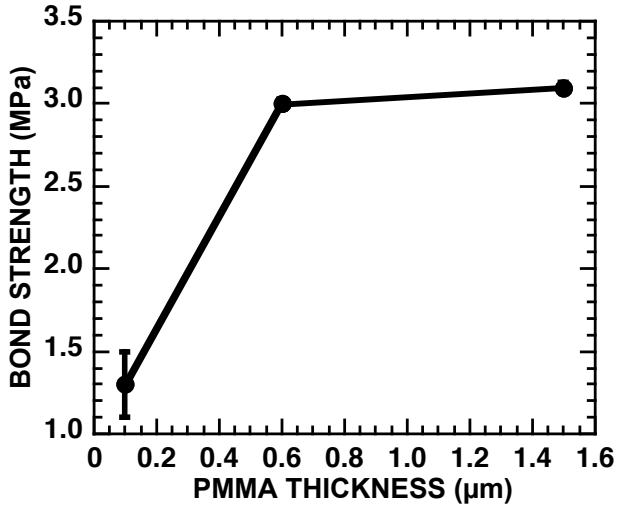

Fig. 2.6 Dependence of bond strength on PMMA thickness. Bonding is carried out at 110 °C, 0.4 MPa pressure and 75 Torr pressure for 15 min.

This may be explained due to the fact that thicker layer of PMMA better planarises the glass surface and provides better contact with the Si surface. The 100 μm thick glass being so thin is easily deformed during processing. The bond strength is higher for thicker PMMA layer since it can provide some compensation to the glass deformation. With 600 nm thick PMMA, the bond strength is 3.0 MPa compared to the lower bond strength of 1.3 MPa with 100 nm thick PMMA.

2.3.2. Sealing of Integrated Channels

The sealing of 350 nm wide, 100 nm deep Si channels with electrodes is demonstrated in Fig. 2.7.

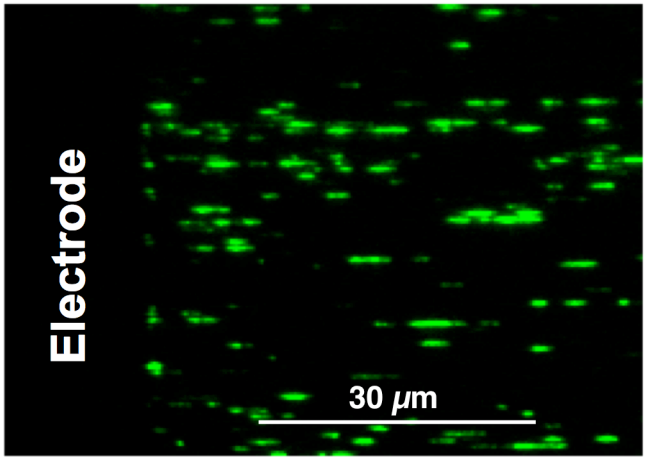

Fig. 2.7 λ-DNA molecules at 5 pM concentration in TRIS-EDTA buffer (pH=8.0, σ=150 μS/cm) at equilibrium in 350 nm wide, 100 nm deep horizontal channels integrated with vertical Cr/Au electrodes.

5 pM λ-DNA molecules in tris-ethylenediamine tetraacetic acid (TRIS-EDTA) buffer (1 mM, pH=8.0, σ=150 μS/cm) are introduced into the channels at the inlet fluidic port, where they are subsequently pumped through the channels due to evaporation from the outlet end. After a number of DNA pass through the channels, the pumping is stopped by hydrating the outlet end with the same buffer. Figure 2.7 shows λ-DNA molecules

partially stretched at equilibrium in channels next to an integrated electrode. The DNA molecules are in straight lines and they are well confined in the channels. Thus we have demonstrated a fluidic system where nanochannels are integrated with electrodes and in subsequent sections we will demonstrate control over the position and motion of DNA molecules in similar channels.

2.3.3. Wetting of Channels

To observe the fluid flow in the channels, the meniscus in motion is recorded. Spontaneous filling of the channels by DI water due to capillarity induced pressure is observed. Capillary pressure depends on the surface properties of the channel sidewalls and the dimensions of the channels. In our sealed fluidic system, 3 channel walls are compromised of –OH terminated Si surface that are hydrophilic, and one sidewall is PMMA which is hydrophobic. The PMMA-to-Si bonding provides a tight seal without any fluid leakage.

100 nm deep Si channels with widths ranging from 3 to 100 μm are filled with DI water through the fluidic ports at the ends of the channel. The fluid is instantly sucked into the channels by the capillary force, indicating that the PMMA does not flow into the channels during the bonding process and there is no problem of PMMA clogging even for small channels of 100 nm deep. The position of the capillary meniscus inside the channels is recorded as a function of time as shown in the Fig. 2.8. The flow velocity decreases with time. It is 0.65 mm/s initially for the 50 μm wide channels, and it decreases to 0.29 mm/s after 3 s. This is due to the fact that while the capillary force driving the flow remains constant, the amount of fluid being pulled along which dissipates energy through viscous shearing increases with time. The flow velocity also

increases with channel width since the resistance to the fluid is less for wider channels. The 100 μm wide channel has a flow velocity of 0.36 mm/s after 3 s, while the 50 μm wide channel shows a lower flow velocity of 0.29 mm/s.

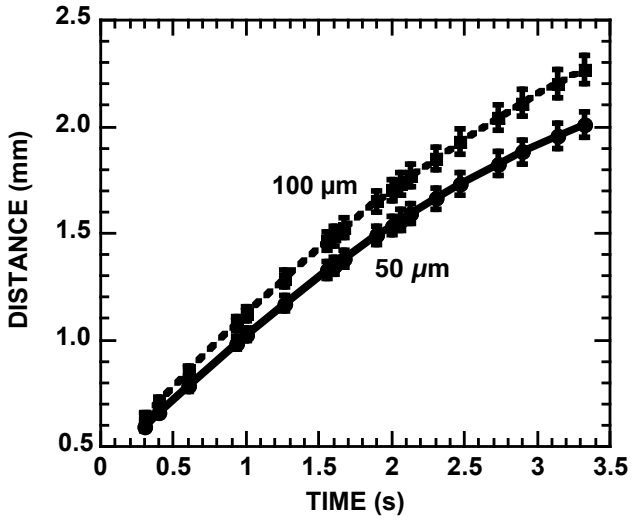

Fig. 2.8 DI water flow as a function of time in 50 and 100 μm wide, 100 nm deep Si channels.

The capillary force F_c driving the fluid in a sealed channel is expressed as [64]:

$$F_c = 2(d + w)(\gamma_{sa} - \gamma_{sl}) \tag{2.3}$$

where d is channel depth, w is channel width, γ_{sa} is surface tension between channel surface and air, and γ_{sl} is surface tension between channel surface and fluid. For given fluid and channels, the capillary force is directly proportional to the channel dimensions. Hence, the capillary filling velocity is higher in wider channel as seen in Fig. 2.8. The velocity does not scale proportionally with the channel width in spite of increase in capillary force with width. The reason is due to increase in volume of fluid in the channel, which results in the capillary force pulling higher volume of fluid through the channel.

DNA molecules are introduced into the fluidic system by capillary action of hydrophilic Si channels. Figure 2.9 shows T2-DNA molecules driven into the channels by the capillary action. 5 pM T2-DNA molecules in TRIS-EDTA buffer (1 mM, pH=8.0, σ=150 μS/cm) are introduced at the inlet of the channels, while the outlet is open to air. The DNA molecules immediately enter the channels due to the capillary action and they are subsequently pumped through the channels due to evaporation from the outlet port. The DNA molecule is partially stretched near the entrance of the channel array. Once inside the channel, it is in a stretched state due to the entropic force present in the channel and the hydrodynamic flow of the fluid. Although this method does not offer control over the velocity of DNA molecules, it enables the molecules to be introduced into the channels without the need for electrophoresis or pressure driven flow.

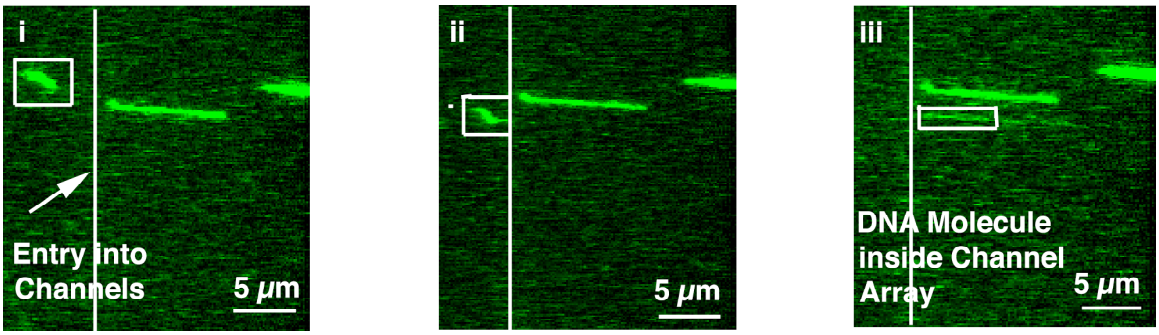

Fig. 2.9 T2-DNA molecules at 5 pM concentration in TRIS-EDTA buffer (1 mM, pH=8.0, σ=150 μS/cm) are pumped into 500 nm wide, 100 nm deep channels by capillary force. DNA molecules are introduced at inlet port and outlet port is open to air.

2.4. Conclusion

In this chapter, the fabrication technology of a fluidic system has been developed to integrate electrodes in sealed Si micro- and nano-channels. Electrodes on glass are integrated with Si channels by bonding Si to glass using PMMA as an adhesive layer. The fabrication technology has been used to realize an integrated fluidic system that

enables the control of the motion of DNA molecules in multiple channels using an ac electric field. Channels sealed with PMMA can withstand capillary pressure above 3 MPa. Electrodes are integrated with nanochannels without fluid leakage. The Si micro- and nano-channels exhibit good wetting property and DNA molecules are introduced in 350 nm wide channels using capillary flow. The fabrication technology has been used to realize an integrated fluidic system that enables the control of the DNA motion in multiple channels using an ac electric field.

CHAPTER 3
IMMOBILIZATION OF DNA MOLECULES IN MICROCHANNELS FOR HIGH THROUGHPUT SINGLE-MOLECULE ANALYSIS

3.1. Introduction

DNA mapping has been used to discover genetic biomarkers for early disease and cancer detection [65]. Different technologies are used for DNA mapping and they vary by their throughput, cost, and complexity [20]. In bulk technology, DNA mapping by sequence detection using PCR amplification offers high throughput [66]. However, due to the multiple steps involved in performing PCR, they are costly and complex. On the other hand, in single-molecule technologies, the DNA sequences are detected directly, without amplification, on individual molecules using fluorescence. Since PCR is not performed, single-molecule analysis lowers the cost and complexity compared to bulk techniques [67].

Single-molecule DNA mapping involves analysis of hundreds of immobilized and stretched DNA molecules to collect multiple data points on the locations of specific sequences along the stretched DNA strands [40]. Statistical analysis on the data is performed to eliminate false positives that might occur when sequences are detected at incorrect locations on a few of the strands. Current fluid flow based techniques are capable of immobilization and stretching of large numbers of DNA molecules [38]. However, the DNA molecules are overstretched, which is undesirable since it hinders interactions of the DNA molecules with fluorescent labels and proteins that are essential to performing mapping [24].

We present a DNA immobilization technique called protein assisted DNA immobilization (PADI) to immobilize and stretch but not overstretch hundreds of DNA molecules in microchannels. Performing DNA stretching in microfluidic systems offers several advantages. First, overstretching of the DNA molecules is avoided by using shear flow of the microchannels to stretch DNA molecules [44]. Second, low concentration of DNA molecules is required for analysis [68]. Third, the DNA molecules are confined within the channel, enabling easier detection and automated analysis of the DNA molecules.

The PADI technique is capable of high throughput analysis as hundreds of DNA molecules are immobilized and stretched rapidly in minutes. Control over the number of immobilization points of the strand to the microchannel surface is demonstrated. This feature allows optical mapping and DNA-protein interaction studies to be performed in the microchannels. Capability for DNA mapping is demonstrated by detecting specific sequences along the DNA strand using restriction enzymes. Single-molecule transcription is performed on the stretched DNA molecules in the microchannels.

In this chapter, DNA immobilization using the PADI technique is shown in section 3.2, along with the discussions of DNA stretching in fluid flow and protein adsorption to surfaces. The number of DNA immobilized in microchannels and the DNA stretch length are presented in section 3.3. The ability to perform DNA mapping and transcription in microchannels are presented in section 3.4.

3.2. DNA Immobilization and Stretching

The forces generated in a fluid flow are able to stretch DNA molecules. The DNA stretching dynamics in a fluid flow are analyzed by considering flow as having two

components, shear and extensional [44]. The stretched length depends on the component influencing the DNA molecules. DNA molecules can be immobilized on surfaces either by hydrophobic-hydrophobic or electrostatic interactions. The PADI technique uses hydrophobic interactions between DNA-interacting proteins and hydrophobic surface to achieve DNA immobilization [43]. There are several methods to generate hydrophobic surfaces and one of them is the use of polymers. Proteins have several hydrophobic molecules incorporated in them, hence they can adsorb on hydrophobic surfaces by hydrophobic-hydrophobic interactions. In this section the mechanism of the PADI technique will be described along with DNA stretching dynamics in fluid flow and protein adsorption to surfaces.

3.2.1. Immobilization and Stretching by PADI Technique

Immobilization of DNA molecules is performed as follows. DNA binding proteins such as restriction enzymes or RNA polymerases (RNAP) are allowed to bind to the DNA molecules in bulk solution at non-specific segments whereupon they diffuse along the DNA in search of target sequences at a rate faster than in a three dimensional diffusion-limited search. Whether or not the protein finds a specific binding site on the particular DNA strand used, the result is a DNA-protein complex with multiple proteins of ~5 nm in size wrapped around each DNA molecule. When this DNA-protein complex is subjected to a hydrodynamic flow inside a channel, it stretches out as depicted in the Fig. 3.1 .

When the DNA-protein complex reaches the channel surface, the proteins on the DNA adsorb to the surface, resulting in immobilization of the stretched DNA molecule inside the channel. Several steps are involved in the PADI technique including

fabrication of a microfluidic system to generate fluid flow, stretching of DNA-protein complex in fluid flow, and protein adsorption to microchannel surface. In each of these steps, a number of factors influence DNA immobilization and stretching and they will be explained below.

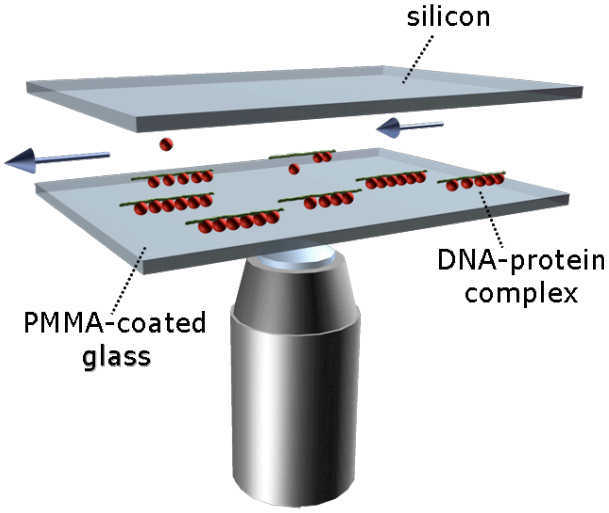

Fig. 3.1 DNA-interacting proteins (circles) bound to stretched DNA molecules (straight lines) adsorb to PMMA coated glass.

3.2.2. DNA Stretching by Fluid Flow

DNA molecules experience shear and elongational forces in fluid flow [44]. Fluid flow between two parallel stationary plates is an example of pure shear flow. Pure shear flow has a velocity gradient perpendicular to the flow direction, since the fluid velocity is zero at the plate boundary and maximum at the center of the gap between the two plates. A coiled DNA molecule in shear flow is stretched due to the velocity gradient that exerts a drag force on the coil. As the strand starts to unravel into a stretched state, the drag force on the stretched strand reduces compared to the coiled state, since the surface area of the coil is greater than that of a stretched strand. The decrease in force causes the strand to recoil. In coiled state, the drag force on the molecule increases again, causing the DNA molecule to unravel and the cycle continues between the stretched and the

coiled states. Hence the length of the DNA molecule fluctuates when stretched in shear flow. It is shown that the maximum average length of the DNA molecule does not exceed 0.4 times the contour length in shear flow [44].

DNA molecules experience elongational force in a channel whose fluid flow velocity varies along the length of the channel. The fluid flow velocity gradient exerts an elongational force on the DNA molecules. For example, when DNA molecules are flown into a channel from an inlet port whose cross-sectional area is typically larger than that of the channel, the DNA molecules experience elongational force at the boundary of the inlet port and the channel [69]. Coiled DNA molecules under the influence of the elongational force are stretched by the presence of two gradients. First is the velocity gradient perpendicular to fluid flow, as in shear flow. Second is the velocity gradient in the direction of fluid flow, as in the case of a channel with varying cross-sectional area. Dynamics of DNA stretching by elongational flow is different from shear flow. Unlike in shear flow, DNA molecules do not recoil following in the presence of elongational flow. Therefore, DNA molecules are stretched to longer length in elongational flow compared to shear flow.

3.2.3. Protein Adsorption in Channels

Protein adsorption to surfaces is a complex phenomenon involving a number of factors that include hydrophobic interaction, electrostatic force, hydrogen bonding, and van der waals force between the surface and the protein [70]. Proteins have a complex three-dimensional structure and composed of molecules with different properties. A typical protein surface is constituted of hydrophobic, hydrophilic, and ionic molecules. Hence protein adsorption to surfaces cannot be explained by a single factor but by a

combination of forces and interactions. Proteins adsorb on all types of surfaces: metals, hydrophobic, hydrophilic, and charged. Adsorption efficiency depends on both the properties of the protein and of the surface [71]. A common trend found in most proteins is that they adsorb most efficiently on hydrophobic surfaces [72]. Hence hydrophobic polymers such as PMMA often adsorb a larger number of proteins compared to hydrophilic surfaces such as glass.

For efficient DNA immobilization using the PADI technique, microfluidic systems should have good wetting property to generate high flow rate and the microchannels should have hydrophobic surfaces for protein adsorption. The structure and materials of the microfluidic system are shown in Fig. 3.2. The system consists of microchannels etched in Si and bonded to glass using PMMA as an adhesive layer. The glass enables high resolution imaging of DNA and protein molecules immobilized in the sealed channel. PMMA serves the dual role of bonding layer and hydrophobic surface onto which the DNA-interacting proteins are adsorbed, leading to DNA immobilization. Prior to PMMA bonding, the Si channels are cleaned in a 1:1 H_2SO_4:H_2O_2 solution, which creates a hydrophilic surface. A hydrophilic Si channel surface is important for three reasons. First the hydrophilicity of the Si surface prevents immobilization of DNA molecules, which reduces background fluorescence thus enabling single-molecule imaging of DNA molecules immobilized on the PMMA. Second the hydrophilicity draws the buffer solution into the microchannel at high flow rate by capillarity, hence a drop of DNA-protein complex introduced at the inlet as shown in Fig. 3.2 is immediately pumped into the channel by the capillary action. Finally, 1:1 H_2SO_4:H_2O_2 clean activates the Si

surface with hydroxyl groups (-OH), enabling strong and uniform PMMA bonding of Si to the glass substrate.

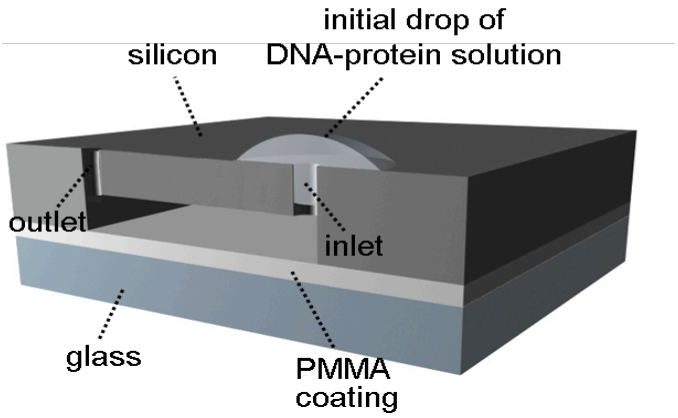

Fig. 3.2 Schematic cut-away representation of cross-sectional area of Si microchannel bonded to glass using PMMA as adhesive layer.

3.3. Number of Immobilized DNA and Stretched Length in Microchannels

High throughput DNA immobilization in microchannels is demonstrated in this section. The immobilization process of DNA molecules is captured with total internal reflection fluorescence (TIRF) microscopy and fluorescent labeled proteins. The number of immobilized DNA molecules and their stretched lengths are analyzed.

3.3.1. Analysis of Protein Assisted DNA Immobilization Process

The DNA-protein complex is introduced at one end of the channel using a pipette. The fluid is immediately sucked into the channel by capillary action, resulting in rapid immobilization of stretched DNA molecules in the channel as shown in Fig. 3.3 (a). The inlet end of the channel acts as a reservoir for fluid entering into the channel and the outlet end is open to the atmosphere for fluid to evaporate (Fig. 3.2). The continuous evaporation of the fluid from the outlet opening drives the fluid from the reservoir into

the channel, which results in a continuous flow of the DNA-protein complex into the channel.

The immobilization and stretching process of a single molecule is captured using a TIRF microscope. DNA-protein complex is formed by mixing 6.7 pM T7 DNA molecules with 5 nM T7 RNAP proteins in TRIS-EDTA (1 mM, pH=8.0, σ=150 μS/cm) buffer. The evaporation-driven flow inside the microchannel stretches the DNA-protein complex and transports it to the PMMA surface where it initially adsorbs at a single point followed by complete attachment (Fig. 3.3 (b)). The DNA is initially out of focus because it is attached at one end to the PMMA surface while the rest of backbone is in the solution (second image in Fig. 3.3 (b)), where it cannot be seen easily with TIRF (TIRF imaging relies on the evanescent wave that decays exponentially with distance, limiting the observation region to ~100 nm from the surface). The DNA comes into focus once it is completely adsorbed to the surface (third image in Fig. 3.3 (b)).

The immobilization and stretching process is also demonstrated using labeled DNA-interacting proteins. 3 nM RNA polymerase proteins labeled with fluorescent molecules are mixed with 0.7 pM T7 DNA molecules in TRIS-EDTA (1 mM, pH=8.0, σ=150 μS/cm) buffer in bulk followed by introducing the DNA-protein complex into the microchannel. Figure 3.4 shows T7 DNA molecules immobilized on the PMMA-coated glass in the microchannel in the presence of T7 RNAP labeled with fluorescent antibodies. Each arrow indicates an individual labeled protein molecule that is bound to the DNA strand and immobilized on the microchannel surface. Apart from using labeled proteins, a denaturing agent such as urea can be used to show that the DNA molecules are immobilized by adsorption of the DNA-interacting proteins to the channel surface. Urea

can be used to denature proteins, which results in disassociation of the DNA-protein complex. If urea is introduced into a microchannel in which DNA molecules are already immobilized by the DNA-protein complex, the immobilized DNA molecules could be released due to protein denaturation by the interaction with the urea, while the labeled proteins remain attached to the channel surface. This would be a further proof that the DNA molecules are immobilized by the DNA-protein complex.

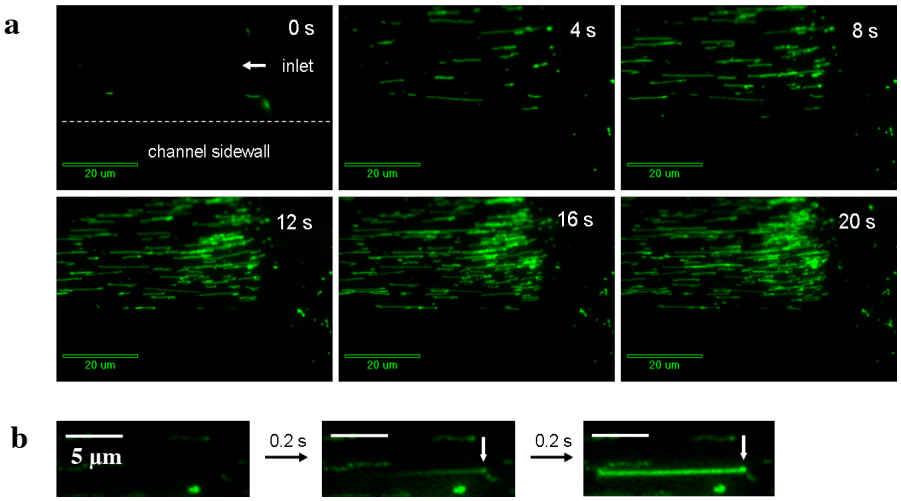

Fig. 3.3(a) Sequence of images of DNA immobilization and stretching by PADI. T7 DNA molecules (6.7 pM) were mixed with T7 RNAP (5 nM) and then introduced into microchannel. Direction of fluid flow is indicated by arrow. (b) Close-up showing DNA molecule adsorbing at one point (indicated by white arrows) followed by complete adsorption of DNA molecule.

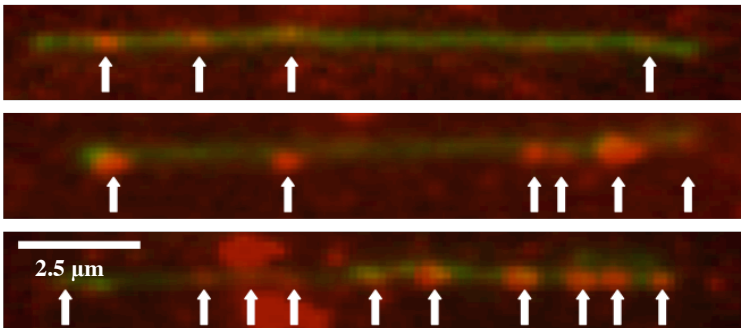

Fig. 3.4 T7 DNA molecules (thin lines, 0.7 pM) immobilized and stretched with assistance of T7 RNAP (bright dots, 3 nM). Arrows indicate positions of bound T7 RNAPs.

Different proteins are used for DNA immobilization as shown in Table 3.1. Successful T7 and λ-DNA immobilization at 5 pM concentration in TRIS-EDTA (1 mM, pH=8.0, σ=150 μS/cm) buffer has been achieved with DNA-interacting proteins such as restriction enzymes, as well as DNA and RNA polymerases. Immobilization is not observed in the presence of proteins that do not interact with the DNA molecules such as bovine serum albumin (BSA) since the DNA-protein complex is not formed. DNA molecules are also not immobilized in the absence of proteins due to the lack of DNA-protein complex. Some of the DNA-interacting proteins listed in the table do not have specific recognition sites on DNA molecules, hence non-specific interactions between DNA and proteins can be used to immobilize DNA molecules. A pocket presented in the structure of the DNA-interacting proteins fits into the DNA strand regardless of the sequence. The electrostatic attraction between positive ions in the protein pocket and negatively charged DNA strand drives the interactions that cause the protein to bind to the DNA molecule.

Table 3.1 Proteins tested for DNA immobilization.

Proteins	**Immobilization**
BamH l, Eco R V, Eco R l, Sma l (Restriction Enzymes)	YES
T4 DNA Polymerase (DNA Replication)	YES
T7 RNA Polymerase (Transcription)	YES
BSA (not a DNA-Interacting Protein)	NO
- (No Proteins)	NO

3.3.2. Number of Immobilized DNA Molecule in Microchannels

Hundreds of DNA molecules can be immobilized and stretched in the microchannel using the PADI technique. The capillary action of the microchannel pumps the DNA molecules into the channels, resulting in rapid immobilization of stretched DNA molecules. Immobilization and stretching of hundreds of DNA molecules is achieved in minutes. Figures 3.5 (a) and (b) show the result of immobilized and stretched λ-DNA molecules at 5.5 pM using T7 RNA polymerase at 10nM in TRIS-EDTA (1 mM, pH=8.0, σ=150 μS/cm) buffer in 100 μm wide and 1 μm deep channel after 2 min of pumping.

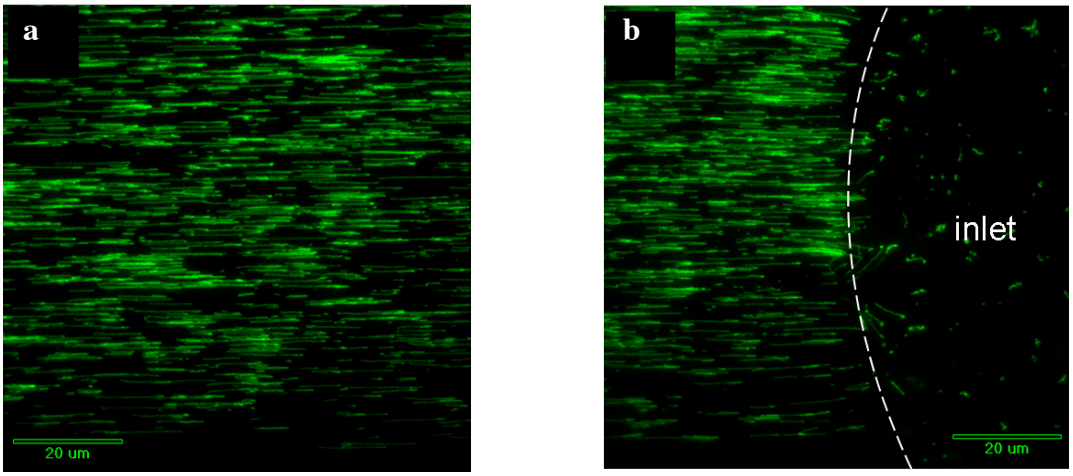

Fig. 3.5 Images of λ-DNA (5.5 pM) stretched onto PMMA-coated glass in 100 μm width and 1 μm deep channel in presence of T7 RNAP (10 nM) (a) at 200 μm from inlet and (b) near inlet. Direction of flow is from right to left.

The number of molecules adsorbed onto the PMMA-coated glass surface was counted at various positions in the microchannel as shown in Fig. 3.6. Approximately 40% of the adsorbed DNA molecules are found within 86 μm (the width of field of view when a 100× objective is used) from the inlet for the 100 μm wide and 1 μm deep channel. Such a high percentage of molecules is found near the inlet because the channel

is initially dry and the number of DNA molecules adsorbed after the fluid is introduced into the channel exhibits an exponential decay with distance shown in Fig. 3.6, presumably because the molecules are depleted from the solution by adsorption near the entrance region. Using diffusion-limited adsorption to the surface, the distance downstream from the inlet that the DNA molecules will travel (X_{inlet}) before being adsorbed is expressed as:

$$X_{inlet} = \frac{vd^2}{2D} \tag{3.1}$$

where v is fluid velocity, d is depth of the channel (1 μm), and D is DNA diffusivity (~0.5 $\mu m^2/s$).

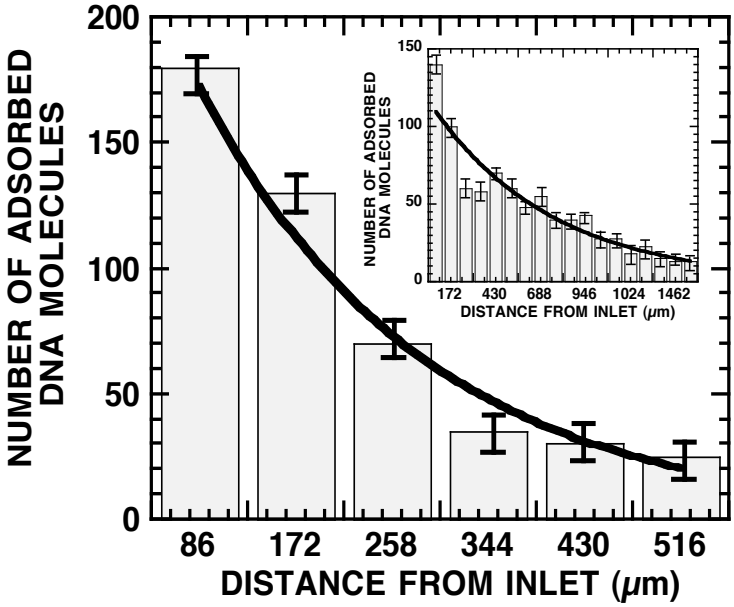

Fig. 3.6 Number of λ-DNA at 9.2 pM adsorbed in presence of 1.7 nM T7 RNAP in TRIS-EDTA (1 mM, pH=8.0, σ=150 μS/cm) buffer as function of distance from channel inlet is fitted to a single exponential ($n = N_0 e^{-x/D}$), yielding adsorption decay distances of D_1=183±18 μm in 1 μm deep channel and D_3=619±59 μm in 3 μm deep channel (inset). Flow was stopped 2 min after introduction of DNA solution by hydrating other end of microchannel.

Thus at the fluid velocity of 200 μm/s, which is measured by tracking 20 nm fluorescent nanoparticles near the center of the channel, the DNA adsorption decay distance is on the order of 200 μm. The adsorption decay distance agrees well with the

decay distance of 183 μm that we have obtained by fitting the number of adsorbed DNA molecules as a function of distance to a single exponential fit for the 1 μm deep channel (Fig. 3.6). Since the fluid velocity is inversely proportional to the channel depth (d) at constant evaporation rate, the DNA adsorption decay distance is directly proportional to d. The DNA adsorption decay distance increases to 619 μm when the depth of the channel is tripled to 3 μm (Fig. 3.6 inset), suggesting that the scaling is valid within the experimental error.

We also have immobilized DNA molecules in channels whose dimensions (100 nm depth, 350 nm width) are smaller than the radius of gyration of λ-DNA (~500 nm) as shown in Fig. 3.7

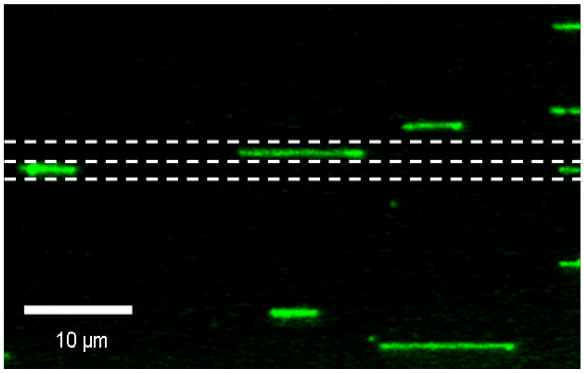

Fig. 3.7 6.7 pM λ-DNA molecules immobilized and stretched with assistance of 0.5 nM T7 RNAP in TRIS-EDTA (1 mM, pH=8.0, σ=150 μS/cm) buffer in series of parallel 100 nm deep and 350 nm wide channels. Dashed lines represent channel sidewalls which are omitted in other areas in figure for clear representation.

The number of DNA molecules immobilized is less in these channels than those found in 1 μm and 3 μm deep channels because the DNA molecules are entropically blocked from entering the channel, due to the small channel size. By using channels with step changes in height, one could exclude large molecules from the channel, and in a downstream process, bleed away small DNA molecules, and thereby concentrate molecules of some desired size [73].

3.3.3. DNA Stretched Length by PADI

We rarely observe overstretched DNA molecules with the PADI technique. The maximum value of the stretch ratio (x/L_c), which is defined as the stretch length (x) divided by the contour length (L_c), is 1.2, and only ~2% of the adsorbed DNA molecules had a stretch ratio greater than unity. The mean stretch ratio of 9.2 pM λ-DNA molecules immobilized using 1.7 nM RNAP in TRIS-EDTA (1 mM, pH=8.0, σ=150 μS/cm) buffer within 86 μm (the width of the field of view) from the inlet is 0.56 for 1 μm deep channel (Fig. 3.8). At this stretch ratio, the force (F) stretching the DNA is expected to be ~0.1 pN according to the worm-like chain model [74]:

$$F = \frac{k_B T}{p}\left[\frac{1}{4}\left(1-\frac{x}{L_c}\right)^{-2} - \frac{1}{4} + \frac{x}{L_c}\right] \tag{3.2}$$

where p is persistence length (~66 nm for YOYO-stained λ-DNA), k_B is Boltzmann constant, T is temperature, x is stretched length, and L_c is DNA contour length. This is much weaker than the force needed to overstretch DNA molecules (~65 pN). With the relaxation time of ~0.1 s for DNA in water and the average fluid velocity of 200 μm/s, the DNA chains should relax by the time they travel 20 μm into the channel, assuming that they are most strongly stretched by the extensional flow at the entrance to the channel. After entering the channel, the extensional flow is replaced by shear, which is not as effective in stretching the DNA [69]. Therefore the mean stretch ratio should decrease with distance from the inlet, as shown in Fig. 3.8.

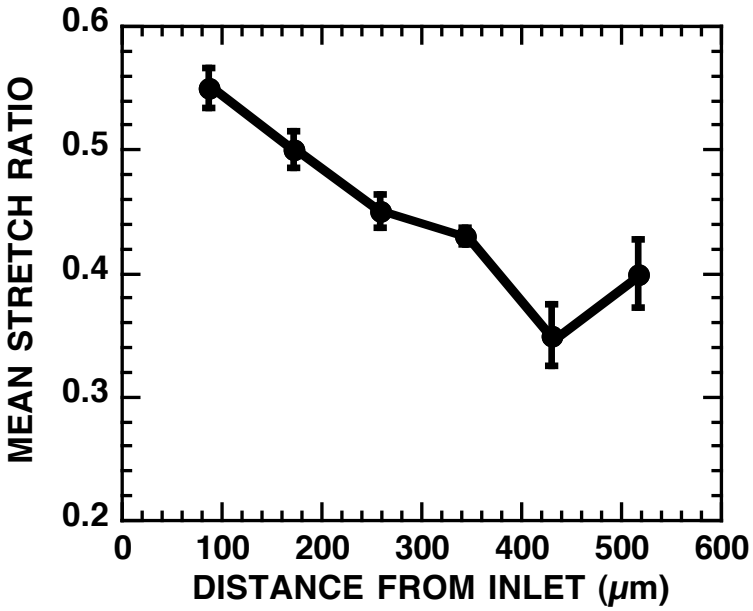

Fig. 3.8 Mean DNA stretch ratio is plotted as function of distance in 1 μm deep channel.

3.3.4. Control of DNA Attachment to Surface

The degree of attachment along the DNA backbone to the surface can be controlled by varying the protein concentration. Increasing the protein concentration increases the number of proteins interacting with the DNA within its radius of gyration, leading to more attachment points on the PMMA-coated glass. Figure 3.9 shows the result of 1 pM T7 DNA attachment in a microchannel for two different RNAP concentrations in TRIS-EDTA (1 mM, pH=8.0, σ=150 μS/cm) buffer. For an RNAP concentration of 5 nM, the DNA remains attached at multiple points after photocleavage for 40 s (Fig. 3.9 (a)), indicating that the DNA was firmly fixed to the PMMA-coated glass at multiple places. In the case of 0.5 nM RNAP, there are fewer attachment points (Fig. 3.9 (b)).

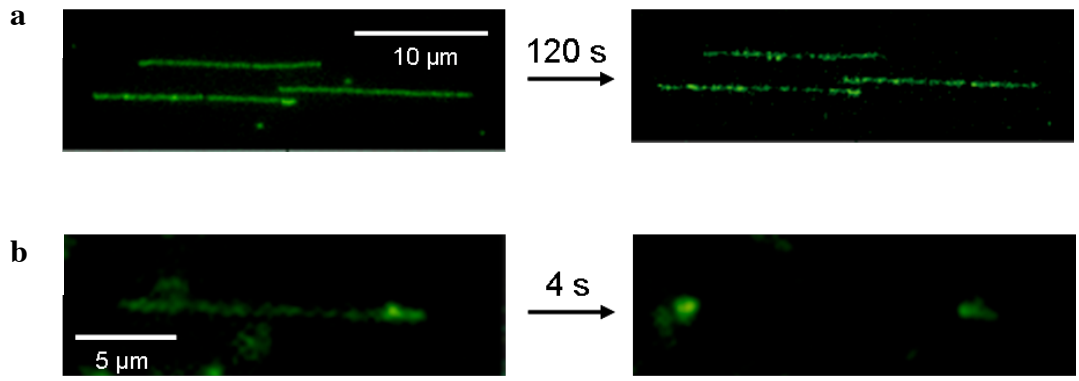

Fig. 3.9 T7 DNA molecules were immobilized at (a) 5 nM and (b) 0.5 nM T7 RNAP followed by DNA photocleavage by exposure to illumination. After photocleavage, DNA fragments coil back to many or few attachment points provided by adsorbed proteins; coiled DNA fragments can be observed as bright spots on surface seen in right hand side of (b).

Depending on the application, different degrees of DNA attachment can be obtained. For example, in optical mapping, DNA has to be tightly bound to the surface so that the restriction fragments are retained on the surface. In the case of studying DNA-protein interactions with proteins that translocate along the DNA contour as they catalyze a biochemical reaction such as transcription, it is preferable to have the DNA attached at two points only (preferably the molecular extremities, if possible) with the rest of the backbone free from the surface so that the interaction is not hindered by the substrate.

3.4. Single Molecule Analysis

Optical mapping and DNA-protein interactions are studied using the PADI technique. Optical mapping is based on the measurement of fragment lengths of surface-deposited DNA molecules after digestion with restriction enzymes [29]. In order to determine the DNA fragment lengths, the strand needs to be firmly attached to the surface so that it does not recoil following digestion with restriction enzymes. On the other hand, in DNA-protein interaction studies, it is required that the DNA strand only

attachs at the two ends and be free from surface attachment for most of its length so as not to hinder protein motion along the strand. For example, transcription on stretched DNA molecules is observed only if most part of the DNA strand is free from attachment to the substrate. In this section, optical mapping and single-molecule transcription are demonstrated.

3.4.1. Optical Mapping

The PADI technique can be used to generate simultaneously many DNA templates for optical mapping applications as shown in Fig. 3.10. We first immobilized 1 pM λ-DNA molecules with 3 nM T7 RNAP in TRIS-EDTA (1 mM, pH=8.0, σ=150 μS/cm) buffer and then introduced type II restriction enzyme Sma I into the microchannel. The concentration of T7 RNAP was adjusted to provide enough protein molecules to hold

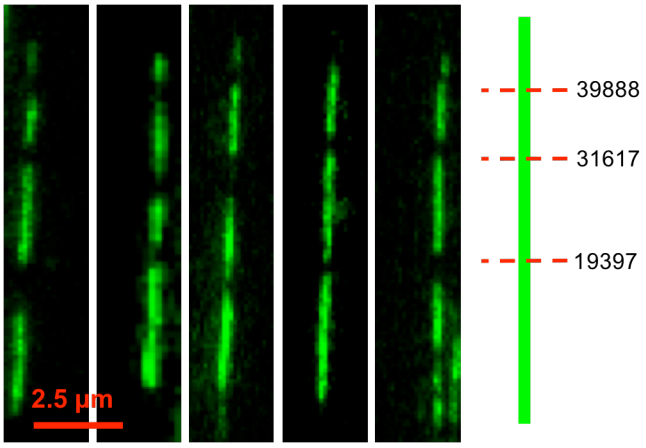

Fig. 3.10 λ-DNA molecules were stretched and immobilized with T7 RNAP followed by enzymatic cleavage by Sma I. DNA molecules were incubated in dark with Sma I at room temperature for 2 h before imaging. Location of predicted cleavage sites for Sma I on λ-DNA is shown on right.

the DNA at several points along the backbone so that the DNA molecule remains anchored to the surface after the cleavage by Sma I, yet the attachment points were not so numerous as to sterically hinder the enzymatic digestion.

We note that a double digestion by two different restriction enzymes may be observed if the DNA is immobilized with one restriction enzyme such as EcoR I rather than RNAP, followed by cleavage by another restriction enzyme such as Hind III. The first restriction enzyme that assists the immobilization needs to bind to the target sequence in the absence of a divalent metal ion to prevent the cleavage prior to the immobilization. This DNA-restriction enzyme complex is then immobilized in the microchannel by PADI, followed by the introduction of the second restriction enzyme along with the divalent metal ion so that both first and second restriction enzymes can cleave the DNA.

We also note that the method works over a range of RNAP concentrations of 0.5 to 17 nM under the conditions of our experiments. At RNAP concentrations much below than 0.5 nM, we do not observe enough adsorption of DNA molecules, and at concentrations well above 17 nM, the time it takes for DNA molecules to imbibe into the microchannel dramatically increases, presumably due to clogging of the channel near the inlet by the protein molecules. There seems to be an optimum protein concentration of around 1 nM at which DNA is immobilized at multiple points, but not so many as to hinder further enzymatic reaction. The optimum concentration may vary from one DNA-binding protein to another, depending on the protein properties. While the number of attachment points could easily be controlled with RNAP by adjusting the concentration to the optimum value, we experienced a limited control over it with commercially

purchased restriction enzymes, apparently due to the presence of highly concentrated BSA, which is mixed in the solution as a stabilizer. Typically in an undiluted stock solution, ~10 nM of restriction enzyme is mixed with 3 μM of BSA, whereas 2 μM of RNAP is readily available commercially without BSA. Therefore, when a restriction enzyme solution is diluted to the optimum concentration (~1 nM), it is BSA, which is present in the solution at the concentration 300 fold higher than the restriction enzyme, that primarily adsorbs on the PMMA-coated surface, presumably leaving little room for proteins on DNA to be adsorbed. The presence of such a high concentration of BSA in the solution also considerably increases the time for imbibition, hindering further increase in the protein concentration.

3.4.2. Single-molecule Transcription

We have also investigated whether transcription can be observed on DNA molecules immobilized by proteins. Transcription on single combed T7 DNA molecules that are not overstretched has been previously demonstrated [24]. In this study, we have demonstrated transcription on DNA immobilized using the PADI technique as shown in Fig. 3.11. Newly synthesized RNA transcripts can be detected with TIRF microscopy as bright dots, when enough fluorescent uridine triphosphates (UTPs) are incorporated into the growing RNA chain. To verify whether this *in vitro* transcription can be observed on DNA molecules immobilized in the microchannel by the PADI technique, we immobilized and stretched 1 pM T7 DNA molecules with the assistance of 1 nM T7 RNAP in TRIS-EDTA (1 mM, pH=8.0, σ=150 μS/cm) buffer, followed by the introduction of transcription buffer containing nucleotriphosphates (200 μM of nucleo triphosphates (NTPs), 8 μM Alexa Fluor 546-UTP), and 100 nM of fresh T7 RNAP. We

observe bright dots showing RNA transcripts synthesized along the DNA strands as shown in Fig. 3.11.

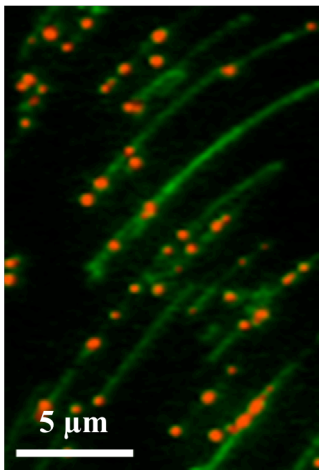

Fig. 3.11 Alexa Fluor 546-UTP labeled RNA transcripts (bright dots) formed along YOYO stained T7 DNA (lines).

3.5. Conclusion

In summary, we have developed a novel DNA immobilization method that utilizes the specific or non-specific interactions between the DNA and DNA binding proteins to immobilize and stretch but not overstretch large numbers of DNA molecules onto a substrate at physiological hydration and pH conditions. In this way, the DNA molecules can be stretched and immobilized inside a microchannel with a high throughput when introduced by a capillary force. Many different DNA binding proteins such as restriction enzymes, DNA polymerase, and RNAP can be used to achieve DNA immobilization irrespective of binding sequence specificity. The number of attachment points along the DNA contour is controlled by varying the protein concentration. The biological activity of the immobilized DNA molecules was tested by digesting the DNA with restriction enzymes in the microchannel. Single-molecule transcription, which

places stringent requirements on the immobilized DNA with respect to surface interactions and stretch lengths, is also successfully demonstrated in the microchannel.

CHAPTER 4
IMMOBILIZATION, STRETCHING, AND MOVEMENT OF DNA MOLECULES IN CHANNELS USING AC VOLTAGE

4.1. Introduction

Precise placement of DNA molecules in microchannels enables access to specific sequences on a DNA strand. This capability is useful in performing experiments such as molecular manipulation or repair of specific sequences using DNA-interacting proteins. In order to control DNA placement in channels, control over its immobilization location and its motion along the channels are required.

Currently, hydrodynamic flow [37] and electric field [5] based techniques have been shown to allow immobilization and stretching of DNA molecules in channels. However, the location of immobilization of DNA molecules cannot be controlled using the existing techniques. Another drawback in the current electric field based techniques is very few DNA molecules can be immobilized on the electrodes [75].

DC electrophoresis is used to control the motion of negatively charged DNA molecules in channels [67]. A voltage is applied across the channels that are in contact with the electrodes, therefore driving the DNA molecules towards the positive electrode. However, due to the large separation between the electrodes across the channel, a large dc voltage is required to create sufficient electric field to generate DNA motion. The high voltage often results in bubble formation in the channel when voltage is applied.

We have developed a technique to immobilize and stretch DNA molecules across an electrode gap in channels using an ac voltage. Large numbers of DNA molecules are

immobilized on the electrodes without chemical modification to the DNA molecules or the electrode surface. Using an appropriate electrode design and fluid at pH of 5.8 and 8.0, DNA immobilization, stretching, and movement across the electrode gap are controlled using an ac voltage.

The different forces that act on the DNA molecules in the presence of an ac field in fluids will be discussed in section 4.2. Techniques to control DNA immobilization and stretching at acidic and physiological pH will be presented in section 4.3. Control of DNA motion in channels using low ac voltage will be shown in section 4.4.

4.2. AC Voltage Induced Forces

An ac voltage is used to prevent electrolysis of the buffer solution near the electrodes, which often occurs when large dc voltage is applied. Electrolysis is not desirable since it can lead to bubble formation, resulting in blockage of the channels and no fluid can flow through. DNA molecules in a buffer solution experience a number of forces in the presence of an ac voltage. DNA molecules are influenced by the electric field through direct interactions with the ions present around the negatively charged strand. In addition, the applied voltage exerts a force on the fluid, and the resulting fluid flow influences the motion of the DNA molecules. Some of the voltage induced forces on DNA molecules are restricted to within the electrode gap or near the electrodes, while other forces influence DNA molecules present >1mm from the electrodes. Therefore various forces influence DNA molecules to different degrees depending on the location of the DNA with respect to the electrodes. In this section, different forces that influence the DNA molecules in microchannels due to an ac field will be discussed.

4.2.1. Dielectrophoretic Force

Any type of materials, whether they are neutral, charged, polar, or non-polar, will be polarized by an electric field. Interactions of this induced dipole with the surrounding electric field can lead to a number of effects such as lateral movement, rotation, orientation, and deformation. In the case of particles suspended in a non-uniform electric field, the interaction of field induced charges on each side of the dipole will result in a non-uniform force acting on the particles. The non-uniform force results in a lateral motion of the particles. This effect is referred to as dielectrophoresis. The dielectrophoretic force, F_D, exerted by an electric field, E, on a spherical object of radius, r, is expressed as [76]:

$$F_D = 2\pi\varepsilon_f r^3 \mathrm{Re}\left[K(\omega)\right]\left|\nabla E^2\right| \tag{4.1}$$

where ε_f is dielectric constant of fluid and $K(\omega)$ is given by:

$$K(\omega) = \left(\frac{\varepsilon_p^* - \varepsilon_m^*}{\varepsilon_p^* + 2\varepsilon_m^*}\right) \tag{4.2}$$

where ε^* is the complex permittivity of particle (ε_p^*) and fluidic medium (ε_m^*) and is given by:

$$\varepsilon^* = \varepsilon - j\frac{\sigma}{\omega} \tag{4.3}$$

where σ is conductivity and ω is frequency.

The dielectrophoretic force is due to the electric field gradient acting on the particles and is proportional to the volume of the particles. Therefore smaller particles require higher field gradient to control the particles. The dielectrophoretic force is dependent on the frequency of the electric field as indicated in the $K(\omega)$ term and it is

also referred to as Clausius-Mossoti (CM) factor. The value of the CM factor also depends on whether the particles are more or less polarizable than the medium. If the particles are more polarizable than the medium, then the CM factor is positive. This means the particles experience positive dielectrophoresis and they move towards the regions of maximum electric field gradient. On the other hand, if the particles are less polarizable than the medium, then the CM factor is negative. This means the particles experience negative dielectrophoresis and they move towards the regions of minimum electric field gradient. Hence the direction of the particle movement is dependent on the relative properties of the particles with respect to the fluidic medium. Dielectrophoretic force is a short range force since the electric field gradient rapidly decays from the electrode edges and high electric field gradient is required to control the particles [76]. Typically, particles present in the electrode gap and near the electrode edges are influenced by the dielectrophoresis force since the maximum electric field gradient is located at the edges of the electrodes and in the gap.

For DNA molecules, they are highly polarizable due to their negative charges. Most buffer solutions used in the DNA experiments have polarization factor lower than the DNA molecules. Hence the DNA molecules often experience positive dielectrophoresis. The motion of DNA molecules due to dielectrophoresis is often directed towards the electrode edges.

4.2.2. Torque

Due to the large length (20 μm) to width (2 nm) ratio of DNA molecules, they experience a torque under the influence of an electric field. For example, a high aspect ratio particle when polarized in an electric field tends to align itself with the longest axis

parallel to the electric field. In other words, the electric field exerts a torque on the particle. A long flexible molecule such as DNA tends to align and stretch parallel to the electric field due to the torque, T_r, which is given by [77]:

$$T_r = D_p \times E \tag{4.4}$$

where D_p is induced dipole and E is electric field. In contrast to the dielectrophoretic force, the torque depends on the electric field and not its gradient. Hence the torque is a long range force capable of exerting its influence outside the electrode gap.

4.2.3. Electrothermal Flow

Typically an ac voltage of 1 to 20 V is applied across microfabricated electrodes in a fluidic medium to manipulate suspended particles. The applied voltage generates power within a small volume of the fluid near the electrodes. The dissipated power leads to localized heating of the fluid near the electrodes, resulting in the generation of temperature gradient in the fluid. A variation in the temperature of the fluid causes local changes in the permittivity and conductivity of the fluid. These changes will give rise to an electrothermal force in the fluid, causing fluid to flow in the channels. The electrothermal force per unit volume, F_E, is expressed as [78]:

$$F_E = \frac{1}{2}(E\nabla T)E\frac{\varepsilon(\alpha-\beta)}{1+(\omega\varepsilon/\sigma)^2} - \frac{1}{4}\varepsilon\alpha|E|^2\nabla T \tag{4.5}$$

where E is electric field, T is temperature, ε is permittivity, σ is conductivity, ω is frequency, and α, β are given by:

$$\alpha = \frac{\left(\frac{\nabla\varepsilon}{\nabla T}\right)}{\varepsilon},\ \beta = \frac{\left(\frac{\nabla\sigma}{\nabla T}\right)}{\sigma} \tag{4.6}$$

The electrothermal force depends on the permittivity and conductivity gradients. It influences fluid near the electrode edges and in the electrode gap since the force is dependent on the gradients. The fluid flow generated by the electrothermal force due to ac voltage applied to a parallel electrode is a circulatory fluid motion across each electrode. The direction of the fluid motion is determined by the direction of the electric field relative to the thermal gradients [79]. The electrothermal fluid flow can be the dominating force near the electrodes. If suspended particles such as DNA experience the electrothermal force, the DNA molecules will continuously circulate on top of the electrodes.

4.2.4. Induced Charge Electro-Osmosis

Particles suspended in fluid in the presence of a electric field are polarized, resulting in the formation of surface charges near the particles' surface. The surface charges move in response to a changing electric field, moving the fluid in the vicinity of the surface charges. This fluid motion results in net force acting on the suspended particles and causing them to move. This phenomenon is referred to as induced charge electro-osmosis (ICEO). The fluid motion is known as the slip velocity, u_s, and it is related to the electric field as [80]:

$$u_s = -\frac{\varepsilon_f \varsigma}{\nu} E_{ll} \tag{4.7}$$

where ε_f is dielectric constant of fluid, ς is zeta-potential, E_{ll} is parallel component of electric field, and ν is fluid viscosity. The equation indicates that the slip velocity, which causes particle motion, is proportional to electric field. Hence ICEO is a long range

phenomenon since electric field spreads out to the fluid in the channel that is far from the electrodes.

4.3. DNA Immobilization and Stretching Across Electrode Gap

We have developed an ac voltage based DNA immobilization and stretching technique where large numbers of DNA molecules are immobilized and stretched across an electrode gap in a microchannel. The DNA molecules are immobilized at pH of 5.8 and 8.0 to Au electrodes. The DNA molecules do not require any end labeling and the electrodes do not require any surface modification for DNA immobilization. DNA immobilization across an electrode gap at one end and two ends of the electrodes are demonstrated.

4.3.1 Electrokinetic Forces to Immobilize and Stretch DNA Molecules

The electrokinetic stretching of DNA molecules in fluid involves several forces acting on the molecules. For example, the dielectrophoretic force is caused by the induced dipole along the backbone of the DNA molecules. This force is directed towards the electrode edges. The second force is the torque exerted on the induced dipole by the electric field. For a DNA molecule with one end immobilized on the electrode, the torque tends to elongate the DNA molecule parallel to the electric field [81]. The third force is the electrothermal force acting on the fluid, which is generated by the gradients in conductivity and permittivity of the fluid caused by the field induced fluid heating [78]. When an ac field is applied between 2 electrodes in a fluidic system, each electrode induces a circulatory fluidic motion across the electrodes. These 2 circulating fluids in the electrode gap prevents the DNA molecules attached to an electrode to be stretched

beyond the range of the corresponding circulating fluid [82]. The torque and direction of the electrothermal induced fluid flow result in the DNA stretching [83]. The direction of the fluid flow depends on the direction of the electric field and temperature gradient. Thus the electrothermal induced fluid flow patterns have a complex relationship with different factors such as electrode design, conductivity and permittivity of fluid, microchannel dimensions, frequency and magnitude of the electric field [79]. A change in any of the above factors can perturb the electric field or the temperature gradient, leading to different flow patterns. In order for the attached DNA to stretch, the fluid has to flow from the edge of the electrode towards the electrode gap.

4.3.2. Immobilization and Stretching of DNA Molecules at One End

DNA molecules are immobilized at one end of the electrodes and stretched across the electrode gap due to the electrokinetic forces. In this section, electrostatic immobilization and stretching of DNA molecules at one end is demonstrated at pH of 5.8 and 8.0 in microchannels.

4.3.2.1. Immobilization and Stretching at Acidic pH in Large Channels

In this set of DNA experiments, 2-morpholinoethanesulfonic acid monohydrate (MES) buffer (25mM, pH=5.8, σ=370 μS/cm) is used. The pH of the buffer is set to 5.8 to enable DNA immobilization to the Au electrode [37]. 0.6 ng/μl of λ-DNA with contour length of 16.5 μm is introduced into the microchannels with integrated electrodes. These Si microchannels are 100 μm wide and 75 μm deep, therefore there is little confinement of the DNA molecules in these channels. 20/50 nm thick Cr/Au electrodes

on 100 µm thick glass are bonded to the Si microchannels using PMMA as an adhesive layer.

DNA stretching depends on the direction of the electrothermal induced fluid flow and the flow patterns in the microchannel. A 100 KHz ac voltage is applied to the electrodes. The direction of the induced fluid flow near the electrode edge changes as the voltage is ramped up. At lower voltages, the DNA molecules move towards the electrode edges. At higher voltages, the DNA molecules start moving away from the electrode edge towards the gap.

DNA are immobilized on Au electrodes irrespective of the fluid flow direction. In order for the attached DNA to be stretched outward from the electrode edge, the electrothermal induced flow should cause the fluid to flow away from the electrode edges. Figures 4.1 (a)-(c) show DNA stretching in the 100 µm wide, 75 µm deep microchannel at different voltages.

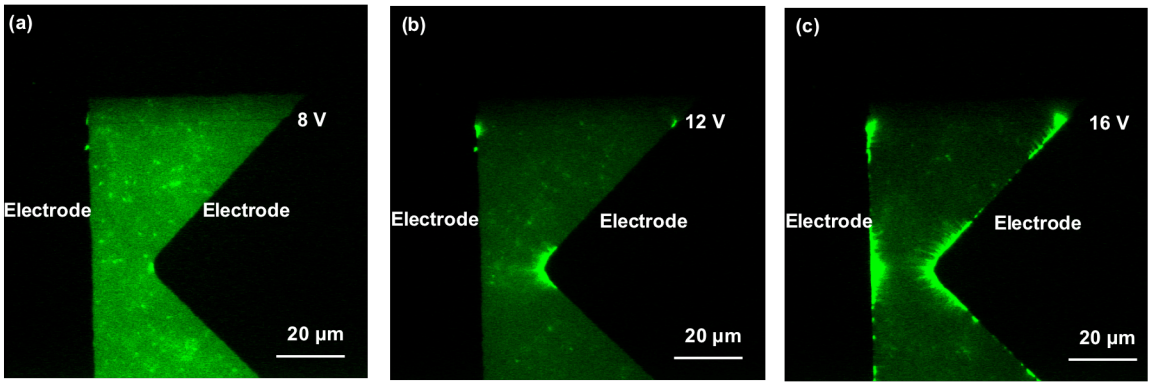

Fig. 4.1 DNA stretching for different voltages at 100 KHz in 100 µm wide and 75 µm deep Si microchannel. (a) DNA stretching starts at tip of pointed electrode at 8 V. (b) Larger number and area for stretched DNA molecules near tip of pointed electrode at 12 V. (c) DNA molecules stretched at both straight edge and pointed electrodes at 16 V.

At 8 V, DNA stretching begins near the pointed tip of the electrode as shown in Fig. 4.1 (a), since the electrothermal induced fluid flow is away from the electrode edge only near the electrode tip where the electric field is highest. Figure 4.1 (b) shows an increase in the number of DNA molecules and the expanded area for stretched DNA near the electrode tip at 12 V. At 16 V, as shown in Fig. 4.1 (c), DNA molecules are stretched along the pointed and straight edge electrodes since the electric field is high enough along all electrode edges to cause electrothermal induced fluid flow away from both electrode edges.

Large number of DNA molecules are immobilized and stretched in a single step along the electrode edges in the microfluidic channel. It allows one end of the DNA molecules to be fixed at the electrode edge and the other end to be stretched out to different lengths by the electric field. This capability is particularly useful for studying single molecule DNA-protein interactions. The fluid flow pattern is different for microchannels with shallower depth. For a 3 μm deep channel, the induced flow is towards the electrode edge at voltages up to 20 V and for frequencies varying from 25 KHz to 1 MHz. The electric field and temperature distributions perpendicular to the electrode surface are different for shallower channels, resulting in different flow patterns.

Figure 4.2 shows the variation of DNA stretch lengths with voltage. At 100 KHz, maximum stretch length of 10.8 μm is obtained for DNA molecules stretched from the pointed electrode tip. At 200 KHz, the stretch length is lower due to the reduced torque acting on the DNA molecules. The maximum stretch length at 200 KHz is 4 μm. No DNA stretching is observed at 1 MHz. Longer stretch lengths of DNA molecules are obtained consistently at 100 KHz compared to other frequencies.

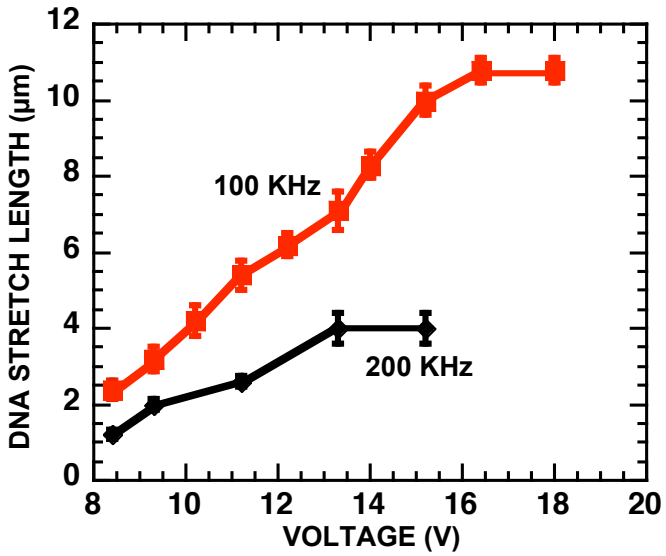

Fig. 4.2 Variation of stretch length of λ-DNA molecule as voltage is applied at 100 and 200 KHz. Length is measured from edge of electrode to end of stretched DNA molecule.

4.3.2.2. Immobilization and Stretching at Physiological pH in Small Channels

Immobilization and stretching of large number of DNA molecules on electrodes have been shown in buffer solution with pH of 5.8. However, the rate of catalysis, which is an indicator of the efficiency of enzymatic actions, is maximum near physiological pH of 8.0 [84]. Immobilization is typically not performed at pH of 8.0 since fewer number of DNA molecules can be immobilized [28]. By reducing the channel dimensions, for example using microchannels that are 500 nm wide and 100 nm deep, immobilization of large number of DNA molecules to the electrodes are obtained at physiological pH of 8.0, rather than at acidic pH.

λ-DNA molecules at 5 pM concentration in TRIS-EDTA buffer (pH=8.0, σ=150 μS/cm) are introduced at the inlet port of 500 nm wide and 100 nm deep channels integrated with electrodes having a 20 μm gap. DNA molecules are flown into the channels by the capillary action and are brought to rest by hydrating the outlet port. A

100 KHz ac field is then applied across the electrodes, which is slowly ramped up from 1 to 18 V. The electrothermal force induced flow moves the DNA molecules towards the electrodes, which results in some of the DNA molecules being immobilized on the electrodes. Beyond 8 V, the immobilized DNA molecules begin to stretch and the stretched length increases with the applied voltage. Figure 4.3 shows λ-DNA molecules stretched at 16 V. The smaller channels improve DNA immobilization to the electrodes due to the greater possibility of DNA molecules being in contact with the electrode surface compared to 100 μm wide and 75 μm deep channels.

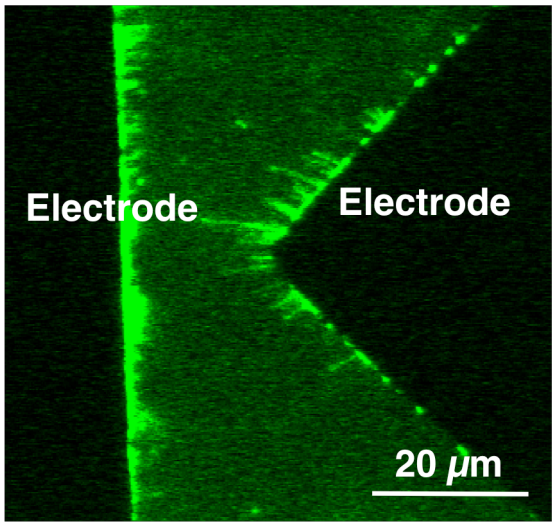

Fig. 4.3 λ-DNA molecules at 5 pM concentration in TRIS-EDTA buffer (pH=8.0, σ=150 μS/cm) immobilized and stretched across electrode gap using 100 KHz ac voltage at 16 V in 500 nm wide and 100 nm deep channels. DNA molecules are immobilized at one end of Cr/Au electrodes and stretched by ac field.

Figure 4.4 shows the variation of DNA stretch length with voltage. A maximum stretch length of 12 μm is obtained for DNA molecules stretched from the pointed electrode tip. The stretched length is determined from the edge of the electrode to the end of the DNA molecule. DNA molecules are attached at different positions from the edge

of the electrode, therefore DNA molecules with different stretched lengths are observed in Fig. 4.3. The electrothermal flow drives the DNA molecules towards the electrode surface and during this process the DNA molecules contact the electrode surface and get immobilized at different locations with respect to the electrode edge.

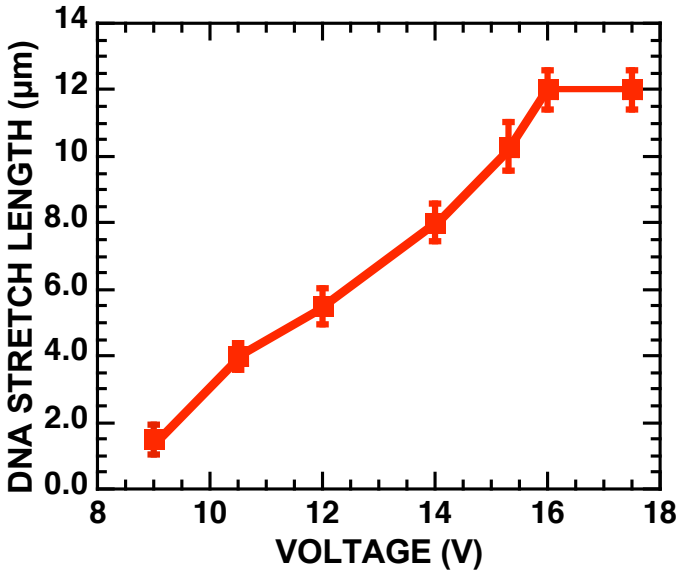

Fig. 4.4 Variation of stretched lengths of λ-DNA molecule in TRIS-EDTA (pH=8.0, σ=150 μS/cm) buffer as ac voltage is applied at 100 KHz.

4.3.3. Immobilization and Stretching of DNA Molecules at Two Ends

In addition to attaching the DNA molecules at one end on an electrode and stretch them, it would also be useful to immobilize both ends of the DNA molecules. A floating electrode is incorporated between the electrode gap for this purpose as shown in Fig. 4.5. T2 DNA molecules at 5 pM concentration in MES buffer (25 mM, pH=5.8, σ=370 μS/cm) are introduced in the channels. Since the voltage is applied between the straight edge and pointed electrodes and not to the floating electrode, the electrothermal induced fluid flow in the vicinity of the floating electrode edge is minimized. This allows DNA molecules to be immobilized at both ends and stretched across the electrodes. When a

second force such as hydrodynamic flow of the fluid containing DNA molecules is applied in addition to the electric field, the DNA molecules can overcome the resistance due to the electrothermal induced flow of the floating electrode and the other end of the DNA molecule can be attached to the floating electrode.

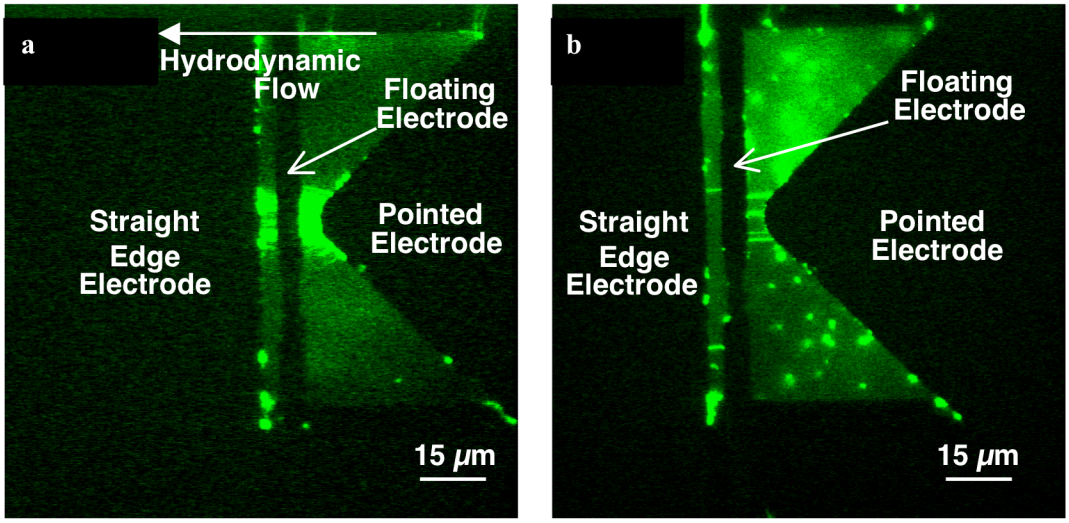

Fig. 4.5 (a) Attached T2 DNA molecules stretched in presence of 100 KHz and 13 V peak-to-peak electric field and hydrodynamic flow in 100 μm wide and 16 μm deep microchannel. Direction of flow is from right to left as indicated by arrow. (b) Stretched DNA molecules in absence of electric field and hydrodynamic flow.

As shown in Fig. 4.5 (a), a 6 μm wide floating electrode is placed near the center of the 15 μm wide electrode gap and the fluid containing the DNA molecules is flown from the right to the left hand side of the microchannel after the DNA molecules are attached at the edge of the electrodes and stretched by the electric field. The hydrodynamic flow of the microchannel is initiated by dehydrating one end of the microchannel, leading to fluid pumping by evaporation. Large numbers of T2 DNA with contour length of 55.8 μm are immobilized at the pointed electrode and stretched across the electrode gap in the presence of both the electric field and the hydrodynamic flow in the microchannel. Some of the DNA molecules may cross over the floating electrode and bridge the gap to the straight edge electrode.

The fluid flow as characterized by tracing the velocity of DNA molecules 20 μm from the microchannel sidewalls is ~124 μm/s. DNA molecules immobilized at both ends in the absence of electric and hydrodynamic forces are shown in Fig. 4.5 (b). The electric field is switched off while the hydrodynamic flow is allowed to continue for ~2 min and then the flow is stopped by hydrating the outlet port. While some of the DNA molecules recoil back, a few remain to be stretched and immobilized at both ends near the edges of the pointed and floating electrodes. With the floating electrode, we have demonstrated that multiple stretched DNA molecules can be immobilized at both ends across the electrode gaps. This capability would enable the realization of complex network such as inverters and adders from DNA-templated carbon nanotube transistors, where precise placement of stretched DNA across electrodes is needed.

4.4. DNA Molecule Movement Outside Electrode Gap

Motion of DNA molecules outside the electrode gap is controlled using low ac voltage. The motion of the DNA molecules is due to the ICEO phenomenon which has a long range influence over DNA molecules. ICEO induced motion results in DNA molecules moving away from the electrodes. The details of the mechanisms generating the DNA motion will be described in the next chapter. The velocity of the DNA molecules is controlled by varying the voltage across the electrodes. Electric field induced stretching of DNA molecules at a distance of 1110 μm from the electrodes is also demonstrated.

4.4.1. DNA Velocity Outside Electrode Gap

The control of the velocity of DNA molecules present outside the electrode gap has been demonstrated in microchannels. The fluidic system consists of a 100 μm wide, 20 μm deep Si microchannel integrated with a sharp tip and a straight edge electrode pair separated by 20 μm. 3-ng/μl concentration of λ-DNA molecules in DI water is introduced into one of the fluidic ports of the Si channel. The fluid is instantly pumped into the channels by the capillary action and it continues to flow due to pumping by evaporation from the fluidic port at the other end of the channel. The fluid flow is brought to rest by introducing fluid in both fluidic ports. The initial size of the coiled DNA molecules is 500 nm in diameter before they are introduced into the channel and when they are stationary inside the channel in absence of any external force. After the fluid flow is stopped, a 100 KHz sinusoidal voltage is applied across the two electrodes.

At lower voltages, the DNA molecules in the vicinity of the electrodes are influenced by the dielectrophoretic and electrothermal forces. Beyond a threshold voltage, the DNA molecules near the electrode begin to move away from the electrode. With further increase in voltage, the DNA molecules begin to move. Figure 4.6 shows the velocity of the DNA molecules at the centre of the channel for various applied voltages and at a distance of 1110 μm away from the centre of the electrode gap. The velocity of the DNA molecules increase with the applied voltage, since ICEO induced motion is proportional to electric field.

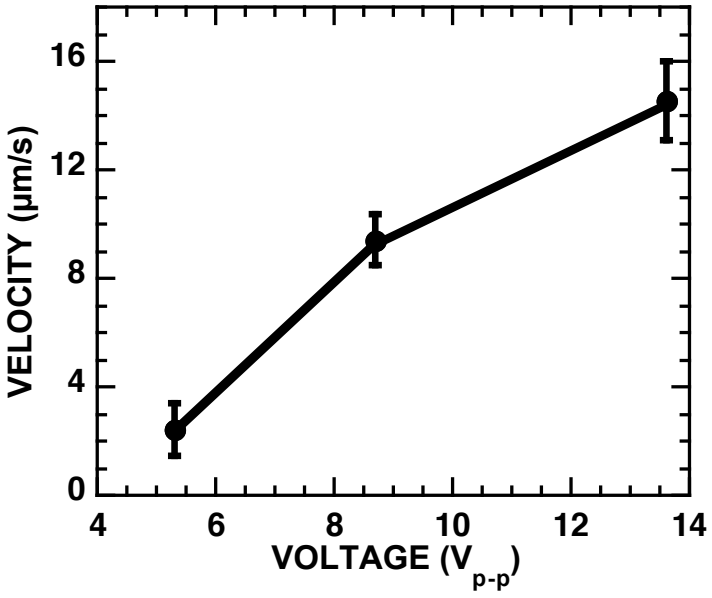

Fig. 4.6 Velocity of DNA molecules in Si microchannels for different applied ac voltage.

4.4.2. DNA Stretching Outside Electrode Gap

The ICEO phenomenon is used to stretch the DNA molecules tethered on the PMMA surface inside the microchannel as shown in Fig. 4.7. λ-DNA molecules at 5 pM concentration in DI water (pH=7.8, σ=200 μS/cm) are introduced in the channels. It has been shown that DNA molecules can bind one of their ends on PMMA surface [28]. The stretched DNA molecules are located at a distance of 1110 μm from the electrode gap. The boundaries of the 100 μm wide channel are indicated by the two solid lines in Fig. 4.7. A 100 KHz sinusoidal voltage is applied with 13.6 V peak-to-peak, resulting in stretching of the DNA molecules. At this applied voltage, the DNA molecules that are tethered at only one end to the PMMA surface are stretched to 15 μm long. Some DNA molecules are not stretched to this maximum length. The possible reasons for various stretched lengths shown in the figure could be related to multiple attachment points of a single DNA molecule and photo-cleavage of the molecules during image acquisition.

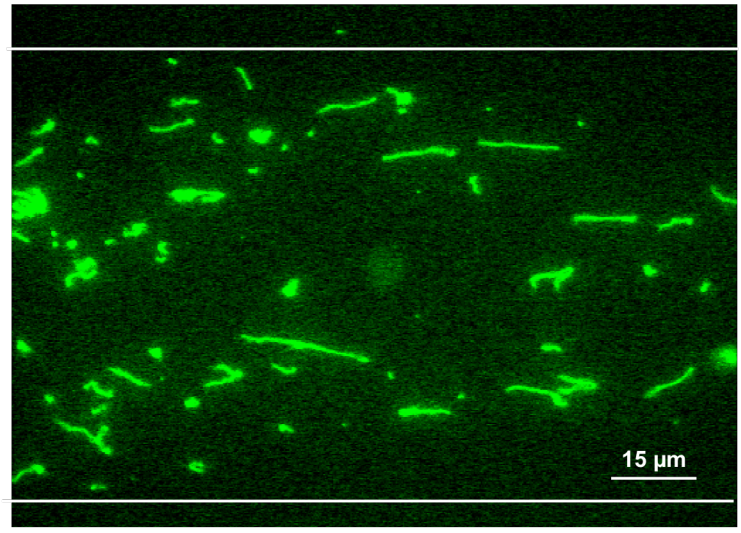

Fig. 4.7. Stretching of tethered DNA molecules in Si microchannel. 3-ng/ul of λ-DNA in DI water is introduced into microchannel.

4.5. Conclusion

A low ac voltage is used to provide controllable DNA immobilization, stretching, and movement in microchannels. Large numbers of DNA molecules are immobilized to the electrodes at acidic and physiological pH without chemical modification to DNA or electrode surface. 100 KHz ac voltage is used to immobilize and stretch λ-DNA molecules in a buffer solution with pH of 5.8 in 100 µm wide and 75 µm deep microchannels. Immobilization and stretching of large number of DNA molecules across an electrode gap is achieved at physiological pH of 8.0 using smaller, confined channels. The stretched length of the DNA molecules is controlled by varying the voltage across the electrode gap. Using a floating electrode, T2 DNA molecules are immobilized at both ends and stretched across a 5 µm wide electrode gap using electric field and hydrodynamic flow in the microchannels. The movement and stretching of DNA molecules outside the electrode gap is made possible based on the ICEO phenomena. The

velocity of the DNA molecules located at a distance of 1110 μm from the electrodes is controlled using a low ac voltage varying from 5.3 to 13.6 V. Stretching of tethered DNA molecules up to 15 μm long located at a distance of 1110 μm from the electrodes is demonstrated.

CHAPTER 5
MECHANISMS OF VOLTAGE INDUCED DNA AND PARTICLE MOTION IN CHANNELS

5.1. Introduction

In fluidic systems for biological [85] and chemical sensing [86] applications, fluid flow is used to direct the transport of particles to specific locations within a micro- or nano-channel to perform biomolecular detection or chemical reactions. A number of biomedical applications require motion of biomolecules such as DNA and proteins in small channels. For example, mapping is performed by imaging DNA molecules moving through 1 μm wide, 100 nm deep channels [41]. DNA and protein separations are performed by transporting the molecules along 300 nm deep channels [87].

The two most common forces used for controlling fluid flow along the channels are pressure gradient [40] and electro-osmosis [88]. In pressure driven flow, a pressure gradient is applied across the channel to control the flow rate. A drawback in this method is that as channel dimensions are reduced, the resistance to fluid flow increases, thereby requiring higher pressure to maintain the same flow rate.

In dc electro-osmosis, a voltage applied across the channel drives the positive charges induced in the fluid due to the preconditioned, negatively charged channel surface towards the negative terminal. The motion of the positive charges moves the fluid along the channel. Electro-osmosis typically requires large dc voltage of 100 V across a 1 cm long channel to generate a fluid flow that transports particles [88], since the electrodes are often placed far apart in the inlet and outlet ports. In addition, the channel

surface is prone to particle adsorption, which alters the surface charge distribution, resulting in flow instabilities [89]. In ac electro-osmosis, a voltage applied across asymmetrical electrodes is used to control the fluid flow in the channels [90], [91]. The asymmetrical shape of the rectangular electrodes allow the electrode with more surface area to generate more surface charges, thereby generating a net motion of fluid in channels. Although fluid flow can be generated at low voltage since the distance between the electrodes is typically <20 μm, ac electro-osmosis is limited by the increase in flow resistance as the channel dimensions are reduced.

We present mechanisms that describe the motion of particles such as DNA and polystyrene nanoparticles generated using low ac voltage but without fluid flow along the channels. The ac voltage induced motion does not require surface modification and is ideally suited to control the motion of particles in channels with small dimensions, as the motion is induced by direct electric field interaction with the particles and not by fluid displacement along the channels. The velocity of the particles is controlled by varying the voltage magnitude.

Current techniques of controlling the motion of particles in channels are discussed in section 5.2. The mechanisms of ac voltage induced DNA and nanoparticle motion in channels are presented and compared to fluid flow generated motion in section 5.3. Electric field simulations are compared with experimental results in section 5.4.

5.2. Current Techniques to Control DNA and Particle Motion in Channels

Pressure gradient and electro-osmosis are the two most common forces used to generate fluid flow in channels to transport particles to a desired location in the channels. In this section, pressure driven and electro-osmotic forces to control particle motion in

channels are discussed. Electro-osmotic phenomena due to dc voltage, ac voltage, and induced charges are introduced in this section.

5.2.1. Pressure Driven Flow

Just as potential difference is used to drive current in conductors, pressure difference drives fluid in channels from high to low pressure points [68]. Pressure driven flow between two parallel plates, such as a microchannel, exhibits parabolic velocity profile across the channel walls. The stationary channel walls result in the velocity of the fluid being zero at the walls and maximum at the center of the channels. The velocity profile, v, from the channel walls to the center of the channel is expressed as [92]:

$$v = \frac{3V_m}{2}\left[1 - \left(\frac{y}{d}\right)^2\right] \tag{5.1}$$

where V_m is mean velocity, y is distance from center of channel, and d is depth of channel.

In order to generate a specific flow rate in the channels, appropriate pressure gradient is required. The relationship between the pressure gradient, Δp, and fluid flow rate, q_f, in the case of fluid flow between two parallel plates is expressed as [92]:

$$\Delta p = \frac{3q_f \nu l}{2d^3} \tag{5.2}$$

where ν is viscosity, l is channel length across which pressure gradient is applied, and d is channel depth. It indicates that the pressure gradient required to generate fluid flow increases with decrease in channel cross-section. Therefore, higher pressure is required to maintain the same flow rate as channel dimensions are reduced. Pressure driven flow is commonly used in channels with depths greater than 20 μm [93].

5.2.2. Electro-Osmosis

Electro-osmosis refers to movement of fluid on a charged surface such as an electrode, charge modified channel surface, or polarized particles. In this section, electro-osmosis due to different charged surfaces are described, along with their applications to generating motion of fluid and particles in channels.

5.2.2.1. DC Electro-Osmosis

In dc electro-osmosis, the surface of the channel is modified to contain negative charges [88]. For example, glass substrates treated with oxygen plasma or 1:1 H_2SO_4:H_2O_2 solution result in the formation of –OH groups on the surface. The oxygen atom in the –OH group is electronegative, thereby resulting in negative ions on the glass surface. In the presence of fluid in the channel, positive ions from the fluid are formed next to the negatively charged channel surface. When a dc voltage is applied across the channel, the positive ions are attracted towards the negative electrode. The moving positive ions drag the fluid in the same direction, resulting in fluid flow along the channel. AC voltage cannot be applied since there will be no net motion of the fluid along the channel as the fluid simply oscillates between the two electrodes. The relationship between electrophoretic mobility, z, of the ionic molecules and electric field, E, is expressed as [94]:

$$z = \frac{EQ}{3\pi\nu d_s} \tag{5.3}$$

where Q is total ionic charge, ν is viscosity, and d_s is Stokes diameter of the ions. This equation shows that the electrophoretic mobility of positive ions near the channel surface is dependent on the electric field and independent of channel dimensions. Therefore,

unlike pressure driven flow, dc electro-osmosis is not limited by the increase in flow resistance in smaller channels. However, a drawback for dc electro-osmosis is a large voltage is required across the channel to generate fluid flow since the electrodes are often placed at a large distance equal to the length of the channel in the inlet and outlet ports. Typically 100 V is required to generate fluid flow in a 1 cm long channel. A second drawback is the adsorption of particles to the channel walls, which alters the surface charges and creates flow instabilities. DC electro-osmotic flow has been generated in both micro- and nano-channels [93], [87].

5.2.2.2. AC Electro-Osmosis

When a voltage is applied to electrodes immersed in a fluid, it attracts oppositely charged ions in the fluid to the electrode surface. In case of ac voltage at frequencies typically between 1 Hz to 100 KHz, the ions on the electrode surface change in response to the changing voltage. The changing ions drag the fluid along, resulting in fluid flow. The phenomenon is similar to dc electro-osmosis except the motion of the ions occurs on the electrode surface rather than on channel walls. Also, the separation between the electrodes in ac electro-osmosis is often smaller compared to dc electro-osmosis.

In the case of symmetrical electrodes, there is no net motion of fluid since the flow is symmetrical for each electrode. A net flow can be generated in asymmetrical electrodes where the width or height of the electrodes is unequal. The direction of the flow is determined by the direction of the fluid pumping force generated by the larger electrode. Compared to dc electro-osmosis, a lower ac voltage is required to generate equivalent flow rate due to the smaller separation between electrodes typically in the order of 20 μm. A drawback of ac electro-osmosis is the increase in flow resistance in

smaller channels. AC electro-osmotic flow has been demonstrated in 100 μm wide and 20 μm deep channels integrated with electrodes with 5 μm gap in the channels [91].

5.2.2.3. Induced Charged Electro-Osmosis

The ICEO phenomenon has been discussed earlier in which electric field interactions with the field induced surface charges on the particles, resulting in fluid flow in the vicinity of the particle surface. The fluid flow results in net force acting on the particles and causing them to move. Although ICEO phenomenon has been observed experimentally [95] and analyzed theoretically [47], it has not been used to generate directional motion of particles in channels. ICEO phenomenon occurs when either a dc or ac voltage is applied. AC voltage is preferred in microfluidic applications since it reduces bubble formation in channels. We will present mechanisms to induce motion of DNA and particles in channels using the ICEO phenomenon and ac voltage without fluid flow along the channels. Hence, unlike pressure driven flow and ac electro-osmosis, ICEO induced DNA and particle motion is not limited by the increase in flow resistance in smaller channels. In addition, only low ac voltage below 20 V is needed to generate motion of DNA and particles in channels.

5.3. AC Voltage Induced Motion of DNA and Particles in Channels

Existing techniques transport DNA and particles in channels by moving fluid in the channels. These techniques are limited either by increase in flow resistance in smaller channels or large voltage required to generate fluid flow in channels. We present an alternative mechanism that generates DNA and particle motion in channels using low ac voltage without using fluid flow along the channels. This mechanism is ideally suited to

control the motion of DNA and particles in channels with small dimensions as the motion is induced by the electric field interactions with the DNA or particles and not by the fluid displacement along the channels. Controlled motion of particles in channels is demonstrated at 100 KHz. The motion of the particles in the presence of fluid flow only, ac voltage only, and both fluid flow and ac voltage are compared.

5.3.1. DNA and Nanoparticle Motion Induced by Fluid Flow Only

5 pM λ-DNA molecules and 15 pM 20 nm polystyrene nanoparticles in TRIS-EDTA (1 mM, pH=8.0, σ=150 μS/cm) buffer are introduced into the channels at the inlet port by the capillary action, while the outlet port is open to air. This leads to continuous pumping of the DNA and nanoparticles into the channels by fluid evaporation. The mean velocity due to fluid evaporation for the DNA molecules and nanoparticles in a 1 μm wide, 400 nm deep channel array is 33 and 65 μm/s, respectively; and in a 10 μm wide, 800 nm deep channel is 80 and 200 μm/s. Due to the smaller size of the 20 nm particles compared to 1 μm radius DNA molecules, the nanoparticles experience stronger Brownian motion. The Brownian motion causes variations in DNA and nanoparticles velocity as shown in Table. 5.1. The 20 nm particles show a velocity variation of 15 μm/s while the DNA molecules have a variation of 1 μm/s in 10 μm wide, 800 nm deep channels. The velocity variation is less in channels with smaller dimensions. The velocity of the DNA molecules is constant along the channels since fluid flow is incompressible. The velocity is higher in wider channels since the coiled DNA molecules move faster in channels with cross-sectional area that is comparable to their coiled volume. Apart from the channel dimension and particle size, the force that a fluid flow exerts on suspended particles is also dependent on the shape of the particles and the location of the particles

with respect to channel walls [96], [97]. The above factors result in fluid flow exerting a greater force on the nanoparticles compared to the DNA molecules, resulting in higher velocity for nanoparticles moved by fluid flow in channels.

Table 5.1. DNA and nanoparticles velocity due to fluid flow only.

Channels	DNA Velocity (μm/s)	Nanoparticles Velocity (μm/s)
1 μm wide 400 nm deep	33±1	66±5
10 μm wide 800 nm deep	80±1	300±15

5.3.2. DNA Motion Induced by Low Frequency AC Voltage

A schematic showing particle motion due to an ac voltage is illustrated in Fig. 5.1. An ac voltage is applied across the parallel electrodes and the applied voltage influences the particles present outside the electrodes. In Fig. 5.1, the particle is assumed to be attracted to the electrodes during the positive period of the cycle and is deflected during the negative period. The distance traveled due to deflection, X_2, is greater than the distance traveled due to attraction, X_1, since the particle is closer to the electrode when deflected, and hence experiences larger electric field as compared to when it is attracted towards the electrode. Thus the direction of the particle motion is away from the electrodes during the first period. During subsequent periods, the particle continues to move away from the electrodes. This proposed mechanism is independent of the size or charge of the particle, or the frequency of the ac voltage. We had captured the motion of DNA molecules at low frequency and it shows that this explanation applies to both DNA and polystyrene nanoparticles which have different properties.

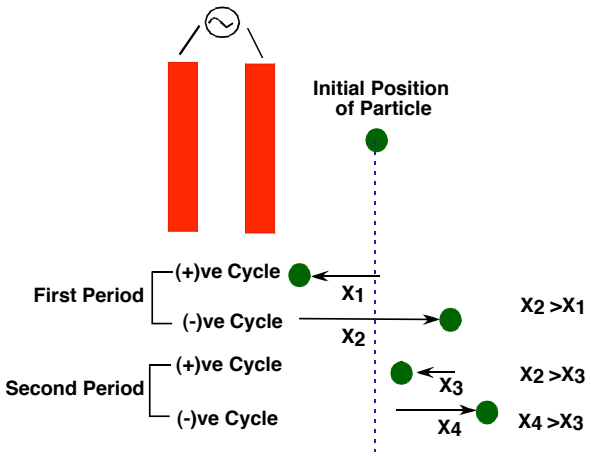

Fig. 5.1 Schematic showing ac voltage induced motion of particle. Particle is alternatively attracted and deflected due to change in voltage polarity. Net deflection distance is greater than attraction distance, hence causing particle to move away from electrodes.

5 pM λ-DNA molecules in TRIS-EDTA (1 mM, pH=8.0, σ=150 μS/cm) buffer are introduced into the channels and brought to rest by hydrating the outlet port. Sinusoidal ac voltage is then applied across the electrodes and it is increased in steps of 0.5 V. Beyond a threshold voltage, the λ-DNA molecules and 20 nm nanoparticles begin to move away from the electrodes. The motion generated by the ac field is due to the ICEO phenomenon [47]. It was proposed that the ac electric field generates fluid flow locally around the particles due to the interactions between the field and the field induced surface charges on the particles, therefore moving the particles along the channels by ICEO. Under ICEO, there is no fluid movement along the channels.

Figure 5.2 shows the movement of λ-DNA molecules induced by 1 Hz sinusoidal voltage at 3.5 V. The DNA molecules are present in a 150 μm wide and 1 μm deep channel at a distance of 100 μm from the electrodes. Figure 5.2 (a) shows the initial position of the DNA molecules before ac voltage is applied. In Fig. 5.2 (b), the DNA molecules are moved to the left during the first half of a cycle at 0.4 s, bringing them

closer to the electrodes. Since DNA molecules are negatively charged, there are positive charges induced on the DNA surface. The fluid flow generated by the field interactions with the surface charges moves the DNA molecules closer to the electrodes. In Fig. 5.2 (c), DNA molecules are moved to the right in the second half of the cycle as they are repelled away from the electrodes by the voltage with opposite polarity.

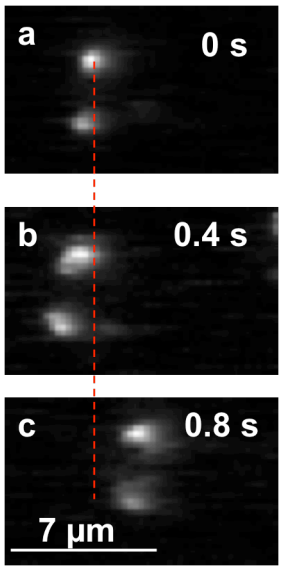

Fig. 5.2 λ-DNA molecules moved by 1 Hz, 3.5 V sinusoidal ac voltage in 150 µm wide, 1 µm deep channel. (a) initial position. (b) DNA molecules move towards electrodes during first half of cycle at 0.4 s. (c) DNA molecules move away from electrodes during second half of cycle at 0.8 s. The net motion after one cycle results in DNA molecules moving away from electrodes with respect to their initial positions.

Since the DNA molecules are closer to the electrodes when they are repelled, the electro-osmotic flow generated around the particles is greater, since the flow is proportional to the electric field. This results in the distance traversed by the DNA molecules to be greater than the first half of the cycle. Hence at the end of the first cycle, the DNA molecules are moved away from the electrode with respect to their original positions. The DNA molecules also experience the Brownian motion, therefore the movement is not in a straight-line. During subsequent cycles, the DNA molecules will

continue to move away from the electrodes. Similar movement is observed for 20 nm polystyrene particles, although they experience more Brownian motion than DNA molecules and hence more velocity variation.

5.3.3. DNA and Nanoparticle Motion Induced by High Frequency AC Voltage

Field induced DNA motions at higher frequency for channels with different dimensions are also investigated. 5 pM λ-DNA molecules in TRIS-EDTA (1 mM, pH=8.0, σ=150 μS/cm) buffer are introduced into the channels and brought to rest, followed by having a sinusoidal ac voltage applied across the electrodes. Figure 5.3 shows the velocity of λ-DNA molecules as a function of 100 KHz applied voltage at a distance of 500 μm from the electrodes.

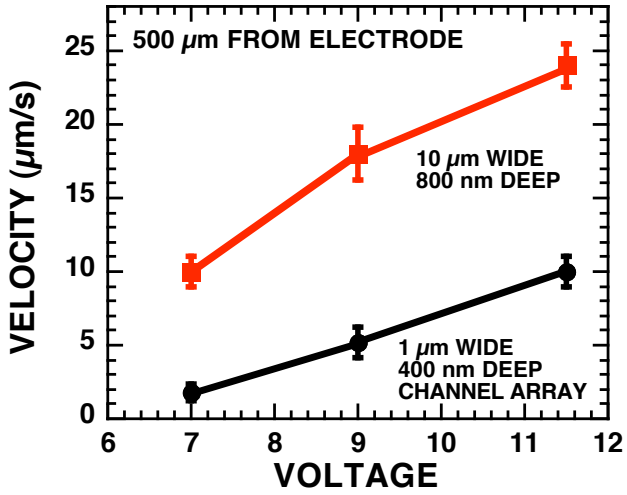

Fig. 5.3 Velocity of λ-DNA molecules varies with ac applied voltage at 100 KHz. DNA molecules are at distance of 500 μm away from electrodes.

The DNA molecules move away from the electrodes and their velocity increases with the applied voltage. They begin to move in the 1 μm wide, 400 nm deep channel array at 6 V. For voltage ranging from 7 to 11.5 V, the DNA velocity in a 1 μm wide, 400

nm deep channel array is 2 to 10 μm/s; and in a 10 μm wide, 800 nm deep channel, the velocity is 10 to 24 μm/s. The velocity of DNA molecules is higher in wider channels due to the larger cross-sectional area of the channels. At 100 KHz applied voltage, the DNA molecules show nearly linear motion with negligible Brownian effect when the movement is recorded at a frame rate of 10 Hz.

The velocity of DNA molecules varies with distance from the electrodes. Figure 5.4 shows the dependence of λ-DNA molecule velocity as a function of distance from the electrodes. The 100 KHz ac voltage is kept constant at 11.5 V. At 500 to 1340 μm from the electrodes, the velocity varies from 10 to 2 μm/s in a 1 μm wide, 400 nm deep channel array and 24 to 9 μm/s in a 10 μm wide, 800 nm deep channel. The decrease in electric field with distance from the electrode causes a reduction in velocity.

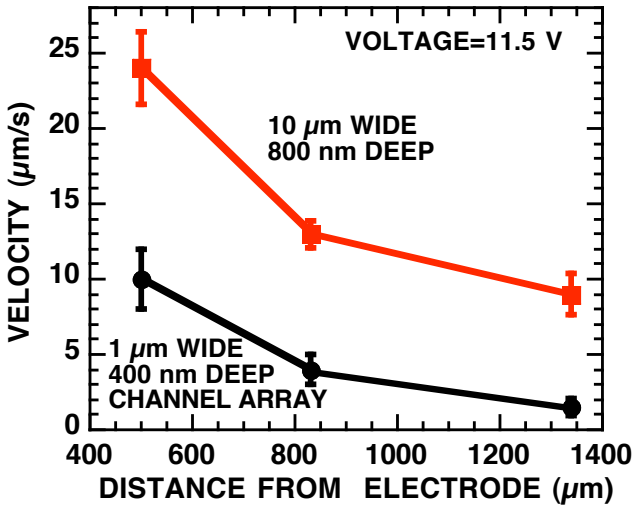

Fig. 5.4 Dependence of λ-DNA velocity with distance from electrodes. AC applied voltage is kept constant at 11.5 V and 100 KHz.

This result indicates that the DNA molecules are not driven by fluid flow along the channel, since the measured velocity of the DNA molecules changes within the same channel while the fluid is not compressible. Although ac field can cause electrothermal or

electro-osmotic induced fluid flow along the channels, these effects do not apply in this case since the measured velocity of DNA molecules is a function of distance from the electrodes. Also, no fluid flow out of the inlet and outlet ports is noticed during the experiments.

Similar ac voltage induced motion of 20 nm polystyrene particles is also observed as shown in Table 5.2. The direction of their movement is away from the electrodes and their velocity increases with voltage and reduces with distance from the electrodes. 15 pM nanoparticles in TRIS-EDTA (1 mM, pH=8.0, σ=150 μS/cm) buffer are introduced into the channels and brought to rest followed by applying a sinusoidal ac voltage applied across the electrodes. The nanoparticles begin to move in 1 μm wide, 400 nm deep channel array at 8.5 V, which is higher compared to the 6 V needed for the DNA molecules. At 10 V and 500 μm from the electrodes, the mean velocity of the 20 nm nanoparticles is 13 μm/s in a 1 μm wide, 400 nm deep channel array and 25 μm/s in a 10 μm wide, 800 nm deep channel. The ICEO phenomenon also depends on the shape of the particle [47], therefore the difference in the shape between DNA molecules and 20 nm particles results in different velocities. Due to the strong Brownian motion, the electric field induced motion in 20 nm particles shows more velocity variations than DNA molecules since the coiled DNA molecules are large in volume and more polarizable due to their negative charges. Compared to motion induced by fluid flow only, 20 nm particles have similar velocity variations in ac voltage induced motion due to the Brownian motion. The velocity of both DNA and nanoparticles are higher due to fluid flow induced motion compared to motion induced by ac voltage.

Table 5.2. Velocity of nanoparticles in channels induced by 10 V ac voltage.

Channels	DNA Velocity (μm/s)	Nanoparticles Velocity (μm/s)
1 μm wide 400 nm deep	6±1	13±5
10 μm wide 800 nm deep	20±1	25±6

5.3.4. DNA Motion Induced by Both Fluid Flow and AC Voltage

The motion of DNA molecules in the presence of both fluid flow and ac voltage is investigated. 5 pM λ-DNA molecules in TRIS-EDTA (1 mM, pH=8.0, σ=150 μS/cm) buffer are pumped into the channels from the inlet port by evaporation from the outlet port. AC voltage at 100 KHz is then applied across the electrodes which is ramped up in steps of 1 V. Figure 5.5 shows the variation of the velocity of DNA molecules in a 150 μm wide and 1 μm deep channel at a distance of 500 μm from the electrode.

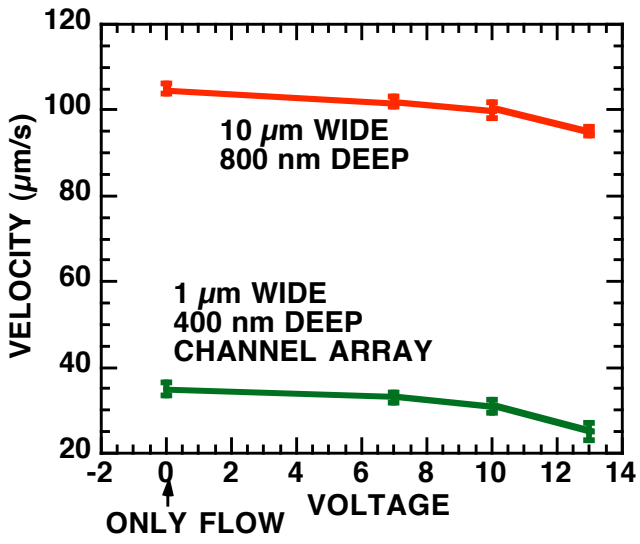

Fig. 5.5 Velocity of DNA molecules at distance of 500 μm from electrode and induced by fluid flow and 100 KHz ac voltage.

The fluid flow velocity is held constant while the voltage is increased from 0 to 13 V. The velocity of the DNA molecules reduces with increase in voltage due to the electrothermal flow generated by the applied voltage, which impedes the fluid flow.

Since the velocity of the DNA induced by the fluid flow only is higher compared to the motion induced by the ac voltage, a decrease in DNA velocity occurs in spite of the increase in DNA velocity due to ICEO at higher voltage.

5.4. Simulations of Electric Field Distribution in Integrated Fluidic System

Voltage induced motion of particles in sealed channels due to ICEO is caused by the electric field interactions with particles. Hence the motion of particles in channels can be better understood by analyzing the electric field distribution in the channels. In this section, simulations of electric field distribution in sealed channels are performed using the comsol software package [98]. The spatial distribution of electric field in channels is simulated and compared to experimental results of ac voltage induced DNA and particle motion in the channels.

5.4.1. Electric Field Distribution For Parallel Electrodes

Electric field distribution due to voltage applied across a pair of parallel electrodes on an insulating substrate such as glass can be solved in spherical coordinates. The equation describing the electric field, E(r), as a function of radial distance, r, due to voltage applied across parallel electrodes is expressed as:

$$E(r) = \frac{V}{\pi}\frac{1}{r}n_{\theta} \tag{5.4}$$

where V is voltage and n_{θ} is normal component of the electric field. Since the electric field is dependent on only one spatial factor, r, which is the radius from the center of the electrode gap, the spatial distribution of the electric field is circular. In addition, since the electric field is inversely proportional to the distance, r, the electric field magnitude decreases linearly with distance from the electrodes.

5.4.2. Simulations of Electric Field Distribution in Sealed Channels

Simulation of the distribution of electric field in the channel is shown in Fig. 5.6 for a pair of 20 μm wide electrodes separated by a 20 μm gap and integrated with a 100 μm wide, 20 μm deep and 860 μm long Si channel. The electric field lines as seen from top of the electrodes is shown in the Fig. 5.6. For the simulations, we use 70 nm thick Au electrodes and 600 nm thick PMMA on top of a 10 μm thick glass, and the channel is in a 30 μm thick Si substrate. The surface area of the glass is 860 × 300 μm^2 and the area of the Si substrate is 880 × 320 μm^3. The electrodes are 300 μm long and the surface area of the PMMA is 800 × 300 μm^2. No PMMA is present in the electrode gap or on the electrode surface. The conductivity values of Au, Si, PMMA, and glass used for the simulations are 10^8, 10^4, 10^{-5}, and 10^{-8} S/m, respectively. The boundary conditions for PMMA, glass, metal, and Si substrates are set as "continuity", where the normal component of the electric field is assumed to be continuous across the boundaries. A +5 V is applied on the left electrode and a -5 V is applied on the right electrode. The direction of the electric field in the gap is pointing from the left to the right electrode. Outside the electrode gap, the electric field distributes circularly into the channel as seen in Fig. 5.6. The electric field originates from the positive electrode and is directed towards the channel walls. The electric field is directed from the outer edge of the left electrode and it is returned towards the outer edge of the right electrode, where it is terminated. When an ac voltage is applied across the electrodes, the directions of the electric field inside and outside of the electrode gap change in each cycle. The change in the directions of the electric field cause the particles outside the electrode gap to move in the opposite directions. Since the deflection of the particles is greater when they are

nearer to the electrodes, the ac voltage induces particle motion due to ICEO results in particles moving away from the electrodes as explained earlier in chapter 4.

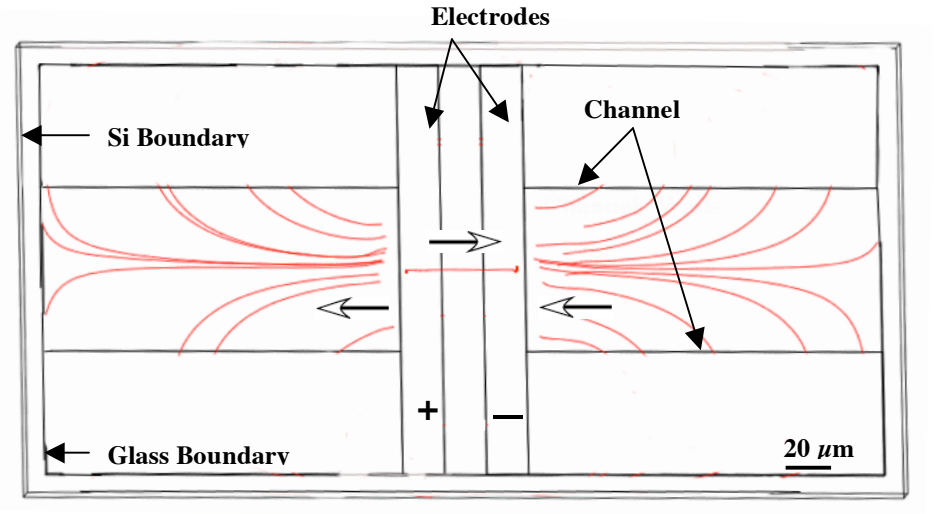

Fig. 5.6. Top view of spatial distribution of electric field due to +5 V and -5 V applied across two parallel electrodes on glass integrated with 100 μm wide and 20 μm deep channel. Boundaries of Si and glass are shown in figure. Directions of electric field in electrode gap and channel are indicated by arrows. In case of ac voltage, directions of electric field change in each cycle, while distribution of electric field is similar.

2D simulations of electric field magnitude inside and outside of the electrode gap in a 20 μm wide and 3 mm long channel are performed. 100 μm wide electrodes are separated by a 20 μm gap and they are placed at the center of the channel as shown in Fig. 5.6. The Au electrodes are assumed to have conductivity of 10^8 S/cm and the Si channel has a conductivity of 10 S/cm. The fluid in the channel is assumed to have a conductivity of 150 μS/cm, which is similar to the TRIS-EDTA buffer used in the experiments. The voltage on the two electrodes are set to +5 V on the left and -5 V on the right electrode. The boundary conditions for channel and medium in the channel are set as "continuity", where the normal component of the electric field is assumed to be continuous across the boundaries. The electric field magnitude for applying 10 V across the 20 μm electrode gap is shown in Fig. 5.7. The center of the electrode gap is set at 0 μm and the two

electrodes edges are located at -10 and +10 μm, as indicated in the figure. The electric field increases towards the electrode edges and reaches a minimum in the center of the two electrodes. Since the electric field originates from the electrode edges and decreases with distance due to the applied voltage, the electric field is maximum at both the electrode edges and reaches a minimum at the center of the electrode gap.

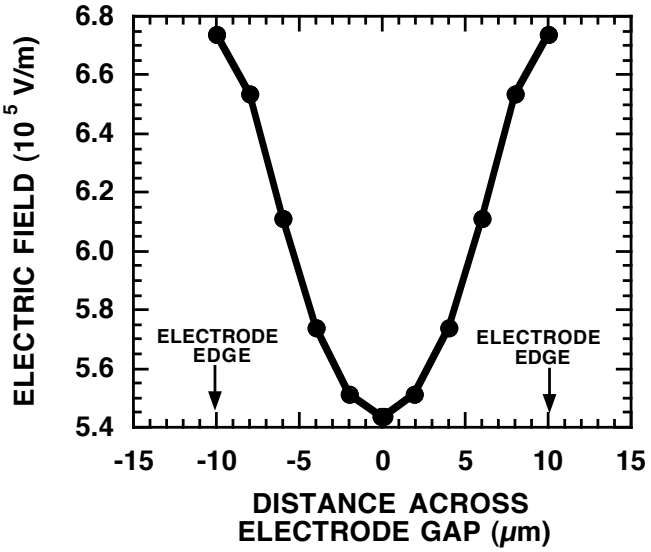

Fig. 5.7. Variation of electric field magnitude across 20 μm wide electrode gap. +5 V is applied on left electrode and -5 V is applied on right electrode. Center of electrode gap is at 0 μm.

The variation of electric field along the channel outside the electrode gap is analyzed. The magnitude of the electric field varies from 1021 V/m near the electrode edge to 5.4×10^{-6} V/m at 1400 μm from the edge. Since the electric field outside the electrode gap arises from the fringe fields, it is lower compared to the electric field in between the electrode gap. Figure 5.8 shows the variation of electric field at a distance of 500 to 1400 μm from the electrode edge at the center of the channel.

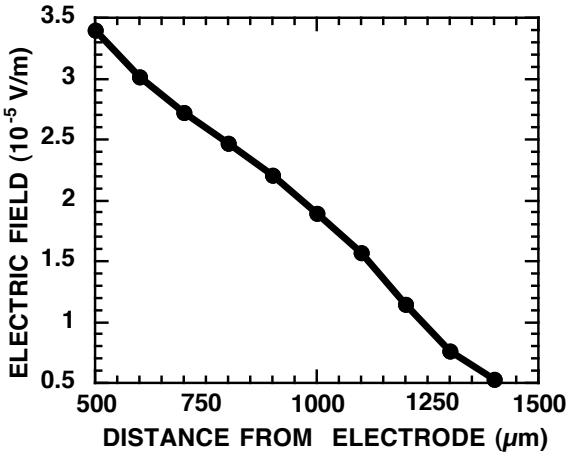

Fig. 5.8. Variation of electric field magnitude at distance of 500 to 1400 μm from electrode edge in center of channel. +5 V and -5 V are applied on electrodes.

The electric field variation across the channel is also analyzed. Figure 5.9 shows the plot of electric field magnitude across the 10 μm wide channel at a distance of 500 μm from the electrode edge. The center of the channel is at 0 μm. The electric field is higher near the channel walls since the electric field is directed from the center towards the channel walls as shown in Fig. 5.6.

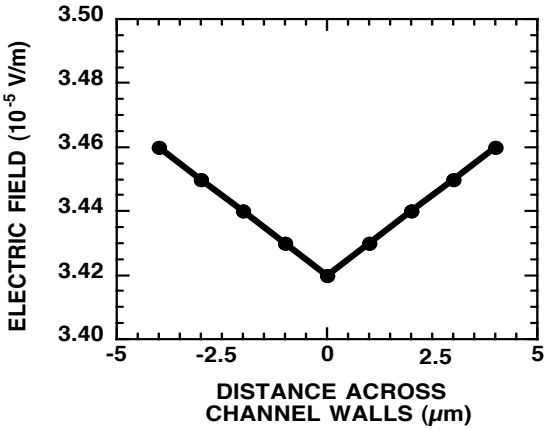

Fig. 5.9. Variation of electric field magnitude across 10 μm wide channel. Center of channel is located at 0 μm. +5 V and -5 V are applied on electrode.

5.4.3. Comparison Between Simulations and Experimental Results

Motion of DNA molecules induced by ac voltage is captured real time in the channels and the trajectory of the DNA movement is compared to the distribution of the

electric field from the simulations. λ-DNA molecules at 5 pM concentration in TRIS-EDTA (1 mM, pH=8.0, σ=150 μS/cm) buffer are introduced into a 100 μm wide and 20 μm deep channel integrated with 20 μm wide parallel electrodes separated by a 20 μm gap. After fluid flow through the channel for 2 min, the pumping is stopped by hydrating the outlet end. An ac voltage is rapidly increased from 0 to 10 V across the electrodes to move the DNA molecules near the electrode edge. Snapshots of the DNA motion near the outer edge of an electrode are captured at different times as shown in Figs. 5.10 (a)-(c).

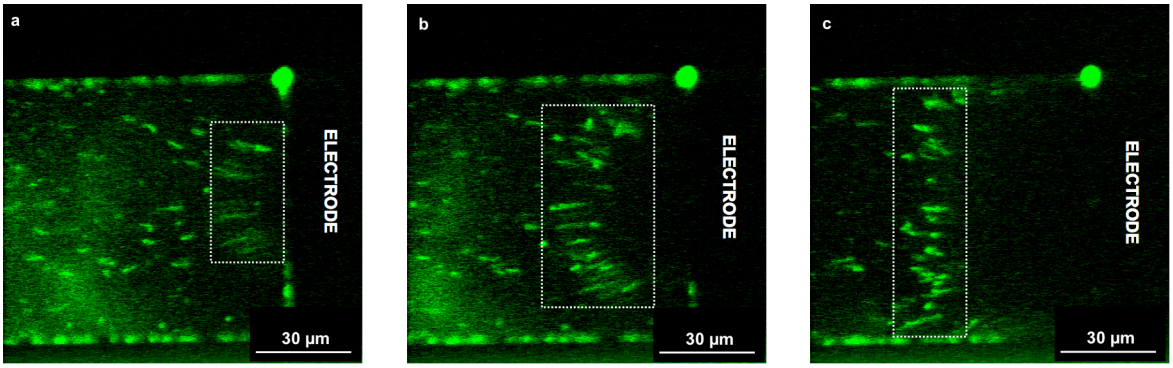

Fig. 5.10 Motion of DNA molecules away from electrode at 10 V in 100 μm wide and 20 μm deep channel at (a) 0 s, (b) 200 ms, and (c) 500 ms. DNA molecules move away from electrode towards channel walls.

The motion of the DNA molecules is away from the electrode edge and they are directed towards the channel walls. The DNA molecules at the center of the channel take longer to reach the channel walls compared to the DNA molecules closer to the walls since their motion follows the electric field distribution as shown in Fig. 5.6. In addition, the electric field is higher near the channel walls than at the center of the channel as indicated in the simulations shown in Fig. 5.9, this variation also contributes to the DNA molecules moving towards the channel walls.

The magnitude of the electric field is found to decrease with the distance from the electrode edge as shown in Fig. 5.7. Experimental results shown in Fig. 5.4 also indicate a decrease in DNA velocity with increase in distance from the electrode. Since the DNA motion is induced by the ICEO phenomenon, which is proportional to the electric field, the results agree with the simulations, which project a reduction in DNA velocity as distance from the electrode edge is increased.

5.5. Conclusion

We have described the mechanisms of ac voltage induced directional motion of DNA molecules and nanoparticles in sealed channels. When an ac voltage is applied, the DNA and particle motion is due to ICEO, which is induced by the electric field interactions with the field induced surface charges on the particles that generate local fluid flow around the particles. The range of electric field induced motion extends beyond 1 mm from the electrodes. Using 100 KHz ac voltage, field induced motion in λ-DNA molecules and 20 nm polystyrene particles are demonstrated in channels of various dimensions. The DNA and particles move in a single direction and away from the electrode edges. Due to their smaller size, the nanoparticles experience stronger Brownian motion compared to DNA, and they have larger velocity variation. Also, since DNA molecules are negatively charged, they are highly polarizable and their motion due to ICEO is induced at lower voltage compared to 20 nm polystyrene nanoparticles. The field induced velocity increases with applied voltage and decreases with distance from the electrodes. This velocity dependence of distance from electrodes indicates that the field induced particle motion is not due to fluid flow along the channel, since fluid flow in channels is incompressible, but the motion is due to ICEO. This technique is ideally

suited to control the motion of particles in channels with small dimensions as the motion is induced by the electric field interactions with particles and not by fluid displacement along the channels, which has higher resistance to fluid flow for channels with smaller dimensions. Simulations of electric field distribution in the channel concur with data obtained from the experiments. The simulated distribution of electric field in the channel is similar to the trajectory of the motion of the DNA molecules captured near the electrode edge at 10 V in a 100 μm wide and 20 μm deep channel. The simulations also indicate that the magnitude of the electric field decreases with the distance from the edge of the electrode, in agreement with the decrease in DNA velocity when the molecules are further away from the electrodes.

CHAPTER 6
SUMMARY AND FUTURE WORK

Micro- and nano-fluidic systems containing electrodes integrated with hydrophilic sealed Si channels have been fabricated and their sealing and wetting properties have been characterized. An immobilization technique, PADI, capable of rapidly immobilizing and stretching hundreds of DNA molecules in microchannels has been demonstrated. A technique to immobilize and stretch DNA molecules across electrode gaps using buffers with acidic and physiological pH in channels has been demonstrated. Mechanisms to control the motion of DNA and nanoparticles in channels by electric field interactions with particles without fluid flow along the channels have been presented. In this chapter, several key achievements in each of the above stated accomplishments will be summarized. A discussion of possible future research in these areas will be proposed.

6.1. Research Accomplished

Accomplishments achieved in the fabrication and characterization of fluidic systems, development of a novel DNA immobilization technique and its application in DNA mapping and DNA-protein interaction studies, DNA immobilization and stretching across electrode gaps in channels using electric field, and development of mechanisms to explain DNA and particle motion in channels induced by an ac voltage will be reviewed in this section.

6.1.1. Fabrication and Characterization of Integrated Fluidic Systems

The fabrication technology for integrating electrodes with sealed Si micro- and nano-channels along with the characterization of the wetting and sealing properties of the fluidic systems were presented in this work. Micro- and nano-channels were patterned and dry etched in Si. Electrodes and PMMA were patterned on a 100 μm thick glass substrate, followed by bonding the Si and glass substrates using PMMA as an adhesive layer. PMMA does not clog small channels during bonding due to its high viscosity at low temperature. Sealing of 350 nm wide and 100 nm deep Si channels with integrated electrodes has been demonstrated. The wetting property of the sealed channels was characterized by monitoring the motion of the capillary meniscus in 100 and 50 μm wide, 100 nm deep channels. The bond strength of PMMA bonding between glass and Si was determined at different bonding temperatures and PMMA thickness. A maximum bond strength of 3 MPa was obtained at a bonding temperature of 110 °C, bonding pressure of 0.4 MPa, and PMMA thickness of 600 nm. The bond strength is high enough to withstand the capillary pressure during the operation of the fluidic systems.

6.1.2. DNA Immobilization Technique for High Throughput Single-Molecule Analysis

A novel DNA immobilization technique, PADI, to immobilize and stretch DNA molecules in microchannels without causing overstretching has been demonstrated. In the PADI technique, DNA-interacting proteins such as restrictions enzymes and RNA polymerase are allowed to bind to the DNA molecule in bulk solution, followed by pumping the DNA-protein complex into a microchannel. The DNA-protein complex is stretched by the flow in the microchannel, followed by the adsorption of proteins present

on the DNA strand to the hydrophobic channel surface, resulting in immobilized and stretched DNA molecules in the microchannel. The immobilization is performed at physiological pH of 8.0 while maintaining continuous hydration of DNA molecules in the channel. Immobilization and stretching of hundreds of λ-DNA molecules in 100 μm wide and 1 μm deep channel is achieved in minutes. The DNA molecules are immobilized using different kinds of DNA-interacting proteins such as restriction enzymes, RNA polymerase, and DNA polymerase. The number of attachment points along the DNA strand to the microchannel surface is controlled by varying the protein concentration from 0.5 to 5 pM. Optical mapping and DNA-protein interactions have been demonstrated in the microchannels. Optical mapping of λ-DNA molecules using Sma 1 restriction enzyme has been performed in a 100 μm wide and 1 μm deep channel. The λ-DNA molecules are first immobilized and stretched in the microchannel, followed by introducing the enzyme Sma 1 into the microchannel. The enzyme Sma I cleaves the stretched DNA strand at specific sequences. The cuts on the DNA molecules are detected and analyzed from the images taken with a fluorescent microscope. Single-molecule transcription is demonstrated on immobilized and stretched DNA molecules in the microchannel. RNA transcripts synthesized by the enzyme RNA polymerase from NTPs are detected along the stretched DNA strand.

6.1.3. DNA Immobilization, Stretching, and Movement in Channels Using AC Voltage

Immobilization and stretching of DNA molecules across electrode gaps has been demonstrated using an ac voltage. DNA molecules in the channels outside of the electrode gap are also moved using an ac voltage. Using MES buffer with pH of 5.8,

DNA molecules are immobilized to the tip of an Au electrode integrated with a 100 μm wide, 75 μm deep microchannel. The immobilized DNA molecules stretched upto 11.5 μm across the electrode gap using a 100 KHz ac voltage. Immobilization of DNA molecules to Au electrodes at physiological pH of 8.0 is achieved by better confinement in smaller, 500 nm wide and 100 nm deep channels. Immobilization of DNA molecules at both ends to the electrodes is demonstrated by incorporating a floating electrode in between the electrode gap. The floating electrode reduces the electrothermal flow near the edge of the electrodes, enabling attachment of the second end of the DNA molecules to the floating electrode.

Velocity of DNA molecules present outside the electrode gap is controlled using an ac voltage applied across the electrode gap. The DNA molecules are moved away from the electrodes and their velocity is controlled by varying the voltage across the electrode gap. Velocity of DNA molecules upto 14.2 μm/s located at a distance of 1110 μm from the electrode gap is demonstrated in 100 μm wide, 20 μm deep channels.

6.1.4. Mechanisms of Voltage Induced DNA and Particle Motion in Channels

Mechanisms of ac voltage induced DNA and particle motion in channels using the ICEO phenomenon have been presented. The DNA and particle motion are induced by electric field interactions with particles and not by fluid flow along the channels. Therefore, this motion is not limited by the increase in flow resistance in smaller channels, making it ideally suited for controlling motion of particles in small channels. The motion of particles is away from the electrodes and the velocity of the particles is controlled by the ac voltage. DNA Velocity upto 10 μm/s is demonstrated in 1 μm wide, 400 nm deep channels using 100 KHz ac voltage. Motion is induced in DNA and 20 nm

polystyrene particles present at a distance >1 mm from the electrodes using a 100 KHz ac voltage. Simulations of electric field distribution in the channels provide a qualitative explanation of the trajectory and velocity variation of DNA motion induced by an ac voltage in channels.

6.2. Future Work

Future work in developing nanofluidic systems for sequence specific DNA-protein interaction studies, nanoelectronics fabrication using self-assembly property of carbon nanotube (CNT) on stretched DNA molecules, and DNA mapping using the PADI technique will be presented.

6.2.1. Next Generation Integrated Nanofluidic Systems

Protein interaction studies and manipulations at specific sequences on the DNA strand have not been possible to date due to the lack of fluidic systems capable of providing precise control over the locations of DNA-protein interactions on the DNA strand. We propose an integrated nanofluidic systems to control DNA-protein interactions and their locations using an ac electric field. We have demonstrated control over the motion and placement of DNA molecules in integrated fluidic systems using an electric field. The velocity and position of the DNA molecules in channels are controlled by varying the voltage. To perform DNA-protein interactions at specific sequences on the DNA molecule, a nanofluidic system capable of accessing specific DNA sequences needs to be developed. This can be achieved by placing a stretched DNA molecule at a specific location within a nanochannel and have proteins interact with the DNA at that location. Such a system would be applied in performing manipulation or repair of specific DNA

sequences using DNA-interacting proteins. Apart from controlling the location of protein interactions, a similar nanofluidic system can be developed to control the protein interactions with the DNA strand using an electric field. Such a system will lead to the development of new nanoscale DNA-protein interaction experiments. In this section, integrated nanofluidic systems for performing sequence specific DNA manipulations and voltage controlled DNA-protein interactions are presented. Examples of single-molecule experiments that could be performed using the integrated nanofluidic system are also presented.

6.2.1.1. Control of Location of DNA Molecules in Nanochannels

In order for the proteins to access specific sequences on the DNA strand, we propose introducing a protein nanochannel perpendicular to the DNA nanochannels as shown in Fig. 6.1. The protein molecules can be focused onto a specific site on the DNA strand.

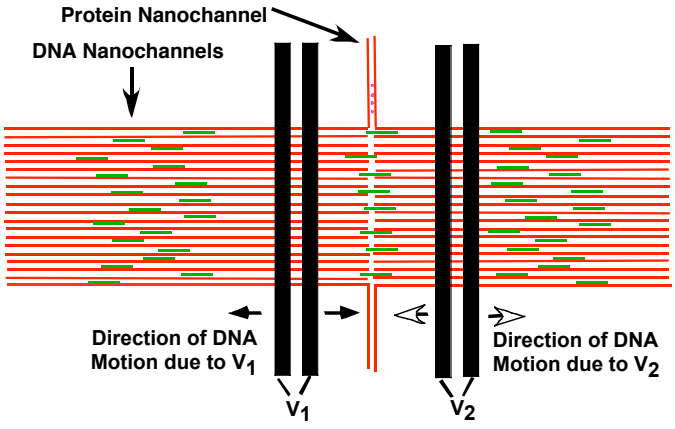

Fig. 6.1 Schematic of integrated nanofluidic system where proteins in vertical nanochannel interact with DNA present in horizontal nanochannel.

The location of the DNA strand with respect to the protein nanochannel can be controlled using a dual electrode pair system. For example, if protein interaction studies

and manipulations are required to be conducted on a sequence present at the left end of the DNA molecule, the stretched DNA strand can be moved by the applied voltage on each electrode pair such that the left section of the strand intersects with the protein nanochannel. The proteins introduced in the nanochannel would then interact with the specific site on the DNA strand.

Currently, studies of how proteins would interact with each other when translocating along the same DNA strand have not been possible due to the lack of fluidic systems capable of controlling the location of one or more protein interactions on the DNA strand. A modified version of the integrated nanofluidic system proposed above can be built to perform protein interactions at two specific locations on the DNA strand. In such a system, two protein nanochannels would intersect with the stretched DNA strand. Proteins from each nanochannel would translocate along the DNA strand, causing them to cross each other and interact on the strand. This study may lead to uncovering new phenomenon of how proteins would interact or coordinate with each other when moving along the same strand.

Apart from the multiple protein translocation studies, the effect of one protein binding to the DNA on other protein interactions on the same DNA strand can also be studied using the dual protein nanofluidic system. Studies have shown that the force applied by proteins such as lac repressor on the DNA strand inhibits other DNA-protein interactions such as transcription process on the DNA strand [99]. Our proposed system would enable studies on distance of influence that proteins exert to inhibit other interactions. For example a protein interaction inhibitor such as lac repressor can be introduced in the first nanochannel and another kind of protein such as a restriction

enzyme, which cuts the DNA strand, can be introduced into the second nanochannel. The distance between the two protein nanochannels can be varied to study how far across the strand the protein inhibitor influences other protein interactions. If the distance between the two protein nanochannels is over 5 μm and the distance of the influence of the protein inhibitor is less than 5 μm from the point of interaction, then the restriction enzyme would cut the DNA molecule, which could be detected with a fluorescent microscope. This is one example of nanoscale DNA-protein interactions that can be performed and studied using the proposed system. Different kinds of DNA-interacting proteins can be chosen and the appropriate experiments can be designed using the nanoscale level control over the motion and position of DNA and protein molecules that this system would be capable of providing.

6.2.1.2. Control of DNA-Protein Interactions Using Electric Field

We have introduced fluidic systems and methods to control the motion and location of stretched DNA molecules in nanochannels and to achieve control over the location of DNA-protein interactions on the stretched DNA strand. We have demonstrated control over the motion of DNA and 20 nm polystyrene particles using an ac voltage. We propose to control the motion and interactions of protein molecules using an ac voltage, in a manner similar to the voltage controlled DNA and nanoparticles motions, to study DNA-protein interactions and the influence of electric field over these interactions. Studies have shown that electric field plays an important role in determining the protein structure and functionality [100], [101]. Electric field originating from ionic molecules is present at the active site of the protein, hence it likely plays an important role in protein interactions with other biomolecules such as DNA [101], [102]. The

electric field distribution in the proteins has been determined from the electrostatic calculations and their intensity is found to be in the order of 1 MV/cm [101]. Generating electric field of 1 MV/cm magnitude is feasible using microfabricated electrodes. Therefore we propose an integrated nanofluidic system to influence and control DNA-protein interactions using electric field derived from the integrated electrodes placed near the site of the DNA-protein interactions. A schematic of our proposed system to study and control DNA-protein interactions using electric fields is shown in Fig. 6.2.

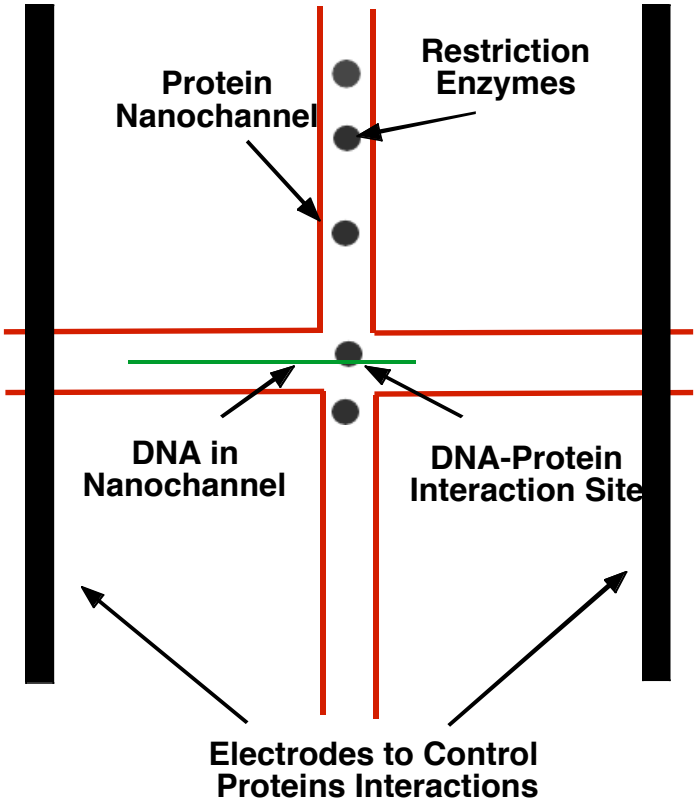

Fig. 6.2 Schematic of integrated nanofluidic system where proteins such as restriction enzymes in vertical nanochannel interact with DNA present in horizontal nanochannel. Electric field in order of 1 MV/cm applied across electrodes can be used to control protein interactions.

In our proposed experiment, a stretched DNA molecule in a nanochannel is located near the electrodes, where sufficient electric field strength can be generated. A protein introduced into the vertical nanochannel would interact with the DNA under the presence of an electric field. The electric field would influence the protein motion and interactions along the DNA strand. For example, if a restriction enzyme is used, then the electric field could be applied such that the cutting of the DNA strand by the restriction enzyme is controlled by the electric field. The cutting action of the restriction enzyme can be detected using a fluorescent microscope. Using this system, experiments can be performed on many kinds of DNA-interacting proteins and the role of the electric field in protein interactions could be better understood.

6.2.1.3. Immobilization of DNA Molecules by Selective Surface Modification

Manipulation of specific DNA sequences using proteins requires immobilization of stretched DNA molecules at specific location in the nanochannels. This would enable proteins to interact with a specific sequence on the stretched DNA molecule. We propose to move DNA molecules to a desired location in the nanochannels using dual electrodes as described in Fig. 6.1, followed by immobilizing the ends of the DNA molecules. The ends can be immobilized at selected sites whose surface is modified to enable DNA attachment, while the rest of the DNA backbone is free from surface interactions as shown in Fig. 6.3.

Surface modification for DNA immobilization can be performed by specific surface patterning using proteins or by changing the surface energy. We have demonstrated DNA immobilization using DNA-interacting proteins in PADI. DNA molecules in the vicinity of a surface patterned with DNA-interacting proteins such as

RNA polymerase would interact with the proteins, causing the strand to be immobilized. This principle can be used to immobilize the two ends of a DNA molecule in the nanochannel by patterning selected areas of the nanochannel with DNA-interacting proteins. DNA molecules can also be immobilized to hydrophobic surfaces at a pH range of 5.5 to 6.6. Hydrophobic treatment of selected areas in a nanochannel would enable the ends of a DNA strand to immobilize on the surface, while the rest of the backbone exposed to the hydrophilic surface is free from surface attachment.

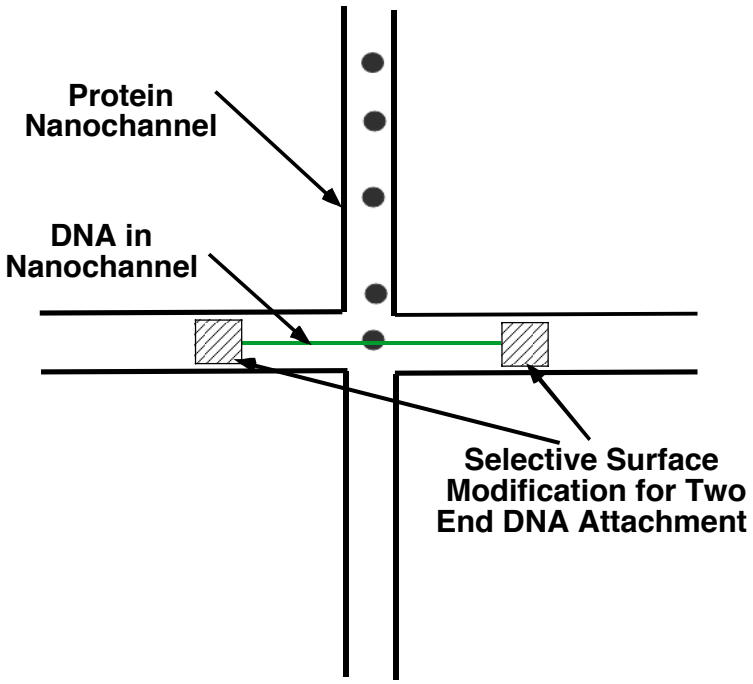

Fig. 6.3 Schematic of nanofluidic system whose surface is modified at specific locations to enable two ends of DNA to attach to channel surface while rest of DNA backbone is free from surface interactions, which enables protein interactions at specific DNA sequences.

6.2.2. Self-Assembly of Carbon Nanotube on DNA Stretched Across Electrode Gaps

CNT transistors have been fabricated using DNA molecules as a template, where the CNT acts as a channel of the transistor [103]. This was first achieved by stretching a DNA molecule, followed by self-assembly of a CNT on the DNA strand. The self-

assembly is achieved by introducing a CNT with recA proteins which recognize specific DNA sequences. Following self-assembly, the DNA molecule is metallized using metal nanoparticles and connected across the microfabricated electrode gaps. A major drawback of the current technology is that the DNA molecules are randomly immobilized and stretched on a substrate using DNA combing. Logic circuits from DNA-CNT transistors cannot be fabricated from randomly placed DNA molecules.

We propose to fabricate DNA-CNT transistors and logic circuits using the techniques of precise DNA immobilization and stretching across electrode gaps that have been presented in this thesis. We have demonstrated the capability to immobilize and stretch DNA molecules controllably across electrode gaps, in contrast to DNA combing, where the DNA molecules are immobilized and stretched at random locations. In order to fabricate logic circuits such as an inverter from DNA-CNT units, we would design the electrodes so that DNA-CNT units are stretched across multiple electrode gaps that are connected in an inverter configuration. Shown in Fig. 6.4 is a schematic of an inverter with two transistors that would be fabricated from the stretched DNA molecules with CNT self-assembled on top. The appropriate type of CNT can be chosen to obtain either a p-type or an n-type transistor.

The top transistor is a carrier of holes, allowing it to act as a positive metal oxide semiconductor (PMOS) device and the bottom transistor is a carrier of electrons, allowing it to act as a negative metal oxide semiconductor (NMOS) device. The two transistors are connected in an inverter configuration. The electrode acts as a gate to modulate the current in the CNT that acts as a channel of the transistor. The CNT can be self-assembled on the DNA molecules either before or after stretching the DNA

molecules. Similar concepts can be applied to the fabrication of more complex logic circuits such as adders and multiplexers. Hence our technique of immobilizing and stretching DNA molecules across electrode gaps can be applied to realizing nanoelectronic logic circuits using self-assembly of CNT, without the need for complex nanofabrication techniques such as nanowires growth and electron beam lithography.

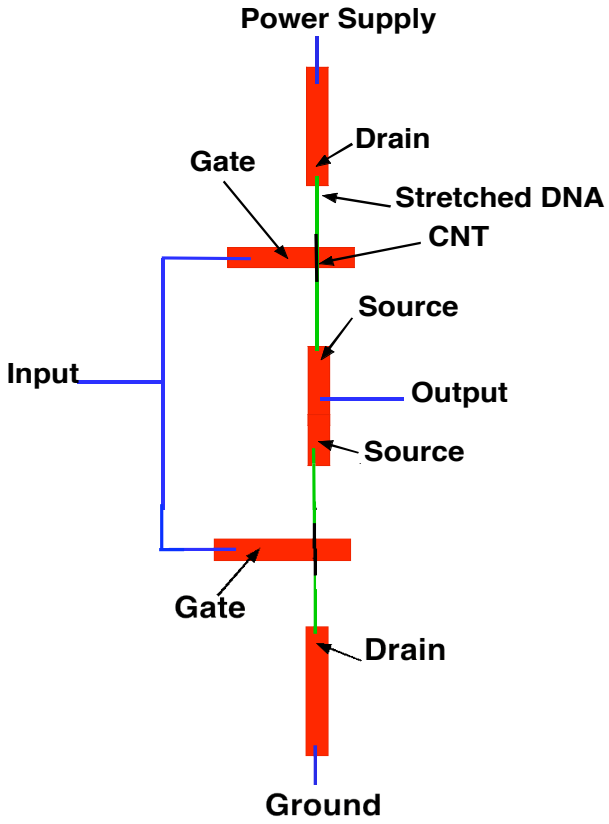

Fig. 6.4 Schematic of inverter fabricated from self-assembly of CNT on stretched DNA molecules. DNA molecules are stretched across electrode gaps that are connected in inverter configuration. Gates modulate current in CNT, which acts as channel of transistor.

6.2.3. Molecular Diagnostics and Biomarker Discovery Using PADI Technique

The crucial requirement for single-molecule DNA analysis for applications in molecular diagnostics and biomarker discovery is the ability to rapidly analyze hundreds of immobilized and stretched DNA molecules. We have demonstrated optical mapping

on stretched DNA molecules. Optical mapping is performed by detecting cuts on the stretched DNA strand due to restriction enzymes, with each cut corresponding to a specific sequence recognized by the restriction enzyme. The number of sequences that can be detected by using restriction enzymes is limited since each enzyme cuts only one type of sequence, and there are only limited numbers of types of restriction enzymes that are available. A capability to detect any desired sequence is required for DNA immobilization and stretching to be useful in biomedical applications.

We propose to improve DNA mapping over the use of restriction enzymes by attaching fluorescent tags that could recognize specific sequences on the DNA strand. Peptide nucleic acid (PNA) is one such molecule whose sequence can be designed so that it is able to attach to a specific sequence on the double strand DNA molecule. PNA structure is similar to the DNA molecule except the backbone does not have sugar and negatively charged phosphate groups but is instead composed of n-(2-aminoethyl)-glycine units linked by peptide bonds [104]. Since the backbone of PNA contains no charged phosphate groups, the binding between PNA/DNA strands is stronger than between DNA/DNA strands due to the lack of electrostatic repulsion. Fluorescent tagged PNA molecules attached to the dsDNA molecule can be detected on the stretched DNA molecules as shown in Fig. 6.5.

Fig. 6.5 Schematic of stretched DNA molecule with fluorescently labeled PNA molecules attached to DNA at specific sequences. Each arrow indicates individual PNA molecule. DNA mapping can be performed by detecting fluorescently labeled PNA molecules on hundreds of immobilized and stretched DNA molecules in microchannel generated using PADI technique.

The combination of the PADI technique and sequence recognition using PNA molecules can be used to rapidly perform sequence detections on the DNA molecule, which is a requirement for molecular diagnostics and biomarker discovery. Other DNA immobilization and stretching techniques such as DNA combing and modified positively charged surfaces cannot be used to perform DNA mapping using PNA tags since the DNA molecules are overstretched, causing structural deformation in the DNA and resulting in instabilities in attachment between the PNA and DNA molecules.

6.3. Conclusions

Future work based on developing integrated nanofluidic systems for sequence specific DNA-protein interactions and electric field controlled interactions has been presented. Fabrication of logic circuits by self-assembly of CNT on DNA molecules has been conceived. DNA mapping using PNA molecules and PADI technique for applications in molecular diagnostics and biomarker discovery has been proposed.

Development of fluidic systems that enable new DNA-protein interaction experiments is essential for understanding the complex steps involved in protein interactions. The ability to control the location of DNA-protein interactions on the DNA strand is key to performing specific sequence manipulations on the DNA molecules using proteins.

The self-assembly property of DNA molecules can be utilized to fabricate nanoelectronics without using complex nanofabrication techniques. Controlled DNA immobilization and stretching of DNA-CNT complex across electrode gaps is essential to realizing transistors and logic circuits from the DNA-CNT complexes.

The ability to detect sequences along the DNA strand is crucial for DNA immobilization and stretching to be useful in biomedical applications. The use of PNA tags combined with the PADI technique allows rapid detection of specific sequences along hundreds of immobilized and stretched DNA molecules.

APPENDIX A
Fabrication of Integrated Fluidic Systems

Electrodes are integrated with Si micro- and nano-channels using PMMA as an adhesive layer for bonding to glass. Electrodes and PMMA are pattered on a 100 μm thick glass, while channels are patterned on a Si substrate. Microchannels with widths ranging from 500 nm – 100 μm are patterned using UV optical lithography. 350 nm wide channels are patterned using nanoimprint. Si channels are typically included in a sample size of 4.5×4.5 cm^2 in a Si substrate. The electrodes and patterned PMMA are typically included in a sample size of 5×5 cm^2 on a glass substrate.

Fabrication of 10 - 100 μm Wide Si Microchannels

a. Spin 1827 resist @4 K RPM for 30 s to 3 μm thick
b. Soft bake for 90 s @110 °C on hotplate
c. Expose using Karl Suss MA6 mask aligner for 15 s with a light intensity of 5 W/cm^2 (The mask typically consists of twelve 100 μm wide channels)
d. Develop in MF319 developer for 60 s
e. Etch in SF_6 plasma at 100 sccm, 100 W, 250 mTorr for 3 min to depth of 1 μm

Fabrication of 500 nm - 1 μm Wide Si Channels

a. Spin 1827 resist @5 K RPM for 30 s to 2.5 μm thick
b. Soft bake for 90 s @110 °C on hotplate

c. Expose using UV optical Stepper ($5X_t$ reduction) for 5 s for 500 nm wide channels with a light intensity of 300 W/cm^2 (The mask consists of fifty 5 μm wide channels and each channel separated by 5 μm)

d. Expose using UV optical Stepper (5 X_t reduction) for 15 s for 1 μm wide channels with a light intensity of 300 W/cm^2 (using the same mask consists of fifty 5 μm wide channels and each channel separated by 5 μm)

e. Develop in MF319 developer for 45 s

f. Etch in Cl_2 plasma at 20 sccm, 600 W ICP power, 200 W rf power, 5 mTorr for 30 s to a depth of 100 nm

Fabrication of 350 nm Wide Si Channels

a. Spin A6 950 K PMMA @4 K RPM for 80 s on 4 inch Si Wafer to 400 nm thick

b. Soft bake for 60 s @180 °C on hotplate

c. Clean Si mold by 1:1 H_2SO_4:H_2O_2 for 20 min and dry in N_2 after water rinse

d. Put 2-3 drops of FDTS and Si mold with 350 nm wide channels in a glass container covered with lid

e. Place the glass container on a hot plate @140 °C for 50 min

f. Place the Si mold with channel side on top of a Si surface coated with 400 nm thick PMMA and place in Obducat Nanoimprinter

g. Apply a pressure of 70 MPa and temperature of 200 °C for 15 min

h. After cooling to room temperature, separate the mold and Si substrate with channels imprinted on PMMA

i. Etch 100 nm deep channels in a LAM RIE system using Cl_2 plasma at 20 sccm, 5 mTorr pressure, 600 W rf power, and 200 W ICP power for 30 s

j. Remove PMMA in acetone @100 °C for 20 min

Fabrication of Inlet/Outlet Holes and 4.5×4.5 cm^2 Si Samples with Channels

a. Clean 4 inch Si wafers with channels in 1:1 H_2SO_4:H_2O_2 for 20 min and dry in N_2 after water rinse

b. Deposit 1 µm thick PECVD oxide over Si channels using SiH_4 at 45 sccm, N_2O at 2000 sccm, He at 250 sccm, 500 mTorr pressure, 100 W rf power, and at 200 °C in GSI PECVD system

c. Spin 9260 resist @2 K RPM for 30 s to 10 µm thick on the back side of the wafer

d. Soft bake for 6 min @110 °C on hotplate

e. Perform back side alignment with alignment marks present on the channels side to alignment marks on the mask with inlet/outlet holes using Karl Suss MA6 mask aligner for 100 s with a light intensity of 5 W/cm^2 (The mask consists of a total of twenty-four 300 µm diameter holes and 500 µm thick border around the 4.5×4.5 cm^2 sample to etch channel chips out of the 4 inch wafer)

f. Develop in 1:3 AZ400K:H_2O developer for 4 min

g. Spin 1827 resist @2 K RPM for 30 s to 4 µm thick on a Si carrier wafer

h. Place the Si wafer with channels on top of the carrier wafer with resist coating and place the channels facing the resist

i. Press the wafers against each other and place them on a hot plate at 110 °C for 8 min

j. Perform through wafer etch for 3 h using a STS DRIE system. A source power of 600 W and a stage power of 100 W are used at 26 mTorr and with 105 sccm SF_6 in the 14 s etch cycles. A 75 W source power is applied with no stage power at 16 mTorr and 40 sccm C_4F_8 in the 4 s passivation cycles.

k. Separate the wafers by removing the resist in PRS 2000 at 100 °C, resulting in 4.5×4.5 cm^2 samples containing Si channels and inlet/outlet holes

Fabrication of Electrodes and PMMA Patterns on 100 µm Thick Glass

a. Clean 5×5 cm^2 glass wafers in 1:1 H_2SO_4:H_2O_2 for 20 min

b. Dry glass wafers using N_2 gas following rinsing in DI water

c. Evaporate 20 nm thick Cr and 50 nm thick Au on glass using Enerjet Evaporator

d. Spin 1827 resist @4 K RPM for 30 s to 3 µm thick

e. Soft bake for 90 s @110 °C on hotplate

f. Expose using MJB6 mask aligner for 15 s with a light intensity of 5 W/cm^2 (The mask consists of twelve electrode pairs and the distance between electrode in each pair is 15 µm)

g. Develop in MF 319 developer for 90 s

h. Etch Au in 4g:1g:50ml KI:I_2:H_2O solution for 45 s

i. Etch Cr in CR-14 etchant for 45 s

j. Remove resist in PRS 2000 at 100 °C for 4 h

k. Spin A6 950 K PMMA @2.5 K RPM to 600 nm on glass wafer with Cr/Au patterns

l. Soft bake for 60 s @180 °C on hotplate

m. Evaporate 10 nm thick Ti using Enerjet Evaporator

n. Spin 1827 resist @4 K RPM for 30 s to 3 µm thick

o. Soft bake for 90 s @105 °C on the hotplate (The soft bake should be done below the glass transition temperature of PMMA to prevent damage of PMMA)

p. Expose using MJB6 mask aligner for 15 s with a light intensity of 5 W/cm^2 (The mask consists of 12 set of rectangle patterns with each pattern exposing areas near electrode gap and metal pads)

q. Develop in MF 319 for 30 s

r. Etch Ti in 40:1:1 H_2O: H_2O_2:HF solution for 10 s

s. Etch PMMA using O_2 plasma at 100 sccm, 250 mTorr pressure, and 100 W power for 10 min in a RIE system

t. Remove 1827 resist using PRS 2000 at room temperature for 45 min (The removal should be done at room temperature to prevent the PMMA from peeling of from the glass surface)

u. Remove Ti in 40:1:1 H_2O: H_2O_2:HF solution for 10 s (The etch time should not be greater than 13 s to prevent the etchant from damaging the PMMA surface)

Bonding of Si Channels with Glass Containing Electrodes

a. Clean Si wafer with channels and inlet/outlet holes in 1:1 H_2SO_4:H_2O_2 for 20 min

b. Dry Si wafer using N_2 gas following rinsing in DI water

c. Clean 4 inch pyrex glass wafer with acetone and isoproponal alcohol (IPA)

d. Put a drop of DI water on center of pyrex wafer and place the glass with patterned electrodes on the drop (The pyrex wafer is used to prevent the glass wafer from bending when it is vacuumed during alignment)

e. Align Si channels with electrodes on glass using EVG 501 aligner

f. Transfer the aligned wafers from the aligner to EVG 501 bonder

g. Perform bonding at 0.4 MPa pressure, 75 Torr vacuum, and 110 °C for 20 min

h. After cooling to room temperature, detach the bonded wafers from the pyrex glass

Bonding of Si Channels with Plain Glass for PADI Technique

a. Clean Si wafer with channels in 1:1 H_2SO_4:H_2O_2 for 20 min

b. Dry the Si wafer using N_2 gas following rinsing in DI water

c. Clean 5×5 cm^2 glass wafer in 1:1 H_2SO_4:H_2O_2 for 20 min

d. Dry the glass wafer using N_2 gas following rinsing in DI water

e. Spin A6 950 K PMMA @2.5 K RPM to 400 nm thick on glass wafer

f. Soft bake for 60 s @180 °C on hotplate

g. Place the Si and glass wafers in EVG 501 bonder

h. Perform bonding at 0.4 MPa pressure, 75 Torr vacuum, and 110 °C for 20 min

APPENDIX B
DNA and Protein Sample Preparation

Labeling DNA Molecules with YOYO Fluorescent Probes

a. Prepare unlabled DNA (Sigma-Aldrich, St. Louis, MO) sample to a concentration of 1.5 ng/µl in TRIS-EDTA buffer

b. Prepare YOYO-1 dye (Invitrogen Corporation, Carlsbad, CA) to a concentration of 0.1 µM in TRIS-EDTA buffer

c. Mix 1 ng of DNA to 3 µl of 0.1 µM YOYO dye for 5:1 base to dye ratio DNA molecules

Preparing Labeled DNA Molecule Sample

a. Mix required amount of DNA sample to specific concentration in TRIS-EDTA buffer

b. Centrifuge the DNA sample for 10 s

Preparing DNA-Protein Complex for PADI Technique

a. Mix required amount of labeled DNA sample to specific concentration in TRIS-EDTA buffer in a vial

b. Mix required amount of proteins with the DNA sample

c. Centrifuge the DNA-protein complex for 10 s

APPENDIX C
Fluorescent Microscope Interface and Operation

Interfacing Fluidic System to Fluorescent Microscope (Fig. A1)

a. Connect electrodes on glass to contact pads on Printed Circuit Board (PCB) using a wire bonder

b. Place the wafer-PCB unit on microscope objective with glass facing the objective and Si wafer with channels and inlet/outlet holes on top (This configuration enables access to inlet/outlet ports present on top and at the same time electrical contact to electrodes)

c. Power supply is connected to contact pads of the PCB board using probe connectors

d. Focus the microscope objective at the inlet port followed by focusing at the channel

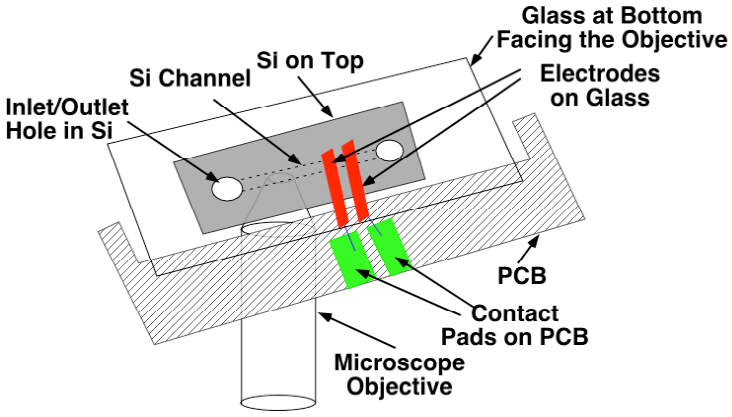

Fig. A1. Schematic of microscope setup showing one channel and a pairs of inlet/outlet holes in Si integrated with an electrode pair. The bonded Si and glass wafers are wire bonded to a PCB board. The wafer-PCB board unit is placed on top of a microscope objective with glass facing the objective piece. The inlet/outlet holes in Si are accessible from the top while the channels in Si shown as dotted lines are not visible from the top. (not drawn to scale).

Microscope Operation

a. Switch on fluorescent lamp

b. Switch on stage power

c. Switch on microscope power

d. Through Metavue software enable fluorescent light through the microscope objective (Select Acquire/Exposure)

e. Put two drops of oil on the objective piece

f. Place the wafer-PCB unit on the microscope objective

g. Focus the objective using the wheel located at the base of the microscope

h. Pictures are taken by clicking the Acquire button

i. Videos are recorded as Stream/Stream Acquisition/Acquire

Avoiding Bubble Formation

a. When filling a channel array with narrow channel width, including a channel with wider channel width that is parallel to the narrow channels allows unobstructed capillary filling of fluid, thus reducing bubble formation

b. Using a buffer such as TRIS-EDTA, which has higher surface tension with oxidized Si surface compared to H_2O, will result in faster filling of channel thus reducing bubble formation in channels

c. Raise the voltage across electrodes slowly in range of 0-20 V to reduce bubble formation

d. Frequency >50 KHz reduces bubble formation

e. Voltage >20 V increases bubble formation

References

[1] R. Riehn, M. Lu, Y. Wang, S. F. Lim, E. C. Cox, and R. H. Austin, "Restriction mapping in nanofluidic devices", *Proc. Natl. Acad. Sci. U.S.A.*, vol. 102, pp. 10012-10016, 2005.

[2] T. R. Strick, V. Croquette, and D. Bensimon, "Single-molecule analysis of DNA uncoiling by a type II topoisomerase", *Nature*, vol. 404, pp. 901-904, 2000.

[3] C. Bustamante, Z. Bryant, and B. S. Smith, "Ten years of tension: single-molecule DNA mechanics", *Nature*, vol. 421, pp. 423-427, 2003.

[4] A. M. van Oijen, P. C. Blainey, D. J. Crampton, C. C. Richardson, T. Ellenberger, and X. S. Xie, "Single-molecule kinetics reveal base dependence and dynamic disorder of lambda exonuclease", *Science*, vol. 301, pp. 591-605, 2003.

[5] H. Kabata, O. Kurosawa, I. Arai, M. Washizu, S. A. Margarson, R. E. Glass, and N. Shimamoto, "Visulatization of single molecule dynamics of RNA polymerase sliding along DNA", *Science*, vol. 262, pp. 1561-1563, 1993.

[6] R. G. Sosnowski, E. Tu, W. F. Butler, J. P. Connell, and M. J. Heller, "Rapid determination of single base mismatch mutations in DNA hybrids by direct electric field control", *Proc. Natl. Acad. Sci. U.S.A*, vol. 94, pp. 1119-1123, 1997.

[7] M. G. Strainic, J. J. Sullivan, A. Velevis, and P. L. deHaseth, "Promotor recognition by e-coli RNA polymerase: effects of the up element on open complex formation and promotor clearance", *Biochemistry*, vol. 37, pp. 18074-18080, 1998.

[8] E. Petricon, D. Ornstein, and L. Liotta, "Clinial Proteomics: Applications of prostrate cancer biomarker discovery and detection", *Urol. Oncol.*, vol. 22, pp. 322-328, 2004.

[9] V. Espina, E. Woodhouse, J. Wulfkuhle, H. Asmussen, E. Petricoin, and L. Liotta, "Protein microarray detection strategies: focus on direct detection technologies", *J. Immunol. Methods*, vol. 290, pp. 121-133, 2004.

[10] X. S. Xie and J. K. Trautman, "Optical studies of single molecules at room temperature", *Annu. Rev. Phys. Chem.*, vol. 49, pp. 441-480, 1998.

[11] M. B. Miller "Practical DNA technology in school", *J. Biol. Education.*, vol. 28, pp. 203-211, 1994.

[12] M. Unlu, M. E. Morgan, and J. S. Minden, "Difference gel electrophoresis: a single gel method for detecting changes in protein extracts", *Electrophoresis*, vol. 18, pp. 2071-2077, 1997.

[13] T. Kuukasjarvi, M. Tanner, S. Pannanen, R. Karhu, T. Visakorpi, and J. Isola, "Optimizing DOP-PCR for universal amplification of small DNA samples in comparative genomic hybridization", *Genes Chromosomes Cancer*, vol. 18, pp. 94-101, 1997.

[14] L. Chen, A. Manz, and P. J. Day, "Total nucleic acid analysis integrated on microfluidic devices", *Lab Chip*, vol. 7, pp. 1413-1423, 2007.

[15] J. H. Kim, V. R. Dukkipati, S. W. Pang, and R. G. Larson, "Stretching and immobilization of DNA for studies of protein-DNA interactions at the single-molecule level", *Nanoscale Res. Lett.*, vol. 2, pp. 185-201, 2007.

[16] M. Sotomayor and K. Schulten, "Single-molecule experiments in vitro and in silico", *Science*, vol. 316, pp. 1144-1148, 2007.

[17] J. D. Wulfkuhle, L. A. Liotta, and E. F. Petricon, "Proteomic applications for the early detection of cancer", *Nature Rev*., vol. 3, 267-275, 2003.

[18] P. H. Dear "One by one: Single molecule tools for genomics", *Brief Func. Genomic Proteomic*., vol. 1, pp. 397-416, 2003.

[19] I. Braslavsky, B. Hebert, E. Kartlov, and S. R. Quake, "Sequence information can be obtained from single DNA molecules", *Proc. Natl. Acad. Sci. U.S.A.,* vol. 100, pp. 3960-3964, 2003.

[20] J. Shendure, R. Mitra, C. Varma, and G. M. Church, "Advanced sequencing technologies: methods and goals", *Nature Rev. Genet*., vol. 5, pp. 335-344, 2004.

[21] K. M. Herbert, A. L. Porta, B. J. Wong, R. A. Mooney, K. C. Neumann, R. Landlick, and S. M. Block, "Sequence resolved detection of pausing by single RNA polymerase molecules", *Cell*, vol. 125, pp. 1083-1094, 2006.

[22] C. Bai, C. Wang, X. S. Xie, and P. G. Wolynes, "Single molecule physics and chemistry", *Proc. Natl. Acad. Sci. U.S.A.,* vol. 96, pp. 11075-11076, 1999.

[23] Y. Kimura and P. R. Bianco, "Single molecule studies of DNA binding proteins using optical tweezers", *Analyst*, vol. 131, pp. 868-874, 2006.

[24] Z. Gueroui, C. Place, E. Freyssingeas, and B. Berge, "Observation of fluorescence microscopy of transcription on single combed DNA". *Proc. Natl. Acad. Sci. U.S.A.,* vol. 99, pp. 6005-6010, 2002.

[25] J. Jing, J. Reed, J. Huang, X. Hu, V. Clarke, J. Edington, D. Housman, T. S. Anaanthraman, E. J. Huff, B. Mishra, B. Porter, A. Shenker, E. Wolfson, C. Hiort, R. Kantor, C. Aston, and D. C. Schwatrtz, "Automated high resolution optical mapping using arrayed, fluid fixed DNA molecules", *Proc. Natl. Acad. Sci. U.S.A.,* vol. 95, pp. 8046-8051, 1998.

[26] T. Yamamoto, O. Kurosawa, H. Kabata, N. Shimamoto, and M. Washizu, "Molecular surgery of DNA based on electrostatic micromanipulation", *IEEE Trans. Indst. Appl.*, vol. 36, pp. 1010-1017, 1990.

[27] L. Bai, T. J. Santangelo, and M. B. Wang, "Single-molecule analysis of RNA polymerase transcription", *Annu. Rev. Biomol. Struct.*, vol. 35, pp. 343-360, 2006.

[28] J. F. Allemand, D. Bensimon, L. Jellien, A. Bensimon, and V. Croquette, "pH-dependent specific binding and combing of DNA", *Biophys. J.,* vol. 73, pp. 2064-2070, 1997.

[29] D. C. Schwartz, X. Li, L. Hernandez, S. P. Ramnarain, E. J. Huff, and Y. K. Wang, "Ordered restriction maps of saccharomyces cerevisiae chromosomes constructed by optical mapping", *Science*, vol. 262, pp. 110-114, 1993.

[30] A. Ashkin, J. M. Dziedic, J. E. Bjorkholm, and S. Chu, "Observation of a single-beam gradient force optical trap for dielectric particles", *Opt. Lett.*, vol. 11, pp. 288-294, 1986.

[31] K. C. Neuman and S. M. Block, "Optical trapping", *Rev. Sci. Instrum.*, vol. 75, pp. 2787-2809, 2004.

[32] S. B. Smith, L. Finzi, and C. Bustamante, "Direct mechanical measurements of the elasticity of single DNA molecules by using magnetic beads", *Science*, vol. 258, pp. 1122-1126, 1992.

[33] C. Gosse and V. Croquette, "Magnetic tweezers: micromanipulation and force measurement at the molecular level", *Biophys. J.*, vol. 82, pp. 3314-3329, 2002.

[34] M. Washizu, O. Kurosawa, I. Arai, S. Suzuki, and N. Shimamoto, "Applications of electrostatic stretch-and-positioning of DNA", *IEEE Trans. Indst. Appl.*, vol. 31, pp.447-456, 1995.

[35] V. Namasivayam, R. G. Larson, D. T. Burke, and M. A. Burns, "Electrostretching DNA molecules using polymer enhanced media within microfabricated devices", *Anal. Chem.*, vol. 74, pp. 3378-3385, 2002.

[36] W. A. Germishuizen, C. Walti, R. Wirtz, B. M. Johnston, M. Pepper, A. G. Davies, and A. P. J. Middelberg, "Selective dielectrophoresis manipulation of surface-immobilized DNA molecules", *Nanotechnology*, vol. 14, pp. 896-902, 2003.

[37] A. Bensimon, A. Simon, A. Chiffaudel, V. Croquette, F. Heslot, and D. Besimon, "Alignment and sensitive detection of DNA by a moving interface", *Science*, vol. 265, pp. 2096-2098, 1994.

[38] X. Michalet, R. Ekong, F. Fougerousse, S. Rousseaux, C. Schurra, N. Hornigold, M. van Slegtenhorst, J. Wolfe, S. Povey, J. S. Beckmann, and A. Bensimon, "Dynamic molecular combing: stretching the whole human genome for high-resolution studies", *Science*, vol. 277, pp. 1518-1523, 1997.

[39] M. Chopra, L. Li, H. Hu, M. A. Burns, and R. G. Larson, "DNA molecular configurations in a evaporation droplet near a glass surface", *J. Rheology*, vol. 47, pp. 1111-1132, 2003.

[40] E. Y. Chen, N. M. Goncalves, R. A. Haeusler, A. J. Hatch, J. W. Larson, A. M. Maletta, G. R. Yantz, E. D. Carstea, M. Fuchs, G. G. Wong, S. R. Gullans, and R. Gilmanshin, "DNA mapping using microfluidic stretching and single-molecule detection of fluorescent site-specific tags", *Genome Res.*, vol. 14, pp. 1137-1146, 2004.

[41] W. Reisner, K. J. Morton, R. Riehn, Y. M. Wang, Z. Yu, M. Rosen, J. C. Sturm, S. Y. Chou, E. Frey, and R. H. Austin, "Statics and dynamics of single DNA molecules confined in nanochannels", *Phys. Rev. Lett.*, vol. 94, pp. 196101-4, 2005.

[42] Y. M. Wang, J. O. Tegenfeldt, W. Reisner, R. Riehn, X. J. Guan, L. Guo, I. Golding, E. C. Cox, J. Sturm, and R. H. Austin, "Single-molecule studies of repressor-DNA interactions show long-range interactions" *Proc. Natl. Acad. Sci. U.S.A.,* vol. 102, pp. 9796-9801, 2005.

[43] V. R. Dukkipati, J. H. Kim, S. W. Pang, and R. G. Larson, "Protein-assisted stretching and immobilization of DNA molecules in a microchannel", *Nano Lett.*, vol. 6, pp. 2499-2504, 2006.

[44] D. E. Smith, H. P. Babcock, and S. Chu, "Single-molecule dynamics in steady shear flow", *Science*, vol. 283, pp. 1724-1727, 1999.

[45] V. R. Dukkipati and S. W. Pang, "Precise DNA placement and stretching in electrode gaps using electric fields in a microfluidic system", *Appl. Phys. Lett.*, vol. 90, pp. 083901-3, 2007.

[46] V. R. Dukkipati and S. W. Pang, "Integration of electrodes in Si channels using low temperature polymethlymethacrylate bonding", *J. Vac. Sci. Tech. B*, vol. 25, pp. 386-372, 2007.

[47] M. Z. Bazant "Induced-charge electrokinetic phenomenon: theory and microfluidic applications", *Phys. Rev. Lett.*, vol. 92, pp. 066101-4, 2004.

[48] G. C. Randall, K. M. Schultz, and P. S. Doyle, "Methods to electrohoretically stretch DNA: microcontractions, gels, and hybrid gel-microcontraction devices", *Lab Chip*, vol. 6, pp. 516-525, 2006.

[49] J. P. Urbanski, T. Thorsen, J. A. Levitian, and M. Z. Bazant, "Fast ac electro-osmotic micropumps with nonplanar electrodes", *Appl. Phys. Lett.*, vol. 89, pp. 143508-1 - 3, 2006.

[50] C. A. P. Petit and J. D. Carbeck, "Combing of molecules in microchannels (COMMIC): a method for micropatterning and orienting molecules of DNA on a surface", *Nano Lett.*, vol. 3, pp. 1141-1146, 2003.

[51] R. H. Horng, P. Han, H. Y. Chen, K. W. Lin, T. M. Tsai, and J. M. Zen, "PMMA-based capillary electrophoresis electrochemical detection microchip fabrication", *J. Micromech. Microeng.*, vol. 15, pp. 6-10, 2005.

[52] L. J. Guo, X. Cheng, and C. Chou, "Fabrication of size-controllable nanofluidics channels by nanoimprinting and its applications for DNA stretching", *Nano Lett.*, vol. 4, pp. 69-73, 2004.

[53] B. Yang and S. W. Pang, "Multiple level nanochannels fabricated using reversal UV nanoimprint", *J. Vac. Sci. Tech. B*, vol. 24, pp. 2984-2987, 2006.

[54] H. L. Wang and Y. Wang, "Flow in microchannels with rough walls: flow pattern and pressure drop", *J. Micromech. Microeng.*, vol. 17, pp. 586-596, 2007.

[55] M. Madou, *Fundamentals of microfabrication: the science of miniaturization*, Boca Raton, FL: CRC Press, 2002.

[56] Q. Y. Tong and U. Gosele, *Semiconductor wafer bonding: science and technology*, Hoboken, NJ: John Wiley & Sons, 1999.

[57] P. Mao and J. Han, "Fabrication and characterization of 20 nm planar nanofluidic channels by glass-glass and glass-silicon bonding", *Lab Chip*, vol. 5, pp. 837-844, 2005.

[58] F. Nikalus, G. Stemme, J. Q. Lu, and R. J. Gutmann, "Adhesive wafer bonding", *J. Appl. Phys.*, vol. 99, pp. 031101-28, 2006.

[59] Y. Xia and G. M. Whitesides, "Soft lithography", *Annu. Rev. Mater. Sci.*, Vol. 28, pp. 153-184, 1998.

[60] H. Sato, H. Matsumura, S. Keino, and S. Shoji, "An all SU-8 microfluidic chip with built-in 3-D fine microstructures", *J. Micromech. Microeng.*, vol. 16, pp. 2318-2322, 2006.

[61] V. Studer, A. Pepin, and Y. Chen, "Nanoembossing of thermoplastic polymers for microfluidic applications", *Appl. Phys. Lett.*, vol. 80, pp. 3614-3616, 2002.

[62] B. Bilenberg, T. Nielsen, B. Clausen, and A. Kristensen, "PMMA to SU-8 bonding for polymer based lab-on-chip systems with integrated optics", *J. Micromech. Microeng.*, vol. 14, pp. 814-818, 2004.

[63] N. R. Tas, J. Haneveld, H. V. Jansen, M. Elwenspoek, and A. van den Berg, "Capillary filling speed of water in nanochannels", *Appl. Phys. Lett.*, vol. 85, pp. 3274-3276, 2004.

[64] L. J. Yang, T. J. Yao, and Y. C. Tai, "The marching velocity of the capillary meniscus in a microchannel", *J. Micromech. Microeng.*, vol. 14, pp. 220-225, 2004.

[65] K. M. Phillips, J. W. Larson, G. R. Yantz, C. M. D'Antoni, M. V. Gallo, K. A. Gillis, N. M. Goncalves, L. A. Neely, S. R. Gullans, and R. Gilmanshin, "Application of single molecule technology to rapidly map long DNA and study conformation of stretched DNA", *Nucleic Acis Res.*, vol. 33, pp. 5829-5837, 2005.

[66] K. Zhang, A. C. Martiny, N. B. Reppas, K. W. Barry, J. Malek, S. W. Chisholm, and G. M. Church, "Sequencing genomes from single cells via polymerase clones", *Nature Biotech.*, Vol. 24, pp. 680-686, 2006.

[67] K. Jo, D. M. Dhingra, T. Odjik, J. J. de Pablo, M. D. Graham, R. Runnheim, D. Forrest, and D. C. Schwartz, "A single-molecule barcoding system using nanoslits for DNA analysis", *Proc. Natl. Acad. Sci. U.S.A.,* vol. 104, pp. 2673-2678, 2007.

[68] T. M. Squires and S. R. Quake, "Microfluidics: fluid physics at the nanoliter scale", *Rev. Mod. Phys.*, vol. 7, pp. 977-1026, 2005.

[69] T. T. Perkins, D. E. Smith, and S. Chu, "Single polymer dynamics in an elongational flow", *Science*, vol. 276, pp. 2016-2021, 1997.

[70] W. Norde, "Adsorption of proteins from solution at the solid liquid interface", *Adv. Colloid Interface Sci.*, vol. 25, pp. 267-340, 1986.

[71] K. Nakanishi, T. Sakiyama, and J. Imamura, "On the adsorption of proteins on solid surfaces, a common but very complicated phenomenon", *Biosci. Bioeng.*, vol. 91, pp. 233-244, 2001.

[72] G. B. Sigal, M. Mrksich, and G. M. Whitesides, "Effects of surface wettability on the adsorption of proteins and detergents", *J. Am. Chem. Soc.*, vol. 120, pp. 3464-3473, 1998.

[73] J. Han, S. W. Turner, and H. G. Craighead, "Entropic trapping and escape of long DNA molecules in submicron size constrictions" *Phys. Rev. Lett.*, vol. 83, pp. 1688-1691, 1999.

[74] J. F. Marko and E. D. Siggia, "Stretching DNA", *Macromolecules*, vol. 28, pp. 8759-8770, 1995.

[75] K. E. Sung and M. A. Burns, "Optimization of dielectrophoretic DNA stretching in microfabricated devices", *Anal. Chem.*, vol. 78, pp. 2939-2947, 2006.

[76] T. Muller, A. Gerardino, T. Schnelle, S. G. Shirley, F. Bordoni, G. D. Gasperis, R. Leoni, and G. Fuhr, "Trapping of micrometer and sub-micrometer particles by

high-frequency electric fields and hydrodynamic forces", *J. Phys. D: Appl. Phys.*, vol. 29, pp. 340-349, 1996.

[77] F. Dewarrat, M. Calame, and S. Schonenberger, "Orientation and positioning of DNA molecules with an electric field technique", *Single Mol.*, vol. 4, pp. 189-193, 2002.

[78] A. Ramos, H. Morgan, N. G. Green, and A. Costellanos, "AC electrokinetics: a review of forces in microelectrode structures", *J. Phys. D: Appl. Phys.*, vol. 31, pp. 2338-2353, 1998.

[79] D. F. Chen and J. H. Du, "Simulation studies on electrothermal fluid induced in a dielectrophoretic microelectrode system", *J. Micromech. Microeng.*, vol. 16, pp. 2411-2419 2006.

[80] T. M. Squires and M. Z. Bazant, "Induced-charge electro-osmosis", *J. Fluid. Mech.*, vol. 509, pp. 217-252, 2004.

[81] A. E. Cohen, "Force-extension curve of a polymer in a high-frequency electric field", *Phys. Rev. Lett.*, vol. 91, pp. 235506-1, 2003.

[82] C. Waiti, P. Tosch, A. G. Davies, W. A. Germishuizen, and C. F. Kaminski, "Establishment of the ac electrokinetic elongation mechanism of DNA by three-dimenional fluorescent imaging", *Appl. Phys. Lett.*, Vol. 88, pp. 153901-153903, 2006.

[83] W. A. Germishuizen, P. Tosch, A. P. J. Middelberg, C. Walti, A. G. Davies, R. Wirtz, and M. Pepper, "Influence of alternating current electrokinetic forces and

torque on the elongation of immobilized DNA", *J. Appl. Phys.*, vol. 97, pp. 014702-7, 2005.

[84] N. P. Stanford, S. E. Halford, and G. S. Baldwin, "DNA cleavage by the EcoRV restriction enzyme endonuclease: pH dependence and proton transfers in catalysis", *J. Mol. Boil.*, vol. 288, pp. 105-116, 1999.

[85] D. C. Pregidon, M. Toner, and P. S. Doyle, "Multifunctional encoded particles for high-throughput biomolecules analysis", *Science*, vol. 315, pp. 1393-1396, 2007.

[86] S. S. Sridharamurthy, L. Dong, and H. Jiang, "A microfluidic chemical/biological sensing system based on membrane dissolution and optical absorption", *Meas. Sci. Technol.,* vol. 18, pp. 201-207, 2007.

[87] Z. Yuan, A. L. Garcia, G. P. Lopez, and D. N. Petsev, "Electrokinetic transport and separations in fluidic nanochannels", *Electrophoresis*, vol. 28, pp. 595-610, 2007.

[88] M. Z. Bazant and T. M. Squires, "Induced-charge electrokinetic phenomenon: theory and microfluidic applications", *Phys. Rev. Lett.*, vol. 92, pp. 066101-1-4, 2004.

[89] A. Oki, S. Adachi, Y. Takamura, K. Ishihara, H. Ogawa, Y. Ito, T. Ichiki, and Y. Horiike, "Electroosmosis injection of blood serum into biocompatible microcapillary dhip fabricated on quartz plate", *Electrophoresis*, vol. 22, pp. 341-347, 2001.

[90] J. P. Urbanski, T. Thorsen, J. A. Levitan, and M. Z. Bazant, "Fast as electro-osmitic miropumps with nonplanar electrodes", *Appl. Phys. Lett.*, vol. 89, pp. 143508-1-3, 2006.

[91] V. Studer, A. Pepin, Y. Chen, and A. Ajdari, "An integrated AC electrokinetic pump in a microfluidic loop for fast and tunable flow control", *The Analyst*, vol. 129, pp. 944-949, 2004.

[92] B. R. Muson, D. F. Young, and T. H. Okiishi, *Fundamentals of fluid mechanics*, Hoboken, NJ: John Wiley & Sons, 2002.

[93] J. M. Macinnes, X. Du, and R. W. K. Allen, "Prediction of electrokinetic and pressure flow in a microchannel T-junction", *Phys. Fluid*, vol. 15, pp. 1992-2005, 2003.

[94] M. Gad-el-Hak, *The MEMS handbook*, Boca Raton, FL: CRC Press, 2001.

[95] V. A. Murtsovkin and G. I. Mantrov, "Study of the motion of anisometric particles in a uniform variable electric-field", *Colloid J. USSR*, vol. 52, pp. 933-936, 1990.

[96] J. P. Matas, J. F. Morris, and E. Guazzelli, "Lateral forces on a sphere", *Oil Gas Sci. Technol. Rev. IFP.,* vol. 59, pp. 59-70, 2004.

[97] D. Stein, F. H. J. van der Heyden, W. J. A. Koopmans, and C. Dekker, "Pressure driven transport of confined DNA polymers in fluidic channels", *Proc. Natl. Acad. Sci. U.S.A.,* vol. 103, pp. 15853-15858, 2006.

[98] COMSOL Inc., Burlington, MA, 2006.

[99] S. Blumberg, M. Pennington, and M. Jens-Christian, "Do femtonewton forces effect genetic function? a review" *J. Biol. Phys.*, vol. 32, pp. 79-95, 2006.

[100] M. W. Rochlin and H. B. Peng, "Localization of intracellular proteins at aceylcholine receptor clusters induced by electric fields in xenopus muscle cell", *J. Cell Sci.*, vol. 94, pp. 73-83, 1989.

[101] I. T. Suydam, C. D. Snow, V. S. Pande, and S. G. Boxer, "Electric fields at the active site of an enzyme: direct comparison of experiment with theory", *Science*, vol. 313, pp. 200-204, 2006.

[102] B. Honig and A Nicholls, "Classical electrostatics in biology and chemistry", *Science*, vol. 268, pp. 1144-1149, 1995.

[103] K. Karen, R. S. Berman, E. Buchstab, U. Srivan, and E. Braun, "DNA-templated nanotubes field-effect transistor", *Science*, vol. 302, pp. 1380-1382, 2003.

[104] V. V. Demidov "New kids on the block: emerging PNA-based DNA diagnostics", *Expert Rev. Mol. Diagn.*, vol. 2, pp. 89-91, 2002.